The Application of Robust Optimization in Power Systems

Final Project Report

Power Systems Engineering Research Center

Empowering Minds to Engineer
the Future Electric Energy System

The Application of Robust Optimization in Power Systems

Final Project Report

Dr. Kory W. Hedman, Project Leader
Akshay S. Korad, PhD Student
Arizona State University

Dr. Muhong Zhang, Co-Investigator
Gregory Thompson, PhD Student
Arizona State University

Dr. Alejandro Dominguez-Garcia, Co-Investigator
Xichen Jiang, PhD Student
University of Illinois at Urbana-Champaign

PSERC Publication: 14-6

August 2014

For information about this project, contact:

Kory W. Hedman
School of Electrical, Computer & Energy Engineering
PO Box 875706
Arizona State University
Tempe, AZ 85257-5706
Fax: (480) 965-0745
Tel: (480) 965-1276
Email: Kory.Hedman@asu.edu

Power Systems Engineering Research Center

The Power Systems Engineering Research Center (PSERC) is a multi-university Center conducting research on challenges facing the electric power industry and educating the next generation of power engineers. More information about PSERC can be found at the Center's website: http://www.pserc.org.

For additional information, contact:

Power Systems Engineering Research Center
Arizona State University
527 Engineering Research Center
Tempe, Arizona 85287-5706
Phone: 480-965-1643
Fax: 480-965-0745

Notice Concerning Copyright Material

Acknowledgements

This is the final report for the Power Systems Engineering Research Center (PSERC) research project titled “The Application of Robust Optimization in Power Systems” (project S-51). We express our appreciation for the support provided by PSERC’s industry members.

Executive Summary

Power system operations are facing and will face new challenges as the level of variable resources increases along with higher levels of demand side uncertainty and area interchange. These added uncertainties make it harder for system operators to obtain robust solutions. Robust optimization allows for the modeling of an uncertainty set and ensures that the chosen solution can handle any possible realization based on this uncertainty set. This project has focused on the application of robust optimization for power system operations and operational planning. Part one of this project report provides an overview of robust optimization as well as it investigates two applications for robust optimization: robust unit commitment and robust corrective topology control. The optimal power flow models used within part one assume a linear approximation of the alternating current optimal power flow formulation. Therefore, part two is a complement to part one by providing a mechanism to test and validate the feasibility of the decision support tool solutions on nonlinear power flows. In summary, this research has developed new power systems decision making tools that utilize robust optimization as well as extensive analysis on the benefits and challenges to implement robust optimization within electric power systems.

Part I: Robust Optimization for Corrective Topology Control and Unit Commitment

In standard optimal power flow (OPF) formulations, the system parameters are assumed to be constant, i.e., they are assumed to be known. However, in real life, system parameters are uncertain, such as system demand, renewable generation, generator availability, and transmission availability. To capture the uncertainty in system parameters related to demand and renewable resources, robust optimization techniques are proposed. The presented report is divided into two parts; the first part discusses the effect of robust corrective topology control on system reliability and renewable integration while the second part deals with the application of robust optimization for the day-ahead security constrained unit commitment problem.

Robust Corrective Topology Control

This research presents three topology control (corrective transmission switching) methodologies along with the detailed formulation of robust corrective topology control. The robust model can be solved offline to suggest switching actions that can be used in a dynamic security assessment tool in real-time. The solution obtained from robust topology control algorithm is guaranteed to be DC feasible for the entire uncertainty set, i.e., a range of system operating states. The proposed robust topology control algorithm can also generate multiple corrective switching actions for a particular contingency, which provides multiple topology control (TC) options to system operators' to choose from in real-time application.

Furthermore, this research extends the benefits of robust corrective topology control to renewable resource integration. In recent years, the penetration of renewable resources in electrical power systems has increased. These renewable resources add more complexities to power system operation, due to their intermittent nature. This research presents robust corrective topology control as a congestion management tool to manage power flows and the associated renewable uncertainty. The proposed day-ahead method determines the maximum uncertainty in renewable resources in terms of do-not-exceed (DNE) limits combined with corrective topology control. Corrective topol-

ogy control can increase DNE limits, for the renewable resources, by a significant amount. Furthermore, the DNE limit methodology, presented in this research, is capable of modeling different types of renewable resource, such as wind and solar, uncertainties simultaneously.

The results obtained from topology control algorithm are tested for system stability and AC feasibility. On IEEE-118 bus test case, significant number of topology control solutions obtained from robust topology control algorithm have produced AC feasible solution. At the same time, it is observed that the effect of topology control on bus voltages are localized around the neighborhood of buses connected by the switched transmission element. In addition to AC feasibility tests, a number of stability studies are carried out to understand the effect of topology control on system stability. It is observed that the perturbation caused by robust corrective topology control solution can be small enough and may not cause any stability issues to system operation; several topology control solutions have shown benefit to system operation.

The future work will involve testing the robust topology control algorithms on larger test systems and investigate the benefits of parallel computational of robust topology control algorithm. The scalability of the robust topology control algorithms, from smaller test systems to realistic systems, will also be studied. Future work will also involve in investigating effects of topology control actions on AC feasibility and system stability.

Key Points

- Three topology control methodologies are presented; out of them, the robust corrective topology control methodology is developed and tested for different scenarios.
- The robust topology control framework, presented in this research, can be used to analyze different types of uncertainties: demand uncertainty and renewable resource uncertainty. The framework can test the impacts of these uncertainties independently as well as simultaneously as well as with or without the proposed corrective transmission topology control actions.
- The methodology to determine the maximum allowable deviation in renewable resources, in terms of do-not-exceed limits, will help to integrate more renewable resources into the system without sacrificing system reliability.

Robust Two-Stage Unit Commitment

This research explored the robust two-stage unit commitment problem with polyhedral uncertainty set. The wind power generation is highly uncertain, which is modeled as a polyhedral uncertainty set. A two-stage robust optimization framework is proposed to find a robust unit commitment solution at the first stage and the dispatch decision can be adjusted in the second stage. Past work has modeled the two-stage decision process to minimize the worst-case total cost including the commitment cost and dispatch cost. In this work, the objective is to minimize the maximum regret for each scenario in the uncertainty set. The regret for a particular scenario refers to the difference between the minimal total cost by fixing the first stage unit commitment decision and the cost of single stage optimal unit commitment solution. Benders' type decomposition algorithm is proposed to solve the problem. Numerical experiments demonstrate that the solutions obtained from this alternative objective function are less conservative comparing to traditional robust model. The

solutions has slightly higher expected cost with respected to the stochastic programming solution, but high reliability.

This research also examined the determination of polyhedral uncertainty sets prior to a robust formulation. With the increasing adoption of the robust programming formulation, the question of how to generate or select uncertainty sets remains open. This work studied two-stage robust unit commitment with polyhedral uncertainty set. With given set of historical data, two types of uncertainty sets based on statistic moments and empirical data are proposed. The computational experiments suggest the selection rule of of uncertainty sets for different confidence levels.

The future work will involve testing of robust unit commitment problem on larger test systems, including developing efficient heuristic and decomposition algorithms which can be implemented in high performance computing framework. Finally, the further work will consider minimax regret model with the n-k security criteria to capture the uncertainty in stochastic resources along with unpredictable contingencies.

Key Points

- The robust unit commitment framework is presented, while considering the uncertainty in renewable resource generation.
- The proposed two-stage robust unit commitment framework has demonstrated that the robust solution obtained from this methodology is less conservative compared with traditional robust model.
- Different types of uncertainty sets generated from historical data that are examined in this research, suggest that carefully selecting uncertainty sets have impacts on the performance of the robust solutions.

Part II: A Zonotope-Based Method for Capturing the Effect of Variable Generation on the Power Flow

In the last decade, there has been an increasing need for developing models to capture the uncertainty associated with electricity generation from renewable resources as they continue to penetrate into the current power system. Such penetration of renewable resources such as wind and solar introduces uncertainties in the power system static state variables, i.e., bus voltage magnitudes and angles. This report proposes a set-theoretic method to capture the effects of uncertainty on the generation side of a power system. Using this method, we can determine whether the power system state variables are within acceptable ranges as dictated by operational requirements. We bound all possible values that the uncertain generation can take by a zonotope and propagate it through a linearized power flow model, resulting in another zonotope that captures all possible variations in the system static state variables. Since the sizes of models of power systems systems have increased over the years, it is important for the developed method to scale easily and be computationally tractable. Zonotopes are easily represented by vectors and matrices, making them ideal candidates for use in large systems. Our method is applicable to both transmission and distribution systems. For verification, we test our proposed method on the IEEE 34-bus, IEEE 123-bus distribution system, and the IEEE 145-bus, 50-machine transmission system. We compare the performance of the proposed method against earlier results using ellipsoids and those solutions obtained through the nonlinear power flow and linearized power flow equations.

Project Publications:

Journal Papers:

- A. S. Korad and K. W. Hedman, “Renewable integration with do-not-exceed limits: robust corrective topology control,” working paper.
- G. Thompson, M. Zhang, and K. W. Hedman, “Data driven robust security constraint unit commitment,” working paper.
- A. S. Korad and K. W. Hedman, “Robust corrective topology control for system reliability,” *IEEE Transactions on Power Systems*, vol. 28, no. 4, pp. 4042-4051, November 2013.
- R. Jiang, J. Wang, M. Zhang, and Y. Guan, “Two-Stage Minimax Regret Unit Commitment Considering Wind Power Uncertainty,” *IEEE Transactions on Power Systems*, vol. 28, no. 3, pp. 2271-2282, August 2013.

Book Chapters:

- A. S. Korad, P. Balasubramanian, and K. W. Hedman,“Robust corrective topology control”, *Handbook of Clean Energy Systems*, Wiley Publications, accepted for publication.

Conference Papers:

- M. Sahraei-Ardakani, A. S. Korad, K. W. Hedman, P. Lipka, and S. Oren,“Performance of AC and DC based transmission switching heuristics on a large-scale Polish system,” in *IEEE PES General Meeting, Washington, DC*, pp.1-5, July 2014.

Student Thesis:

- A. S. Korad, Arizona State University, “Robust corrective topology control for system reliability and renewable integration,” PhD, Anticipated Date of Graduation: January 2015.

Part I
Robust Optimization for Corrective Topology Control and Unit Commitment

Dr. Kory W. Hedman, Project Leader
Dr. Muhong Zhang, Co-Investigator
Akshay S. Korad, PhD Student
Gregory Thompson, PhD Student
Arizona State University

For information about this project, contact:

Kory W. Hedman
School of Electrical, Computer & Energy Engineering
PO Box 875706
Arizona State University
Tempe, AZ 85257-5706
Fax: (480) 965-0745
Tel: (480) 965-1276
Email: Kory.Hedman@asu.edu

Power Systems Engineering Research Center

The Power Systems Engineering Research Center (PSERC) is a multi-university Center conducting research on challenges facing the electric power industry and educating the next generation of power engineers. More information about PSERC can be found at the Center's website: http://www.pserc.org.

For additional information, contact:

Power Systems Engineering Research Center
Arizona State University
527 Engineering Research Center
Tempe, Arizona 85287-5706
Phone: 480-965-1643
Fax: 480-965-0745

Notice Concerning Copyright Material

Table of Contents

List of Figures

List of Tables

Nomenclature

Indices

$\delta(n)^+$	Set of lines with n as the "to" node.
$\delta(n)^-$	Set of lines with n as the "from" node.
g	Generator.
$g(n)$	Set of generators at node n.
k	Transmission asset (line or transformer).
$n(g)$	Node location of generator g.
$n,\ m$	Nodes.
w	Set of wind injection locations.
$w(n)$	Set of wind generators at node n.

Parameters

θ^{max}	Maximum voltage angle difference.
θ^{min}	Minimum voltage angle difference.
B_k	Electrical susceptance of transmission line k.
c_g	Operation cost ($\$/MWh$) of generator g.
c_g^{NL}	No load cost ($\$/MWh$) of generator g.
c_g^{SD}	Shut down cost ($\$/MWh$) of generator g.
c_g^{SU}	Start-up cost ($\$/MWh$) of generator g.
DT_g	Minimum down time for generator g.
$f_k,\ P_k^{max}$	Maximum MVA capacity of transmission line k.
G_k	Series conductance of transmission line k.
M_k	Big M value for transmission line k.
M_n	Big M value for load connected at bus n.
$N1_g$	Binary parameter that is 0 when g^{th} generator contingency occurred and 1 otherwise.
$N1_k$	Binary parameter that is 0 when k^{th} transmission contingency occurred and 1 otherwise.

NSP_t	Minimum non-spinning reserve required for time t.
P_g^{max}	Maximum capacity of generator g.
P_g^{min}	Minimum capacity of generator g.
P_g^{uc}	Real power supplied by generator g (solution obtained from the unit commitment problem).
P_k^{min}	Minimum MVA capacity of transmission line k.
P_w^{fix}	Real power supplied by wind generators connected at bus $w(n)$ (solution obtained from the unit commitment problem).
$Pd_n,\ d_n^{fix}$	Forecasted real part of system demand at bus n.
Q_g^{max}	Maximum reactive power supplied by generator g.
Q_g^{min}	Minimum reactive power supplied by generator g.
Qd_n	Reactive part of system demand at bus n.
R_g^{+c}	Maximum 10 minute ramp up rate for generator g.
R_g^{+}	Maximum hourly ramp up rate for generator g.
R_g^{-c}	Maximum 10 minute ramp down rate for generator g.
R_g^{-}	Maximum hourly ramp down rate for generator g.
R_g^{nsp}	Maximum non-spinning reserve supplied by generator g.
R_g^{SD}	Maximum shut down ramp down rate for generator g.
R_g^{sp}	Maximum spinning reserve supplied by generator g.
R_g^{SU}	Maximum start-up ramp up rate for generator g.
SP_t	Minimum spinning reserve required for time t.
u_g	Unit commitment status of generator g.
UT_g	Minimum up time for generator g.
V^{max}	Maximum bus voltage.
V^{min}	Minimum bus voltage.
$\overline{Z_k}$	Binary parameter for transmission element k; 0 if line is open/not in service; 1 if line is closed/in service.

Variables

λ_{Pn}	Real power LMP at node n.
λ_{Qn}	Reactive power LMP at node n.
θ_n	Voltage angle at node n.
θ_{mn}	Voltage angle difference: $\theta_n - \theta_m$.
d_n	System demand at bus n.
d_{Pn}	Real power demand at bus n.
d_{Qn}	Reactive power demand at bus n.
P_g	Real power supplied by generator g.
P_k	Real power from node m to n for line k.
P_{gt}	Real power supplied by generator g in time t.
P_{kn}	Real power flow along line k at node n.
Q_g	Reactive power supplied by generator g.
Q_k	Reactive power from node m to n for line k.
Q_{kn}	Reactive power flow along line k at node n.
r_{gt}^{nsp}	Non-spinning reserve supplied by generator g in time t.
r_{gt}^{sp}	Spinning reserve supplied by generator g in time t.
S_{kn}	Complex power flow along line k.
u_{gt}	Unit commitment status of generator g in time t; 0 if generator is not in service; 1 if generator is in service.
V_n	Voltage at node n.
v_{gt}	Start-up status of generator g in time t; 0 if generator is not tuned on in time t; 1 if generator is tuned on in time t
w_{gt}	Shut down status of generator g in time t; 0 if generator is not tuned off in time t; 1 if generator is tuned off in time t
Z_k	Binary variable for transmission element k; 0 if line is open/not in service; 1 if line is closed/in service.

1. Introduction

1.1 Motivation

Robust optimization has existing in literature since the 1950s; however, it has not been studied in connection with electrical power systems until recently. The key feature of robust optimization, to utilize uncertainty sets to capture uncertain system parameters, is useful to analyze many power systems operational related studies. The increasing level of intermittent renewable resources in electrical power systems is adding more complexities to power system operations. The standard power system operational tools, present today, are not capable of analyzing these uncertainties to its full extent. As a result, existing power systems optimization packages are either inefficient by overcommitting generation in an ad-hoc fashion in order to handle the uncertainties or the solutions may jeopardize reliability by not accounting for such uncertainties. This research focuses on developing robust optimization based tools and algorithms, which can be used to analyze system uncertainties in power system operations.

1.2 Robust Corrective Topology Control

The proposed robust corrective topology control methodology utilizes existing assets, circuit breakers or electrical switches, to temporarily take high-voltage transmission lines out of service. Typically, taking an available transmission path out of service reduces the transfer capability of electric power across the grid and may degrade system reliability. However, it is also possible that temporarily removing a line can improve the transfer capability and reliability of the system. Since the flow of electric power on one particular transmission path is dependent on the impedances of alternative paths, it is possible to increase the transfer capability on other paths that are left in service by taking out other transmission lines. If the path that has its transfer capability increased is an critical path, e.g., there is excess wind in that region, then taking the line out of service may improve operations.

In most of the system studies today, the modeling of the transmission network is simplified, and limited attention is given to the flexibility in the network topology. To overcome this issue, there is a national push to model the grid by a more sophisticated, smarter way as well as to introduce advanced technologies and control mechanisms into grid operation. One aspect of smart grid aims at making better use of the current infrastructure, as well as additions to the grid that will enable more sophisticated use of the network. This research examines smart grid applications of harnessing the full control of transmission assets by incorporating their discrete state into the network optimization problem, and it analyzes the benefits of this concept for system reliability and renewable resources integration.

1.3 Robust Minimax Regret Unit Commitment

In electric power systems, the unit commitment problem is one of the most complex problems solved today. In prior literature, robust optimization techniques are used to solve the unit commitment problem. However, the solution obtained for the robust unit commitment problem may be expensive as robust optimization hedges against the worst-case possible realization. Therefore, the inclusion of traditional robust optimization into unit commitment is limited, as the theoretical worst-case situation may not occur and system operators may not prefer to adopt such a conservative solution. To overcome this problem, a robust minmax regret unit commitment approach is

proposed in this research.

1.4 Summary of Chapters

Chapter 2 gives a literature review, which provides the basic understanding of transmission switching proposed in literature for various reasons, such as corrective switching, congestion management, and the various techniques adopted are listed. It also covers present industrial practices involving topology control as a corrective mechanism to overcome power systems operational issues.

Chapter 3 provides background information regarding robust optimization. The derivation for the robust topology control algorithm is presented, which converts a complex three stage optimization problem into a two stage problem. The comparison of robust optimization and stochastic optimization is also given.

Chapter 4 presents the effect of demand uncertainties on system reliability. In this chapter, three topology control (corrective transmission switching) methodologies are presented along with the detailed formulation of robust corrective switching algorithm. The results for N-1 reliability analysis with robust corrective switching algorithm are also presented. These studies were conducted on the IEEE 118-bus test case.

Chapter 5 presents the effect of renewable uncertainties on renewable resources integration and system reliability. In this chapter, a robust methodology to determine the do-not-exceed limits for renewable resources is presented, along with a detailed analysis of robust corrective switching algorithm under renewable uncertainties. The simulation results for do-not exceed limits with robust corrective switching algorithm are also presented. These studies were conducted on the IEEE 118-bus test case with two different renewable resource forecasts.

Chapter 6 addresses the practical limitations of the topology control algorithm. The issues associated with the scalability and large computational time of topology control algorithm are discussed in this chapter.

Chapter 7 provides a methodology to solve unit commitment problem, using robust optimization techniques. The objective is to minimize the maximum regret instead of traditional absolute worst overall cost. The alternative objective function is less conservative, but provides robust solutions. A bender's type decomposition algorithm is proposed. The numerical experiments were conducted on the IEEE 118-bust test cases with wind uncertainty.

Chapter 8 discusses and explore the impact of the uncertainty sets to the unit commitment solutions. Two methods to construct uncertainty sets from historical data are proposed and examined in this chapter.

Chapter 9 concludes this dissertation and discusses potential future research that is connected with the main theme of this dissertation, developing a more flexible electric grid.

2. Literature Review

2.1 Introduction

The objective of this research is to study the impact of topology control on system reliability and renewable integration. Past research has identified topology control as a valuable asset that can be used to mitigate various power system operational concerns. This chapter presents a thorough literature review on the motivation for this research, past related research on topology control, and an overview of present industrial operational procedures where transmission control is employed.

2.2 National Directives

The demand of electrical power has increased considerably during the past few years. This increase in system demand causes a great amount of stress on transmission infrastructure; to overcome this issue, there is a national push to create a smarter, more flexible, electrical grid. A smarter grid not only improves the efficiency of the electric transmission systems, but also ensures secure and reliable power system operations. This research is in line with several national directives addressing this need for a smarter and more flexible power grid.

The United States Energy Policy ACT (EPACT) of 2005 calls for advanced transmission technologies, which includes a directive for federal agencies to "encourage ... deployment of advanced transmission technologies," including "optimized transmission line configuration." This research also follows the Federal Energy Regulatory Commission (FERC) order 890, which encourages the improvements in economic operations of transmission grid. It also addresses the Energy Independence and Security Act of 2007: (1) "increased use of...controls technology to improve reliability, stability, and efficiency of the grid" and (2) "dynamic optimization of grid operations and resources." The intention of this research is to harness the control of transmission assets by the dynamic optimization of the transmission grid, and the co-optimization of transmission with generation, using robust optimization techniques, thereby encouraging a smarter, flexible, and more efficient electric network.

2.3 Literature Review: Topology Control

Topology control has been in literature since 1980's and till today it has been used to overcome power systems related operational issues, ssuch as voltage violations, line overloads [1–4], line losses and cost reduction [5–7], system security [8], or a combination of these [9, 10]. In this section, the brief overview of past research related to topology control are presented.

2.3.1 Topology Control as a Congestion Management Tool

Topology control actions are used to manage congestion within the electrical network; [1] proposes topology control actions as a tool to manage congestion in the electrical grid. It discuss ways to solve this problem by genetic algorithms, as well as deterministic approaches. This approach attempt to minimize the amount of overloads in the network since they are not co-optimizing the generation with the topology. Thus, this is a disconnected approach where generation is first dispatched optimally and then this method is employed to reduce network congestion. Once again, the optimal transmission switching concept goes further than this concept since it co-optimizes the generation with the network topology in order to maximize the market surplus. In [11], the

topology control actions are proposed to mitigate transmission network congestion due to high renewable penetration.

In general, it has been assumed that taking transmission elements/lines out of service increases the congestion in the system. This misconception has been proven wrong in [12]. The main reason behind this is that as congestion in the network may increases or decreases, it cannot be assumed that losses must increase with the switching of transmission lines. Network topology optimization allows for a system re-dispatch, which makes it impossible to state the impact on congestion.

2.3.2 Topology Control as a Corrective Mechanism

Past research has shown topology control as a control method for a variety of power system operational problems. The primary focus of past research has been on proposing transmission switching as a corrective mechanism when there are voltage violations, line overloads [1–4], line losses and cost reduction [5–7], system security [8], or a combination of these [9, 10]. While this past research acknowledges certain benefits of harnessing the control of transmission network for short term benefits, they do not use the flexibility of the transmission grid to co-optimize the generation along with the network topology during steady-state operations. In [13], the unit commitment problem with topology control actions are co-optimized, with N-1 reliability, which has shown that co-optimization of topology control actions with unit commitment can provide substantial economic savings, even while maintaining N-1 reliability standards. Furthermore, the use of transmission switching as a corrective mechanism to respond to a contingency has been acknowledged in some past research to have an impact on the cost of generation rescheduling due to the contingency. However, it has not been acknowledged that such flexibility should be accounted for while solving for the steady-state optimal dispatch, probably due to computational difficulties and extended solution time.

In [14], topology control is used as a corrective mechanism in response to a contingency. It also presents the formulation of such a problem and provides an overview of search techniques to solve the problem. This idea is further extended to alleviate line overloading due to a contingency by [2] using topology control heuristics. The limitation of this method is that it is based on topology control heuristics, which does not consider all corrective topology control actions, and does not co-optimize topology control with the generation. In [15], topology control actions are used as a corrective mechanism, with linearized approximate optimal power flow formulation and solved using branch and bound method. The corrective topology control using AC power flow is studied in [9]; however, in this study, it is assumed that the generator dispatch is fixed thereby not acknowledging the benefit of co-optimizing the network topology with generation.

The corrective topology control actions provide optimal results when topology control actions are co-optimized with generation. In [7, 8], a corrective topology control is used to mitigate contingencies, where, a corrective switching algorithm is used to mitigate contingencies, consider the ability to re-dispatch generation. However, due to computational complexity of this problem, this method does not search for the actual optimal topology but rather considers limited switching actions. The review of past research on topology control is provided in [16]. In [3, 10] the topology control actions are used to relieve line overloads and voltage violations.

The optimal transmission switching for contingencies using DC optimal power flow is presented in [17], which shows that in power system operations, using topology control actions, considerable cost benefits can be achieved. Furthermore, reference [17] also shows that co-optimizing topology control with generation can give operational flexibility to system operators' to respond to

emergency situations. Furthermore, in [18] this idea is further extended to determine topology control actions for contingency mitigation in real-time. In this study, the fast DCOPF based heuristic is used to determine candidate topology control actions.

2.3.3 Optimal Topology Control

The bulk electric transmission network is built with redundant paths to ensure mandatory reliability standards, such as NERC requirements for N-1 and these standards require protection against possible worst-case scenarios. However, it is well known that the redundancies in these networks can cause dispatch inefficiency, due to line congestion, or voltage violations. Furthermore, a network branch that is required to be built in order to meet reliability standards during specific operational periods may not be required to be in service during other periods. Consequently, due to the interdependencies between network branches (transmission lines and transformers), it is possible to temporarily take a branch out of service during certain operating conditions and improve the efficiency of the network while maintaining reliability standards. This corrective switching action is the basis for the optimal topology control.

Optimal transmission switching includes the control of transmission assets into the optimal power flow (OPF) formulation in order to co-optimize the network topology simultaneously with the generation. This added level of control to the traditional OPF problem creates a superior optimization problem compared with the traditional OPF formulation. Furthermore, by harnessing the control of transmission and co-optimizing the electrical grid topology with the generation, the optimal transmission switching problem guarantees a solution that is as good as the one obtained by the traditional dispatch formulation.

The concept of a dispatchable network was first introduced in [19], which led to the research work related to optimal transmission switching in [12, 13, 17, 18, 20–23]. This past research has also shown that substantial economic savings can be obtained even for models that explicitly incorporate N-1. For example, in [13, 17] it is observed that savings on the order of $4-15\%$ can be achieved even while maintaining N-1. Note that, this past research has been based on the DCOPF formulation, a linear approximation to the ACOPF problem, which is a lossless model and reactive power flow are ignored.

2.3.4 Topology Control and Minimize Losses

In [5], the topology control actions are used to minimize system losses, which shows that, contrary to general belief, it is possible to reduce electrical losses in the network by opening a transmission line for a short timeframe. Furthermore, in [6], the author proposed a mixed integer linear programming approach to determine the optimal transmission topology, with the objective to minimize electrical transmission losses. Unlike past research, this model searches for an optimal topology, but does not consider the generator re-dispatch. The ideal way to use topology control for loss minimization is to consider the topology control along with generator re-dispatch, which will determine the optimal transmission topology and generator dispatch.

2.3.5 Topology Control for Maintenance Scheduling

Past research focused on the effect of topology control on system reliability. However, topology control actions not only affect the system reliability, but also help to reduce operational cost of the electric grid. Nowadays, system operators consider topology control as a controlling tool in maintenance scheduling of electrical bulk power system. For example, in 2008, the Independent

System Operator of New England (ISONE) saved more than $\$50$ million by considering the impact of transmission line maintenance scheduling on the overall operational costs [24]. However, the study done by ISONE is based on estimating cost instead of employing mathematical optimization tools, which determine the total system cost considering transmission network reliability. Furthermore, the benefit of this research is that it underlines the need of developing more practical mathematical models to solve the maintenance scheduling problem.

2.3.6 Topology Control for Transmission Expansion Planning

The bulk power transmission network is built with redundancies to improve system reliability and/or to improve operational efficiency. Therefore, it is often assumed that topology control actions will reduce operating costs only for poorly planned transmission networks. However, this assumption is not true. Optimal transmission switching and transmission planning are two different optimization problems with different objectives: transmission planning is a long-term problem, which determines the line(s) to build over a long time horizon; on the other hand, optimal transmission switching is a short-term problem, which determines the optimal network for short term benefits, such as reduction in operating cost. The ideal method to obtain better benefits over a long timescale is to consider the optimal transmission expansion plan. Note that, the optimal plan does not guarantee benefits to the system during each individual operating period. As a result, a network can be perfectly planned, but still benefit from short-term network reconfiguration, using optimal topology control actions.

Transmission expansion planning is a complicated multi-period optimization problem. However, in literature, topology control actions are not considered in the planning process. In [25], the methodology for transmission expansion studies with topology control action are presented. The DCOPF based formulation is used in this analysis, considering higher wind penetration. A more detailed analysis for transmission planning with topology control is presented in [26].

2.3.7 Topology Control for System Reliability

The electrical transmission network is designed to handle various contingencies and demand levels. However, such deviations do not exist at the same time with the same intensity. Therefore, a particular line that is required to be in service to meet reliability standards for a specific operating point may not be required to be in service for other operating conditions. Hence, corrective topology control can be used to meet N-1 standards. The NERC policy dictates that after the occurrence of a contingency, the system must be reconfigured and re-dispatched to handle another contingency within 30 minutes. However, in real-time the analysis of N-1 reliability is a complex problem. The real-time dynamic assessment tools used today in power system operation monitor some of these critical contingencies, as it is not possible to monitor all the N-1 contingencies in real-time.

Furthermore, it is possible to improve system reliability by temporarily taking a line out of service. System reliability not only depends on the network topology, it also depends on the generation dispatch solution, e.g., available generation capacity and ramping capabilities of the generators. Since modifying the topology changes the feasible set of dispatch solutions, it is possible to obtain a different generation dispatch solution that was infeasible with the original topology, but is feasible with the modified topology. Even though there may be a line(s) temporarily out of service, this new generation dispatch solution may make the system more reliable if it has more available capacity with faster generators. In [18], N-1 and N-2 contingency analysis for IEEE test cases is presented, which shows that, with topology control actions, $12 - 63\%$ more load can be served

during N-1 contingencies and $5 - 50\%$ more load can be served with N-2 contingencies.

2.3.8 Special Protection Schemes (SPSs)

Corrective switching is one example of topology control that is implemented today [27]. These methods are based on operators' prior knowledge, as specified in [27] on page 107; such actions may also be based on historical information. Ideally, corrective switching algorithms should be solved in real-time. Once the disturbance occurs, the switching algorithm is executed to suggest switching actions to alleviate any constraint violations. This approach is beneficial since the current operating status is known, which ensures the accuracy of the solution. However, the challenge with real-time mechanisms is that they must be extremely fast while also ensuring AC feasibility, voltage stability, and transient stability. Topology control models could be solved offline by estimating the operating state of the system. However, deterministic offline mechanisms also have limitations since the operating state must be predicted prior to the disturbance. Thus, the proposed offline corrective action is, susceptible to problematic reliance on perfect foresight.

Special protection schemes (SPSs), also known as remedial action schemes (RASs) or system integrity protection schemes (SIPSs), are an important part of grid operations. SPSs are used to improve the reliability of the grid and improve the operational efficiency. SPSs are primarily identified and developed based on ad-hoc procedures. The development of such corrective mechanisms like SPSs reflects a change, a push, by the industry to switch from preventive approaches, to the use of corrective approaches. The use of transmission switching as a corrective mechanism can be a powerful tool. For instance, PJM has a number of SPSs that involve post-contingency transmission switching actions [28]. For example, the following action is listed in [28] on page 221: "The 138 kV tieline L28201 from Zion to Lakeview (WEC) can be opened to relieve contingency overloads for the loss of either of the following two lines: Zion Station 22 to Pleasant Prairie (WEC) 345 kV Red (L2221), Zion Station 22 to Arcadian (WEC) 345 kV Blue (L2222)."

In practice, topology control actions are employed during blackouts caused by rare weather conditions [29]. In 2012, due to Superstorm Sandy, PJM lost about 82 bulk electric facilities, which caused extremely high voltages on the system during low load levels. To overcome this high voltage situation, a corrective switching plan was employed, several 500kV lines were switched out to mitigate over voltage concerns during these low load level periods. Note that, the corrective switching methodology employed in this particular case is unknown.

Such operational protocols, like SPSs, are often viewed as a necessary protocols to maintain system reliability. While these transmission switching SPSs do help maintain system reliability, there are alternatives that the operator can employ instead. Possible alternatives may include: re-dispatching the system after the contingency occurs; choosing a different steady-state (no-contingency) dispatch prior to the contingency occurring to ensure there is no overloading; or upgrading the equipment so that it is able to handle these contingency flows. Re-dispatching the system is likely to increase the operating costs. Choosing a different dispatch solution for steady-state operations would increase the operating cost, otherwise, that dispatch solution would have been initially chosen. Investing in new equipment increases the capital cost of the system.

2.3.9 Seasonal Transmission Switching

Topology control actions are used for short term benefits as well as seasonal benefits. For instance, in the state of California, the load requirements are lower in the winter and the probability of an outage is higher due to winter storms. The summer is the exact opposite; during the summer, the

load is the highest in the year, but the probability of outages is lower since there are fewer and less severe storms. As a result, some utilities have determined that it is beneficial to leave certain transmission lines in service during the winter when there is a greater chance of winter storms for reliability purposes, but yet these lines are taken out of service during summer periods since the threat of an outage is lower.

These lines are primarily redundant transmission lines in the lower voltage network. Such redundancies are less important during summer periods when the probability of an outage is lower. Furthermore, these redundant lines can cause overloading concerns during summer periods since the load conditions during the summer are higher. For instance, there can be two parallel lines with different thermal capacity ratings. The lower capacity line, generally a part of the lower voltage network, may reach its capacity first and, therefore, inhibit the higher voltage network from transferring as much power as desired. Due to the higher loading conditions, it is, therefore, preferred to take the redundant, lower capacity line out of service, as long as the line is not necessary to maintain system reliability. Since the outage rates are lower during the summer periods, the operators are able to take the line out of service without jeopardizing system reliability. In contrast, having these redundancies in service during the winter is integral to maintaining system reliability since the probability of an outage is greater. In addition, the redundancies do not cause overloading concerns during the winter since the winter loading levels are lower.

While this operation is acknowledged by utilities today, the tradeoff between protecting against potential contingencies versus the potential for overloads is not well understood. Seasonal transmission switching models that are capable of answering these questions do not exist today, thereby emphasizing the need for further research and development in the area of seasonal transmission switching.

2.3.10 Summary of Literature Review of Topology Control

Topology control actions have been suggested to mitigate many power systems related problems. However, most of those studies are either based on DCOPF or assumes fixed generator dispatch, which has limited the spread of topology control in power system operations. Even though, today, system operators do change system topologies for short term application, these topology control actions are based on operators' prior knowledge or some add-hoc methods. To overcome this issue research presented in this report introduces a robust optimization based topology control methodology, which suggests the topology control actions, that are valid for a range of operating states, are guaranteed DC feasible for the entire uncertainty set.

2.4 Literature Review: Stochastic and Robust Optimization

In the modern decision processes, uncertainty has drawn massive research and practical attention. Traditionally, an optimization model is built based on the point prediction of the modeling parameters. For example, in the electrical power planning problem, an expected load is estimated at a particular time. It has been shown that, with the estimation errors or the nature of parameters, the "true" value of the estimated parameter can be deviating from the estimation. The solution from the deterministic formulation can be suboptimal for the true value of the parameters.

Stochastic programming is proposed to address the uncertainties [30, 31]. In a stochastic programming approach, a prior probability distribution is assumed for the uncertain parameters. A typical objective of stochastic programming formulation is to optimize over the expected value under the probability distribution. When a probability distribution is hard to estimate or the com-

putational difficulty of the explicit form of the expectation, sample based formulations are studied extensive in the recent several decades. Sampling average approximation (SAA) [32, 33] is proposed to model the stochastic programming with a large number of samples, which each sample is assumed to have equal probability. It has been shown that, when the sample size is sufficiently large, the sampling average approximation solutions converges to the stochastic programming solution with true probability distribution of the parameters. The advantage of SAA is the minimal assumptions of the underlining probability distribution. The formulations typically preserve certain structures of the deterministic models, which enable the insights and algorithms from the deterministic models to be adopted to the stochastic models. However, with the large sample size, the stochastic programming formulation grows fast, which can be extremely computational challenging.

While many applications of stochastic programming are optimizing over expected objective function, there are problems requiring probability assurance of the constraints satisfaction such as reliability requirements. Chance constraint programming problem is used to model such problems [30, 31]. Specifically, a solution is feasible in a chance constraint program if it is feasible with certain probability. The chance constraint problem is shown in general a hard problem, which is non-convex even when the deterministic model is a linear program. Risk measures are proposed to approximate the chance constraints with convex constraints [34]. Sampling average approaches are also applied to the chance constraint programming problem [35] and modeled as mixed integer programming problems [36, 37].

Due to the computational challenging of stochastic programming and lack of probability distributional information, robust optimization has been proposed to address uncertainties with limited assumptions on probability distribution of the parameters. The earlier work of robust optimization is back to 1950's [38]. The robust model of a linear program with right hand side uncertainty is a linear program again. However, the resulting solution is too conservative from a practical point of view. Kouvelis and Yu [39] summarize the different type of robust optimization formulation with different objective functions. In recent two decades, the robust optimization is attracting extensive research attention starting from [40–44]. In such prior work, the robust optimization model is to optimize the worst-case objective value on a pre-defined uncertainty set, where the solution is guaranteed to be feasible to any realization of the uncertainty parameters in the uncertainty set. The uncertainty sets are typically parametric closed convex set, such as ellipsoids or polyhedra. The parameters associated with the uncertainty set are used to adjust the conservative choice from the decision maker. Furthermore, adaptive robust model are studied [45, 46], where the decisions are partitioned to two stages. The first stage is to determine partial solution before the observation of the uncertain parameters and the second stage solution will be adaptively adjusted according to the updated parameter information.

With the nature of the power industry and electrical power generation, multistage stochastic programming formulations were proposed and an augmented Lagrangian decomposition framework was studied to solve the problem efficiently (see, e.g., [47], [48], [49], and [50]), targeting load uncertainty for vertically integrated utility companies. Recently, significant research progress has been made in the application of stochastic programming approaches to the deregulated electricity markets (see, e.g., [51], [52] and references therein). Stochastic programming approaches have been used to combine the slow-start generator commitment in day-ahead and fast-start generator commitment in real-time operations (see, e.g., [53] and [54]), estimate the contribution of demand flexibility in replacing operating reserves [55], and solve stochastic security-constrained

unit commitment models (see, e.g., [56], [57], [58], and [59]). Besides these applications, chance-constrained two-stage stochastic programming has been studied to ensure high utilization of wind power output [60], and the parallel computing (see, e.g., [61]) implementation under a cloud computing or high performance computing environment has increased the capacity to solve large-scale two-stage stochastic power system optimization problems. With these processes in the stochastic programs, the computational challenges still exist, especially for the unit commitment with risk measures. Robust optimization is aligned with the high reliability requirements in the power grid. Two-stage or adaptive robust optimization models are studied in [62] and [63]. One of the concern of the application of robust optimization model in the power system is the possible overly conservative nature since it optimizes over the worst-case scenario. Alternative objective of robust optimization can be minimax regret [64], which has been applied in risk-constrained power system planning problems, to model multiobjective tradeoff (see, e.g., [65], [66], and [67]), to handle the uncertainty that emerges in market competition [68], to serve as an alternative of the probabilistic choice approach [69], and to mitigate the vulnerability against intentional attacks while meeting budgetary limits [70]. In this work, we will adopt the minimax regret as the objective to model the two-stage robust unit commitment problem under wind uncertainty and demonstrate the tradeoff between the various objectives and solution qualities.

3. Robust Optimization

3.1 Introduction

The origin of robust optimization goes back to the early days of modern decision theories in the 1950's [71], where it was used to analyse the worst-case scenario of several uncertainties. In the 1970's, Soyster [38] proposed a worst-case model for linear optimization problem such that constraints are satisfied under all possible perturbations of the model parameters. Over the years, robust optimization techniques have been used in many areas, such as operations research [39, 72], control theory [73], logistics [74], finance [75], medicine [76], and chemical engineering [77].

In recent years, robust optimization has gained a great deal of attention in the electrical power system sector; for example, in [62] and [63], two-stage robust optimization techniques are used for unit commitment, which deal with the data uncertainty and attempt to find an optimal solution considering the worst-case uncertainty realization. The solution of the robust optimization problem is guaranteed to be feasible and optimal for a defined uncertainty set [78, 79]. Since the optimal solution is a hedge against the worst-case realization, the solution is often conservative. Robust optimization may not be preferred for many applications due to its conservative nature; however, it is in accordance with the power industry in regards to maintaining reliability.

3.1.1 The Need of Robust Optimization

LP is a type of optimization problem with a polynomial algorithm and generally it is in form of (3.1), where, x is a vector of decision variables such that $x \in \mathbb{R}^n$, cost is represented by c such that $c \in \mathbb{R}^n$, A is an $m \times n$ constraint matrix, and $b \in \mathbb{R}^m$ is the right hand side vector of constraint matrix.

$$\min_x \{c^T x : \ Ax \leq b\} \tag{3.1}$$

The structure of the problem, given in (3.1), is such that there are m number of constraints and n number of variables. The data of the problem are the collection ($c,\ A,\ b$) and are collected in data matrix, D, as shown in (3.2). The dimension of this matrix is $(m+1) \times (n+1)$.

$$D = \left[\begin{array}{c|c} c^T & 0 \\ \hline A & b \end{array}\right] \tag{3.2}$$

Note that, in D, all the parameters are fixed and known prior to solving the LP problem. In most of the real world LP problem all this data is not known; the uncertainty in data is presented due to many reasons, some of them are listed below [80],

1. Prediction error- In many real-life mathematical problems, some of the data entries are unknown at the time problem formulation. Therefore, when the problem is solved, those data entries are estimated by their respective data forecasts. These data forecasts are not exact (by the definition of forecast), which introduces the prediction error. For instance, in case of day-ahead unit commitment problem, the system demand for the next day is unknown; therefore, it is forecasted using system demand forecasting methodologies [81]. It is well understood in the power industry that day-ahead system demand forecast is not accurate; hence, system

operators consider operational reserves in day-ahead unit commitment problem to overcome this inaccuracy and the unpredicted nature of system demand in real-time implementation.

2. Measurement error- In some LP problems, the few parameters in the data matrix, D, are determined based on actual data measurement. Often these measurements are done off-line and may not be measured accurately. This introduces measurement errors in parameter calculations and may introduce considerable uncertainty into the LP problem solution. For instance, the susceptance of transmission lines in power transmission network are determined based on field measurements. In many cases, these measurements are not accurate or do not reflect the true value, as susceptance of transmission line depends on weather condition and changes over time due to operational wear and tear. Therefore, optimal power flow problems solved based on these susceptance values may results in sub-optimal or even infeasible solutions.

3. Implementation error- Sometimes the decision variables determined in a mathematical problem cannot be implemented exactly as they are computed. This practical implementation issue introduces implementation errors in solution. For example, in power system operations, the generators are scheduled and dispatched based on day-ahead unit commitment solution. However, sometimes, due to practical issues, generators deviate from the required set dispatch point; for instance, old generators may not ramp up and ramp down as expected or gas turbine generators fail to produce required power due to higher temperatures in the turbine. In these cases, system operators needs to update the generator dispatch based on present operating conditions.

Traditionally, LP problems are solved by ignoring the data uncertainty. The results obtained from the LP models are implemented or analyzed with small perturbations via sensitivity analysis. It has been shown that even with small perturbation of the data, the solutions from the deterministic LP models can be suboptimal and even infeasible in many real situations [79]. Therefore, consideration of uncertainties is critical in many practical applications.

3.2 Robust Optimization

In recent years, robust optimization has gained lot of attention. Robust optimization guarantees a feasibility, as well as optimality, of a solution for any possible realization in the modeled uncertainty set. This approach considers the worst-case realization of uncertainty within the predetermined uncertainty set. The benefit of robust optimization is that it requires less probability information about uncertainty compared with the stochastic programming approach; however, the solution obtained from robust optimization is generally more conservative than the solution obtained from stochastic programming approach. Due to the conservativeness of robust optimization over stochastic programming, robust optimization has recently become more attractive as a mechanism to model uncertainty [80, 82, 83] in applications with high reliability requirements.

In addition, ensuring reliability and obtaining economically robust solutions are the primary concerns in the power systems sector. Little work has been done to examine the benefits of robust optimization in the electric power industry. Recently, more attention has been given to the application of robust optimization in the power systems sector by [62, 63, 84].

The generic form of deterministic MIP problem is presented in (3.3)-(3.7), where, x is a set of integer variables and y is a set of continuous variables. Other parameters, such as $A, a, B, b, c, E, e,$

F, f, H, h, are data or parameters. The solution obtained from this MIP formulation is optimal/feasible only for the fixed values associated with parameters $A, a, B, b, c, E, e, F, f, H, h$. The basic topology control model, used in research, is a MIP problem. This can be represented in generic form as shown in (3.3)-(3.7), where, variable x represents the status of transmission line, i.e., line in service or line out of service, and variable y represents the set of other continuous variables, such as generator dispatch, line flows, and bus angles.

$$\min_{x,y} \quad c^T x + b^T y \tag{3.3}$$
$$\text{s.t.} \quad Fx \leq f \tag{3.4}$$
$$Hy \leq h \tag{3.5}$$
$$Ax + By \leq a \tag{3.6}$$
$$Ey = e \tag{3.7}$$
$$x \in \{0, 1\}$$

The objective of robust optimization problem is to determine the optimal solution considering the worst-case outcome under the assumed uncertainty set. The generic form of robust optimization problem is given in (3.8)-(3.12), which is a two-stage optimization problem. The first stage of the problem is to determine the solution associated with integer variables which are typically referred as design decisions ; the second stage is to find the worst-case cost or worst-case realization of the continuous variable, y, associated with the integer solution obtained in the previous stage. Traditionally, two-stage robust optimization is actually modeled as a three-stage problem with a middle stage of uncertainty scenario selection, as shown in (3.8)-(3.12). The formulation is attempting to determine an optimal solution of the design and operational cost against the worst-case uncertainty realization. The solution of the robust optimization problem is guaranteed optimal for a pre-defined uncertainty set [62, 63].

$$\min_{x \in \mathcal{X}} \quad \left(c^T x + \max_{d \in \mathcal{D}} \min_{y} b^T y(d) \right) \tag{3.8}$$
$$\text{s.t.} \quad Fx \leq f \tag{3.9}$$
$$Hy(d) \leq h \tag{3.10}$$
$$Ax + By(d) \leq a \tag{3.11}$$
$$Ey(d) = e \tag{3.12}$$
$$x \in \{0, 1\}$$

In (3.8), the term $y(d)$ is used to emphasize the dependency of continuous variable y on the uncertainty, d. The first minimization part of (3.8) minimizes the cost associated with the integer solution. The later part of (3.8), the max-min formulation, known as the evaluation part of robust structure, determines the worst-case cost of decision taken in first part of minimization problem. The evaluation part of the robust formulation is divided into two parts, which makes the robust optimization problem as a three-stage optimization problem as shown in (3.8).

Traditionally, for robust optimization problems, the following assumptions are made prior to solving the problem, which are cited in [80].

1. All the entries in the first-stage decision variables are “here and now” decisions, which

should get specific numerical values as a result of solving the problem, and before the actual data "reveals itself". The second-stage variables are "wait and see" decisions, which will be determined when the data realization is revealed. This assumption indicates that the first-stage solution of the robust optimization problem should be a fixed number/vector, which will be optimal and feasible to the entire uncertainty set with the adaptive second-stage solutions.

2. The decision maker is fully responsible for consequences of the decisions to be made when, and only when, the actual data is within the unspecified uncertainty set. This assumption indicates that the solution is guaranteed to be "robust" only to the uncertainties modeled within the uncertainty set.

3. The constraints in robust formulation are "hard"- we cannot tolerate violations of constraints, even small ones, when the data is within the uncertainty set. This assumption ensures the robustness property of robust optimization problem by enforcing all the constraints and not allowing any relaxations on a constraint level.

3.2.1 Uncertainty Modeling

Uncertainty modeling is a key part of robust optimization. In [62], polyhedral uncertainty sets are used to define demand uncertainties. System demand uncertainty, in [62], is modeled assuming that the system load has an upper, as well as a lower bound, and that the system-wide aggregate load has an upper bound, as shown in (3.13). Similar uncertainty set definition is used [63].

$$\mathcal{D} = \{d \in \mathbb{R}^{N_d} : \sum_{i \in N_d} \frac{|d_i - d_i^{fix}|}{\hat{d}_i} \leq \Delta, d_i \in [d_i - \hat{d}_i, d_i + \hat{d}_i],\ \forall i \in N_d\} \tag{3.13}$$

In (3.13), the set of nodes with uncertain demand is represented by N_d, d_i^{fix} represents the estimated or expected demand, d_i represents the realization in demand, the maximum deviation in demand at node i is represented by parameter $\hat{d}_i$ The total deviation in demand is also bounded by parameter Δ.

In Chapter 4-5 , a simplified uncertainty model is used to represent demand uncertainty. The polyhedral uncertainty set is presented in (4.1); if desired, a more complex polyhedral uncertainty sets can be used instead, as in [63].

$$\mathcal{D} = \{d \in \mathbb{R}^n : d_n^{fix} D_n^- \leq d_n \leq d_n^{fix} D_n^+,\ \forall n\} \tag{3.14}$$

In this uncertainty set, the system demand is bounded by its pre-determined lower and upper limits. The uncertainty description used in (3.14) is more conservative than the uncertainty sets used in [62] and [63]. The size of the uncertainty set is defined by the parameters D_n^+ and D_n^-. When D_n^+ and $D_n^- = 1$, the uncertainty is zero and $\mathcal{D}$ is a singleton, i.e., $d_n = d_n^{fix}$. When $D_n^- \leq 1$ and $D_n^+ \geq 1$, the uncertainty set is a polyhedron and its size is defined by the values of D_n^+ and D_n^-.

Similarly, wind uncertainty is modeled as shown in (3.15). Renewable resources (in this case, wind generation), P_w, are assumed to vary within these pre-determined lower and upper limits, and the size of uncertainty set depends on the parameters D_w^- and D_w^+.

$$W = \{P \in \mathbb{R}^w : P_w^{fix} D_w^- \leq P_w \leq P_w^{fix} D_w^+, \ \forall w\} \tag{3.15}$$

3.3 Comparison Between Robust Optimization and Stochastic Optimization

Uncertainty is an important factor to be considered in the decision making processes. In traditional applications, the uncertainties were ignored or simplified due to computational difficulties. With the advance of the computational power, there are different ways to incorporate uncertainties in decision processes.

Stochastic programming has been one common approach to facilitate the decision processes with uncertainties. It typically assumes probability distributions for uncertain parameters, or incorporates a large number of scenarios, which leads to computationally challenging large scale optimization problems. In stochastic programming formulations, the objective is typically optimizing over the expectation over the uncertain parameters. The feasibility of the solutions is modeled either to be feasible to all scenarios or with probability guarantees. While it is generally difficult to know the exact distribution of the random parameters, sample based methods are popular in the stochastic programming literature. To achieve high probability guarantees, the sample size is typically large and leads to computational challenges of the stochastic programming approaches.

In (3.16), a generic form of stochastic optimization problem with probability constraints is presented, where the uncertainty in optimization framework follows the probability distribution, when $\epsilon \ll 1$, the distribution of data (c, A, b) is represented by P. In simple cases, these uncertainties are modeled with known probability distribution functions; however, in more realistic cases, the probability distribution function is partially know. This may cause a problem in (3.16) such that the partial distribution of P is known and P belongs to a given family $\mathcal{P}$ of probability distributions on the space of the data (c, A, b). In this situations, the accuracy of stochastic optimization problem depends on the availability of possible scenarios and modeling details. If all the possible scenarios are modeled in stochastic framework, the optimization problem become cumbersome and may not be solvable. Therefore, there is a tradeoff between the number of scenarios modeled and the computational time/trackability. Another tradeoff is between the quality of stochastic solution and number of scenarios under consideration. The solution quality of stochastic optimization problem is directly related to number of scenarios under consideration. The primary barrier to stochastic programming is the tradeoff between the computational challenge and the quality of the solution; to get a more accurate solution, it would be preferable to represent additional uncertainties, but then this increases the model complexity, which makes it more difficult to obtain a quality solution.

$$\min_{x,t}\{t : Prob_{(c,A,b)\sim P}\{c^T x \leq t \ \& \ Ax \leq b\} \geq 1 - \epsilon, \forall P \in \mathcal{P}\} \tag{3.16}$$

The robust optimization has gained substantial attention in recent years [62, 63, 84]. This approach is attractive in many aspects over stochastic optimization approach for the problems with high reliability requirements. The main benefit of robust optimization is that it requires moderate information about underlying uncertainties, such as range of uncertainty, type of uncertainty. The robust framework is flexible enough to model each type and size of uncertainty independently, as well as simultaneously. Robust optimization does not requires probabilistic information about the

uncertainty; the solution obtained from robust formulation is guaranteed to be optimal for the entire uncertainty set. Therefore, robust optimization modeling approach is favorable for the electric power sector where ensuring reliability is crucial. Furthermore, robust optimization requires less knowledge concerning the probability distribution as compared to stochastic programming and the computational complexity for robust optimization is typically smaller. In robust optimization, instead of assuming explicitly a probability distribution of uncertainty parameters, an uncertainty set is predetermined to cover the possible realizations. A solution model is robust if it is feasible for all the possible scenarios in the uncertainty set and is robust if it is close to the optimal solution for all the scenarios in the uncertainty set.

Smaller uncertainties can be analyzed by performing a sensitivity analysis [82]. The sensitivity analysis is a tool to analyze the stability properties of an already found solution; there are many application, in literature, which are based on sensitivity analysis to determine the solution quality/robustness. This approach has been used in many system control related problems; however, sensitivity analysis solution does not give guarantees associated with quality of solution and its effectiveness; plus, sensitivity analysis does not hold, if the expected uncertainty is relatively large. Therefore, implementation of solution sensitivity based methods are limited.

3.4 Conclusion

Uncertainty analysis plays an important role in decision making processes. By ignoring the uncertainty, a decision can be sub-optimal, or even infeasible. Stochastic optimization has been one common approach to incorporate uncertainties in decision making process.

This research focuses on robust optimization to understand and model the uncertainties in the decision making process. The solution obtained from robust optimization problem is guaranteed optimal/feasible for the entire uncertainty set. However, robust optimization problems are computationally complex and require special solution techniques to solve the problem.

In recent years, robust optimization has gained attention in the electrical power system community. Robust optimization, would be suitable for power system related problems, as ensuring reliability and obtaining robust solutions are primary concerns in the power systems sector. However, little work has been done to examine the benefits of robust optimization in the electric power industry.

4. Robust Corrective Topology Control for System Reliability

4.1 Introduction

Even though the bulk power grid is one of the most complex systems to date, in practice, the modeling of the transmission network is simplified and limited attention is given to the flexibility in the network topology. Traditionally, transmission lines are treated as static assets, which are fixed within the network, except during times of forced outages or maintenance. This view does not describe transmission lines as assets that operators have the ability to control. Transmission switching has been studied since the 1980s and it was used as a tool to overcome various situations such as voltage violations, line overloads [1–4], line losses and cost reduction [5–7], system security [8], or a combination of these [9, 10].

Recent work has demonstrated that topology control can have significant operational as well as economic impacts on the way electrical power systems are operated today [13, 22, 23, 85]. The concept of a dispatchable network is presented in [19]. Additionally, optimal transmission switching using a direct current optimal power flow (DCOPF) formulation is presented in [85] and [20]; however, these models did not implicitly enforce N-1 reliability constraints. In [17], optimal transmission switching with an N-1 DCOPF formulation was tested on the IEEE 118-bus test case and on the RTS 96 test case. Reference [17] also indicates that substantial savings can be obtained by optimal transmission switching while satisfying N-1 reliability constraints.

There has been recent development of a different transmission switching formulation, [86], which builds on the work of on generalized line outage distribution factors, [87]. With the use of flow canceling transactions, [86] develops a framework that is able to capture the changes in the topology and compares it to the $B-\theta$ formulation used in many preceding transmission switching papers as well as in this research. This formulation is likely to outperform the $B-\theta$ formulation when the number of monitored lines is relatively small, something that is common practice within optimal power flow problems today.

Past literature has shown that topology control can be used to improve system operations and reliability. Such previous work has led system operators to adopt topology control as a mechanism to improve voltage profiles, transfer capacity, and even improve system reliability [27, 88, 89]. However, the adoption of topology control is still limited as there is a lack of systematic topology control tools. Currently, the industry adoption and implementation of topology control is based on ad-hoc methods or the operator's past knowledge. Alternatively, transmission switching decisions can be suggested by a mathematical decision support tool. Many factors have prevented topology control from becoming a more widespread corrective action within system operations. For instance, there have been misconceptions that more transmission is always better than less, concerns over the switching actions' effect on stability, impacts on circuit breakers, computational complexities of topology control algorithms, as well as additional concerns.

Corrective switching is one example of topology control, which is implemented today [27]. These methods are based on operators' prior knowledge, as specified in [27] on page 107; such actions may also be based on historical information. Ideally, corrective switching algorithms should be solved in real-time. Once the disturbance occurs, the switching algorithm is executed to suggest switching actions to alleviate any constraint violations. This approach is beneficial since the current operating status is known, which ensures the accuracy of the solution. However, the challenge of real-time mechanisms is that they must be extremely fast while also ensuring AC feasibility,

voltage stability, and transient stability. Topology control models could be solved offline by estimating the operating state of the system. However, deterministic offline mechanisms also have limitations since the operating state must be predicted prior to the disturbance. The proposed offline corrective action is, thus, susceptible to its problematic reliance on perfect foresight. This rearch introduces the concept of robust corrective topology control, which presents a solution to these current challenges.

Robust optimization has gained a great deal of attention in recent years; for example in [62], a two-stage robust optimization technique is used for unit commitment. It deals with data uncertainty and attempts to find an optimal solution considering the worst-case uncertainty realization. The solution of the robust optimization problem is guaranteed optimal for a defined uncertainty set [78, 79]. Since the optimal solution is a hedge against the worst-case realization, the solution is often conservative. Robust optimization may not be preferred for many applications due to its conservative nature; however, it is in accordance with the power industry in regards to maintaining reliability.

This research proposes the new concept of robust corrective topology control. The main idea is to use transmission switching as a control tool to mitigate constraint violations with guaranteed solution feasibility for a defined uncertainty set. The switching solution obtained from the robust corrective topology control formulation will work for all system states within the defined uncertainty set. The proposed robust corrective topology control tool is tested as a part of contingency analysis, which is conducted after solving a day-ahead unit commitment problem; however, note that the concept of robust corrective topology control is not restricted to such applications. The main concepts discussed in this chapter are summarized below.

1. Three corrective switching methodologies are identified: real-time corrective switching, deterministic planning based corrective switching, and robust corrective switching. Real-time corrective switching is the preferred process for corrective switching, but it requires extremely fast solution times. Thus, with today's technology, the implementation of real-time corrective switching is limited. With today's technology, deterministic planning based corrective switching can be implemented but it requires perfect foresight regarding future operating states. Therefore, implementation of deterministic planning based corrective switching is limited. To fill the technology gap between real-time corrective switching and deterministic planning based corrective switching, a robust corrective switching methodology is proposed.

2. A robust corrective topology control formulation: the robust corrective switching model is a three-stage robust optimization problem. With a pre-determined uncertainty set regarding the nodal injections (or nodal withdrawals), the robust corrective switching model will determine the corrective switching action that will be feasible for the entire uncertainty set. The robust optimization model consists of a master problem and two subproblems. The master problem will determine the corrective switching action and the subproblems will determine the worst-case realization of demand within the uncertainty set (for the associated corrective switching action). The nodal injection uncertainty can be due to generation uncertainty (wind/renewables), demand uncertainty, area interchange uncertainty, as well as other causes of uncertainty. The robust corrective switching framework will work for all these different types of uncertainties. The detailed vision of the robust corrective switching framework as an end-to-end process is also presented.

3. A solution technique for solving the robust corrective switching model is presented: specifically, an iterative procedure is developed to solve the master problem and the subproblems. The master problem is a mixed integer programming (MIP) problem and the subproblems are reformulated into a single subproblem, which is a nonlinear problem. This new subproblem is converted from a nonlinear problem into a MIP problem. The proposed solution technique is tested on the IEEE 118-bus test case.

The chapter is structured as follows: a detailed framework of real-time corrective switching, deterministic planning based corrective switching, and robust corrective switching are presented in Section 4.2. The uncertainty modeling used in this chapter is described in Section 4.3. The generic deterministic corrective switching formulation is given in Section 4.4. The detailed mathematical model for robust corrective switching is given in Section 4.5. The solution method for the corresponding problem is discussed in Section 4.6. The IEEE 118-bus test case is used for the robust corrective switching analysis and the results are presented in Section 4.7.

4.2 Corrective Switching Methodologies

Corrective transmission switching can be used as a control action to respond to an event. This research proposes a robust corrective switching methodology to respond to N-1 contingencies. This section analyzes two existing methods to determine potential corrective switching actions and compares them to the proposed robust corrective switching framework. Note that corrective transmission switching actions may or may not be combined with generation re-dispatch. For the proposed robust corrective switching procedure, generation re-dispatch is taken into consideration.

4.2.1 Real-time Topology Control

The real-time topology control model determines the corrective action(s) to take as a response to an event, e.g., a contingency. The skeleton of the real-time topology control scheme is shown in Fig. 4.1. When a particular contingency occurs, the corrective switching algorithm will determine the switching action in real-time based on the current system state. The resultant switching scheme will be tested to determine if the proposed topology is AC feasible and if the switching action causes instability. If the solution is feasible, it is implemented.

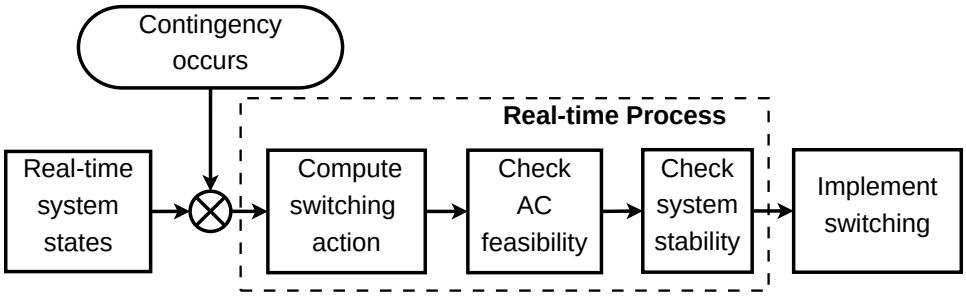

Figure 4.1: Real time topology control scheme.

Ideally, it is preferred to solve for the optimal switching action in real-time because more information is known about the operating state of the grid. However, during an emergency, it is paramount that a corrective action be taken as soon as possible in order to avoid a potential blackout. Real-time corrective switching is a non-convex, nonlinear, MIP problem. Such a problem

cannot be solved in real-time with available tools today. Therefore, heuristics are necessary to generate potential solutions. There are many heuristics for transmission switching that have been previously proposed in literature [90–93]. These heuristics can be used to find decent solutions faster than solving a MIP. However, there is still the overarching concern that they may not be fast enough for practical large-scale applications due to the extreme importance of implementing a solution as fast as possible during an emergency. DCOPF based heuristics would still need to be checked to see if they are AC feasible and any proposed action would need to be confirmed to not cause a stability concern. Therefore, it is difficult to establish the success rate of such heuristics due to the time sensitive nature of real-time corrective actions during emergency conditions. It is also difficult to predict the solution quality of switching actions proposed by heuristics. In [10], a real-time application of topology control is proposed for an AC formulation and they have shown that this can be solved quickly but there is still the issue of transient stability of the switching action and the approach does not take into consideration generation re-dispatch.

Another drawback of such real-time corrective switching heuristics is that they assume the operating state will not change. State estimation would be used to estimate the system state when the algorithm is executed. However, the actual system state when the action is implemented may be different than the assumed system state due to the time it takes to run the algorithm and check for AC feasibility and system stability. While such procedures can be adjusted to reflect multiple operational states, doing so adds additional complexity to the algorithm, which further exposes the approach to the risk that it may not solve fast enough. Overall, real-time topology control mechanisms that rely on heuristics may be fast but there are still practical issues that they do not take into consideration. Thus, there is a need for topology control actions that are robust against operating states in order to increase the likelihood of obtaining a feasible solution when implemented.

4.2.2 Deterministic Planning Based Topology Control

Today, there are special protection schemes involving corrective switching that are determined based on offline analysis, [27]. The main idea of deterministic planning based corrective switching is to determine the corrective switching action offline, e.g., in a day-ahead or a week-ahead time-frame, and then feed this information into a real-time dynamic security assessment tool that can determine if the switching action is feasible. For deterministic planning based corrective switching, an assumption regarding the system state is made and switching actions will be proposed in response to selected contingencies. Then, the switching schemes will be tested for AC feasibility and system stability based on the estimated, assumed system state(s). The benefit of such a procedure is that all of the heavy computational work is done offline. The resultant switching schemes are then fed into a real-time security assessment tool that functions like a lookup table. When the particular contingency occurs, a solution from the lookup table will be selected and tested for system feasibility based on the real-time system states. If a feasible solution is found, it is implemented; if a solution is not found, the operator can resort to traditional corrective means, such as generation re-dispatch. The schematic of the deterministic planning based topology control scheme is shown in Fig. 4.2.

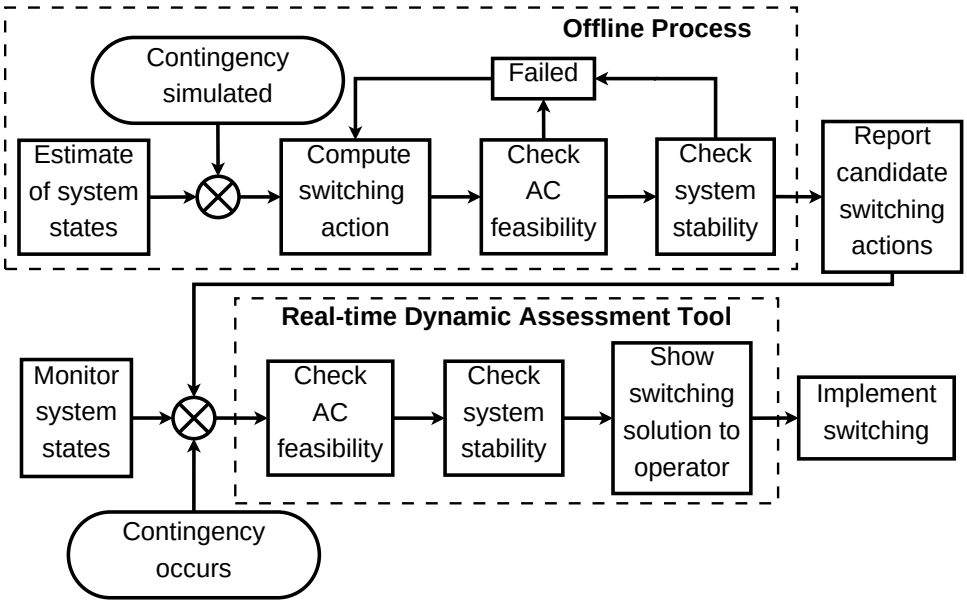

Figure 4.2: Deterministic planning based topology control scheme.

The benefit of a planning based corrective switching approach is that the real-time procedures are minimal, resulting in a fast implementation of the action. However, the drawback is that a deterministic planning based corrective switching procedure requires perfect foresight of the system states. With a small deviation from the estimated operating state, the switching action may cause a blackout instead of preventing a blackout. However, most corrective switching schemes implemented in practice are developed offline [27, 88, 89]. For instance, on Page 8 of [88] it states, "Open or close circuits ... when previously documented studies have demonstrated that such circuit openings reliably relieve the specific condition." As a result, corrective switching is primarily limited to unique situations where the proper corrective action is obvious or it is already a well-known action due to the operator's prior knowledge and experience. In the literature, there are few mathematical models available that can be used to determine corrective switching schemes with guaranteed solution feasibility for a range of operating states. In order to respond to this problem, robust corrective switching is proposed.

4.2.3 Robust Corrective Topology Control

This research proposes the robust corrective switching framework as a response to the limitations of real-time and deterministic planning based corrective switching. The proposed robust corrective switching methodology shown in Fig. 4.3 is a combination of real-time and planning based corrective switching methodologies. Due to robust optimization, the proposed robust corrective switching methodology is superior to deterministic policies with respect to solution reliability. The technology gap between real-time and deterministic planning based corrective switching scheme is reduced by doing most of the heavy computational work offline and the guarantee of solution feasibility for a range of operating states is achieved by developing an uncertainty set over estimated system states. The uncertainty set can be viewed as lower and upper bounds over the system parameters or a range of operating states. The topology control algorithm will find the candidate switching actions based on modeled system states (with uncertainty) and a simulated contingency.

The switching solutions generated by the topology control algorithm will then be tested for AC feasibility and system stability. The resultant switching solutions will be considered as candidate switching solutions for the corresponding contingencies and will be used in connection with a real-time corrective switching algorithm. When a particular contingency occurs, the on-line dynamic security assessment tool will test the proposed robust switching actions to determine the appropriate switching action to take. This process can also be combined with previously proposed real-time corrective switching heuristics since combining these procedures together will increase the likelihood of finding a feasible corrective action fast enough.

The primary feature of robust corrective switching is that the solution is guaranteed to be feasible over a wide range of operating states. The uncertainty set may consist of variable resources, such as generation uncertainty, wind/renewable generation uncertainty, demand uncertainty, and area interchange uncertainty. Furthermore, the topology control algorithm can be used to generate multiple switching solutions for a particular contingency. Note that the presented solution method is designed to determine one topology control solution at a time. However, by updating the solution method termination condition, the presented framework can be used to determine multiple topology control solutions. Providing multiple potential corrective switching solutions to the operator provides added flexibility. This characteristic of robust corrective switching is critical as not all of the solutions generated by the topology control algorithm may be AC feasible or pass the stability check. But due to multiple potential switching actions generated by the topology control algorithm, it is more likely that at least one of them will produce a feasible operating solution.

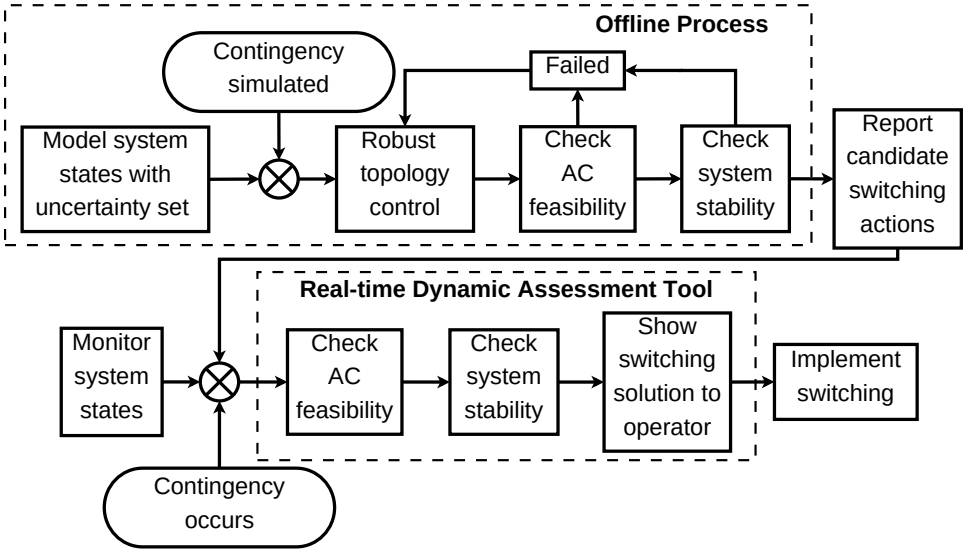

Figure 4.3: Robust corrective topology control scheme.

The timeline of the robust corrective switching scheme works as follows: after solving the day-ahead unit commitment problem, the robust corrective switching algorithm will determine the corrective switching schemes for possible contingencies. This can be seen as a form of contingency analysis, which has been modified to include robust corrective switching and it checks for a robust N-1 solution. These switching actions will be tested for AC feasibility and system stability. All of these calculations will be done offline. Once a particular contingency occurs, the real-time dynamic security assessment tool will evaluate the switching solution (if any) based on the real-

time system states. If any feasible solution is obtained, it will pass the possible switching actions to the operator. Next, the operator will decide whether to implement the switching solution. The benefit of the proposed procedure is that the robust corrective switching scheme obtained from this method does not rely on ad-hoc methods, which enables corrective switching to be more widespread in order to improve operations and reliability.

The robust corrective switching scheme in this research is based on a DCOPF framework and it guarantees the switching solution will be feasible for any operating state modeled by the uncertainty set. Since the optimal power flow (OPF) formulation is not an AC optimal power flow (ACOPF), the proposed solution must also pass an AC feasibility test. As a result, the guarantee that the solution is robust only holds for a DCOPF problem and is not guaranteed for the ACOPF problem. However, by developing a robust corrective switching formulation, we are able to improve the chances that the proposed switching action will, indeed, be feasible as compared to deterministic corrective switching DCOPF schemes. Typically, generation re-dispatch is required to obtain an AC feasible solution, which is one of the primary reasons why corrective switching schemes may be feasible for the DCOPF but are not AC feasible. However, the proposed robust corrective switching scheme is guaranteed to be feasible (for the DCOPF) for a wide range of operating conditions; this substantially increases the chances that the chosen topology solution will have an AC feasible solution since there are many DC solutions to start with. The proposed robust corrective switching procedure can be seen as a mathematical program that is equivalent to the practice used today by operators to identify candidate switching actions based on historical studies showing the action has worked under a variety of operating conditions. Note that the procedure presented in Fig. 4.3 is used to determine corrective topology control actions for a single contingency. For N different contingencies, the procedure described in Fig. 4.3 would be repeated N times.

In robust corrective topology control methodology, it is assumed that with today's technology, the real-time dynamic assessment tool is fast enough to evaluate the topology control action such that the topology control solution can be implemented in realistic timescale. However, with larger test systems, it is possible that the computational time required for topology control solution evaluation, for real-time application, may not be fast enough. To overcome this computational limitation modification to robust corrective topology control methodology, presented in Fig. 4.4, is proposed. In this proposed topology control solution evaluation process, after solving the off-line process, the candidate topology control solutions are made available to real-time applications. In real-time, the real-time dynamic assessment tool will assess the feasibility of topology control action by continuously simulating the contingency and its associated corrective topology control action with real-time system states. When particular contingency occurs, the topology control solution, evaluated in real-time dynamic assessment tool, is made available to operator for implementation. The benefit of this method is that the time required to implement corrective topology control solution is minimal. However, evaluating all possible N-1 contingencies with associated topology control solution, with real-time system states, might be computationally challenging; therefore, to minimize computational burden, only critical contingencies requiring topology control action might be evaluated with real-time system states. This proposed method is similar to the contingency analysis tool, used today in industry, which monitors the critical contingencies, in continuous bases, with real-time system states, to insure N-1 contingency compliance. However, it should be noted that such an approach would limit the capability of corrective topology control to mitigate contingencies, as not all the possible N-1 contingencies are considered for real-time topology control

solution evaluation. Another approach, to overcome computational limitation of real-time evaluation process, is to remove the topology control solution evaluation process with real-time system states. In this approach, the topology control solution will be determined and tested with off-line process and implemented, in real-time, without any evaluations. The success of such a approach heavily depends on accuracy of off-line studies, which can be limit the implementation of corrective topology control in power systems operation. Furthermore, in industry, today, most of the topology control actions are determined and tested in off-line process [94].

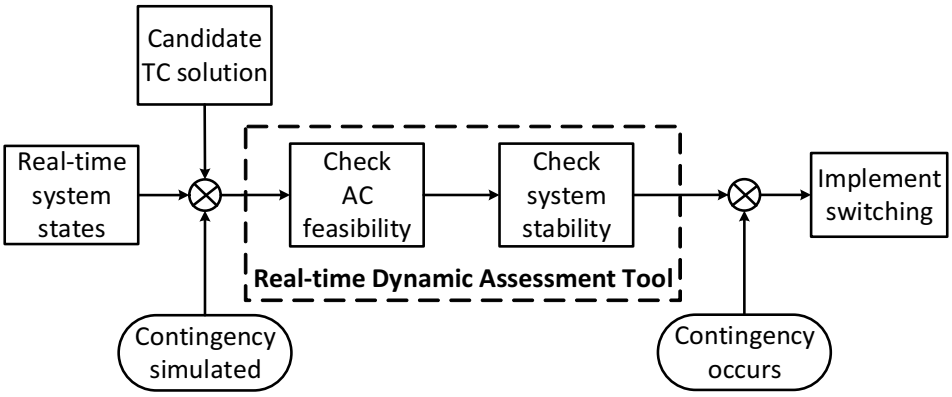

Figure 4.4: Modification to real-time dynamic assessment tool

4.3 Modeling of Demand Uncertainty

Uncertainty modeling is a key part of robust optimization. In [62] and [63], polyhedral uncertainty sets are used to define demand uncertainties; they assume that each load has an upper and lower bound and that the system-wide aggregate load has an upper bound. In this research, a simplified uncertainty model is used to represent demand uncertainty. The polyhedral uncertainty set used in this chapter is presented in (4.1); if desired, more complex polyhedral uncertainty sets can be used instead, as in [63].

$$\mathcal{D} = \{d \in \mathbb{R}^n : d_n^{fix} D_n^- \leq d_n \leq d_n^{fix} D_n^+, \ \forall n\} \tag{4.1}$$

In this uncertainty set, the system demand is bounded by its pre-determined lower and upper limits. The uncertainty description used in (4.1) is more conservative than the uncertainty sets used in [62] and [63]. The size of the uncertainty set is defined by the parameters D_n^+ and D_n^-. When D_n^+ and $D_n^- = 1$, the uncertainty is zero and $\mathcal{D}$ is a singleton, i.e., $d_n = d_n^{fix}$. When $D_n^- \leq 1$ and $D_n^+ \geq 1$, the uncertainty set is a polyhedron and its size is defined by the values of D_n^+ and D_n^-.

4.4 Deterministic Topology Control

Equations (4.2)-(4.6) represent the generic form of deterministic topology control, which includes a DCOPF corrective switching formulation. In this formulation, vector c and b are cost vectors. The parameters $A,\ B,\ E,\ F,,\ f,\ H,\ h$ and g represent the system data. The system demand in this case is the forecasted demand and it is denoted by vector $\bar{d}$; each entry in $\bar{d}$ represents the forecasted demand at each bus, d_n^{fix}. Deterministic corrective switching is a MIP problem. The variable x represents the binary variable associated with the switching action, where $x = 1$ if the line is closed/in service or $x = 0$ if the line is open/out of service. The continuous variable y

represents all of the OPF continuous variables, such as line currents, bus angles, and generator dispatch.

$$\min_{x,y} \quad c^T x + b^T y \tag{4.2}$$
$$\text{s.t.} \quad Fx \leq f, \tag{4.3}$$
$$Hy \leq h, \tag{4.4}$$
$$Ax + By \leq g, \tag{4.5}$$
$$Ey = \bar{d}, \tag{4.6}$$
$$x \in \{0, 1\}$$

4.5 Robust Corrective Topology Control Formulation

In the deterministic corrective transmission switching problem, the switching action is based on a single system state. However, in the robust topology control problem, the switching action is determined based on a range of operating states. The objective of robust topology control is to find a robust switching solution in response to a contingency while not allowing any load shedding for any realizable load within the uncertainty set. It should be noted that demand response can also be used as a control mechanism in response to a contingency; however, this option is not included in this research. Furthermore, in this report the topology control problem is modeled as a feasibility problem; hence, vectors c and b in (4.2) are equal to zero.

The generic form of robust topology control formulation is given in (4.7)-(4.11), which is a two part optimization problem. The first part of the problem is to find a transmission switching solution and the second part is to find the worst-case cost or worst-case realization of demand associated with the switching solution obtained in the previous stage. Robust optimization is seen as being more conservative than stochastic optimization since it minimizes the worst-case approach. While this is often seen as a drawback of robust optimization, this is exactly the motivation: to create a robust, reliable corrective switching methodology.

$$\min_{x \in \mathcal{X}} \quad \left(c^T x + \max_{d \in \mathcal{D}} b^T y(d) \right) \tag{4.7}$$
$$\text{s.t.} \quad Fx \leq f \tag{4.8}$$
$$Hy(d) \leq h, \tag{4.9}$$
$$Ax + By(d) \leq g, \tag{4.10}$$
$$Ey(d) = d, \tag{4.11}$$
$$x \in \{0, 1\}$$

When the system demand uncertainty is zero, the topology control model presented in (4.2)-(4.6) is the same as the model given in (4.7)-(4.11). In (4.11), the term $y(d)$ is used to emphasize the dependency of continuous variable y on the demand uncertainty, d. The second part of the robust formulation is further divided into two parts and results into a three-stage optimization problem as shown in (4.12). The objective of a three stage robust problem is to find a feasible topology under the worst-case demand. The first stage will determine the topology or switching action, whereas stages two and three will determine the feasibility of the switching action for the entire uncertainty set.

$$\min_{x\in\mathcal{X}} \quad \left(c^T x + \max_{d\in\mathcal{D}} \quad \min_{y\in\Omega(x,d)} b^T y\right) \tag{4.12}$$

$$\text{s.t. } Fx \leq f,\ x \in \{0,1\} \tag{4.13}$$

The set $\Omega(x,d)$ is a set of feasible solutions for a fixed topology and demand d, which is represented by $\Omega(x,d) = \{y : Hy \leq h,\ Ax + By \leq g,\ Ey = d\}$. In (4.12), the $\max_{d\in\mathcal{D}} \min_{y\in\Omega(x,d)} b^T y$ part of the problem determines the worst-case cost or demand associated with the switching solution (determined in the first stage) and can be combined together into one problem by taking the dual of $\min_{y\in\Omega(x,d)} b^T y$. The resultant problem is shown in (4.14)-(4.16).

$$\max_{d,\varphi,\lambda,\eta} \quad \lambda^T(Ax - g) - \varphi^T h + \eta^T d \tag{4.14}$$

$$\text{s.t.} \quad -\lambda^T B - \varphi^T H + \eta^T E = b^T, \tag{4.15}$$

$$d \in \mathcal{D},\ \lambda \geq 0, \varphi \geq 0, \eta\ free \tag{4.16}$$

$\varphi,\ \lambda$ and η are dual variables of constraints (4.4), (4.5), and (4.6) respectively. In (4.14), the term $\eta^T d$ is nonlinear. In [62], an outer approximation technique is used to solve this bilinear problem. In [62], the bilinear term, $\eta^T d$, is linearized using a first order Taylor series approximation as shown in (4.17), where $L(d,\eta)$ is a linearized approximation that is linearized across d_j and η_j. Furthermore, the resultant LP problem is solved by employing an iterative process between the outer approximation and the rest of the evaluation problem. The benefit of this method is that it is simple and the resultant optimization problem is a simplified LP. However, this method does not guarantee global optimality; therefore, the solution obtained from this outer approximation method only guarantees local optimality. Furthermore, this approach assumes that the problem is feasible, the corrective topology control problem is a feasibility problem and, thus, it requires a global solution. Therefore, the outer approximation technique is not suitable for the robust corrective switching problem. Hence, in this report, instead of using an outer approximation method, the bilinear term is defined by describing the extreme point of the uncertainty set.

$$L(d,\eta) = \eta_j^T d_j + (\eta - \eta_j)^T d_j + (d - d_j)^T \eta_j \tag{4.17}$$

Since the DCOPF problem is a convex problem, the new subproblem formulation presented by (4.14)-(4.16) can be reformulated into a MIP problem. By classifying all extreme points of the polyhedron representing the uncertainty set, we can guarantee a robust solution due to the convexity of the DCOPF problem, i.e., we can guarantee that all interior points are feasible if the robust solution is feasible for all extreme points of the polyhedron. This reformulation allows us to solve the nonlinear problem (4.14)-(4.16) by mixed integer programming while still being able to guarantee a global optimal solution. This reformulation procedure is also used in [63]. The MIP reformulation for the polyhedron representing the demand uncertainty is shown by (4.41)-(4.44).

The master problem is a MIP problem and represented by (4.18)-(4.19) and the subproblem is represented by (4.14)-(4.16).

$$\min_{x \in \mathcal{X}} \; c^T x \tag{4.18}$$

$$\text{s.t. } Fx \leq f, \; x \in \{0,1\} \tag{4.19}$$

The robust corrective switching formulation used in this chapter is presented in (4.21)-(4.33), with an objective presented by (4.20). The formulation includes generator limit constraints (4.21)-(4.22), generator contingency ramp up and ramp down constraints (4.23)-(4.24), line limit constraints (4.25)-(4.26), transmission switching constraints (4.27)-(4.28), the node balance constraint (4.29), and demand uncertainty (4.30)-(4.31). The maximum number of line switchings per solution are limited by parameter M in (4.32). In this research, only one corrective line switching solution is considered to be implemented in the post-contingency state.

$$\min_{Z_K \in \mathcal{X}} \left(0 \; + \; \max_{d \in \mathcal{D}} \; \min_{P_g, P_k, \theta_n \in \Omega(Z_k, d)} 0 \right) \tag{4.20}$$

$$\text{s.t.} - P_g \geq -P_g^{max} u_g, \; \forall g \tag{4.21}$$

$$P_g \geq P_g^{min} u_g, \; \forall g \tag{4.22}$$

$$-P_g \geq (-R_g^{+c} - P_g^{uc}), \; \forall g \tag{4.23}$$

$$P_g \geq (-R_g^{-c} + P_g^{uc}), \; \forall g \tag{4.24}$$

$$-P_k \geq -P_k^{max} Z_k N1_k, \; \forall k \tag{4.25}$$

$$P_k \geq -P_k^{max} Z_k N1_k, \; \forall k \tag{4.26}$$

$$P_k - B_k(\theta_n - \theta_m) + (1 - Z_k N1_k) M_k \geq 0, \; \forall k \tag{4.27}$$

$$P_k - B_k(\theta_n - \theta_m) - (1 - Z_k N1_k) M_k \leq 0, \; \forall k \tag{4.28}$$

$$\sum_{\delta(n)^+} P_k - \sum_{\delta(n)^-} P_k + \sum_{\forall g(n)} P_g = d_n, \forall n \tag{4.29}$$

$$d_n \leq d_n^{fix} D_n^+, \; \forall n \tag{4.30}$$

$$d_n \geq d_n^{fix} D_n^-, \; \forall n \tag{4.31}$$

$$\sum_{\forall k} (1 - Z_k) \leq M \tag{4.32}$$

$$Z_k \in \{0,1\}, \; P_g, \; P_k, \; \theta_n \;\; free \tag{4.33}$$

The complete robust corrective switching problem is split into two parts: a master problem, and a subproblem. The master problem is $\min_{Z_K \in \mathcal{X}} 0$ with constraints represented by (4.32)-(4.33), which determine the topology. The subproblem is a two part optimization problem, which determines the worst-case demand for a particular topology. The first part of the subproblem is represented by an objective $\max_{d \in \mathcal{D}}$ with constraints (4.30)-(4.31), which determines the worst-case system demand within the uncertainty set. The second part of the subproblem is represented by the objective $\min_{P_g, P_k, \theta_n \in \Omega(Z_k, d)} 0$ with constraints (4.21)-(4.29). This second part of the subproblem is a DCOPF formulation that evaluates the feasibility of the system demand, which is selected in the first part of the subproblem.

The objective of the third stage's dual is given in (4.34), where $\alpha_g^+, \alpha_g^-, \Omega_g^+, \Omega_g^-, F_k^+, F_k^-, S_k^+, S_k^-, L_n$ are dual variables associated with constraints (4.21)-(4.29) respectively. When the second stage and the third stage of the subproblem are combined together, the term $d_n L_n$ in (4.34) makes the objective nonlinear. The nonlinearity of the dual objective is removed by restructuring the nonlinear problem into a MIP problem. The resultant subproblem is given in (4.35)-(4.44), where the dual formulation of the third stage subproblem is combined with the demand uncertainty.

$$\begin{aligned}\max \; & -\sum_{\forall g} P_g^{max} u_g \alpha_g^+ + \sum_{\forall g} P_g^{min} u_g \alpha_g^- \\ & + \sum_{\forall g} (-R_g^{+c} - P_g^{uc})\Omega_g^+ + \sum_{\forall g} (-R_g^{-c} + P_g^{uc})\Omega_g^- \\ & - \sum_{\forall k} P_k^{max} Z_k N1_k (F_k^+ + F_k^-) + \sum_{\forall n} d_n L_n \\ & - \sum_{\forall k} (1 - Z_k N1_k) M_k (S_k^+ + S_k^-)\end{aligned} \tag{4.34}$$

A big-M formulation is used to represent the extreme points of the polyhedron representing the uncertainty set. The drawback of such an approach is that it causes a poor relaxation. To overcome this problem, CPLEX's indicator constraint modeling approach is used to model (4.41)-(4.44).

$$\begin{aligned}\max \; & -\sum_{\forall g} P_g^{max} u_g \alpha_g^+ + \sum_{\forall g} P_g^{min} u_g \alpha_g^- && (4.35)\\ & + \sum_{\forall g} (-R_g^{+c} - P_g^{uc})\Omega_g^+ + \sum_{\forall g} (-R_g^{-c} + P_g^{uc})\Omega_g^- \\ & - \sum_{\forall k} P_k^{max} Z_k N1_k (F_k^+ + F_k^-) + \sum_{\forall n} \eta_n \\ & - \sum_{\forall k} (1 - Z_k N1_k) M_k (S_k^+ + S_k^-) \\ \text{s.t.} \; & -\alpha_g^+ + \alpha_g^- - \Omega_g^+ + \Omega_g^- + L_n = 0, \; \forall g && (4.36)\\ & -F_k^+ + F_k^- + S_k^+ - S_k^- + L_n - L_m = 0, \; \forall k && (4.37)\\ & -\sum_{\delta(n)^+} B_k S_k^+ + \sum_{\delta(n)^-} B_k S_k^+ + \sum_{\delta(n)^+} B_k S_k^- - \sum_{\delta(n)^-} B_k S_k^- = 0, \; \forall n && (4.38)\\ & \alpha_g^+, \alpha_g^-, \Omega_g^+, \Omega_g^- \geq 0, \; \forall g && (4.39)\\ & F_k^+, F_k^-, S_k^+, S_k^- \geq 0, \; \forall k && (4.40)\\ & \eta_n - L_n d_n^{fix} D_n^+ + (1 - D_n) M_n \geq 0, \; \forall n && (4.41)\\ & \eta_n - L_n d_n^{fix} D_n^+ - (1 - D_n) M_n \leq 0, \; \forall n && (4.42)\\ & \eta_n - L_n d_n^{fix} D_n^- + D_n M_n \geq 0, \; \forall n && (4.43)\\ & \eta_n - L_n d_n^{fix} D_n^- - D_n M_n \leq 0, \; \forall n && (4.44)\\ & D_n \in \{0, 1\}\end{aligned}$$

4.6 Solution Method for Robust Corrective Topology Control

The robust topology control problem is a three-stage problem with a master problem and two subproblems. However, it is reformulated into a two-stage problem with a master problem and a subproblem. The solution method proposed in this research is an iterative process between the master problem and the subproblem. The master problem is a MIP, which determines the system topology. The subproblem is a nonlinear problem, which is converted into a MIP and it searches for the worst-case demand for the particular topology. For the proposed solution method, it is assumed that the unit commitment problem is solved prior to solving the robust corrective switching problem.

4.6.1 Initialization

The unit commitment problem is first solved with the fixed, initial topology. The solution of this unit commitment problem, the unit commitment status, the generators' scheduled dispatch, and the acquired reserves, are fed into the robust topology control framework. The first step of solution method is to solve the dual problem given by (4.45), where $\overline{Z}_k$ represents the initial topology. The model presented in (4.45) is the dual of the DCOPF problem. The dual variables of constraints (4.36)-(4.38) are P_g, P_k, θ_n respectively. If the problem is infeasible, then the proposed unit commitment solution is not N-1 reliable and a cut must be added to the master problem in the form of (4.47). The proposed approach will then search for a robust corrective switching action that enables the solution to be N-1 compliant, if such a solution exists.

$$\begin{aligned}\max \; & -\sum_{\forall g} P_g^{max} u_g \alpha_g^+ + \sum_{\forall g} P_g^{min} u_g \alpha_g^- \\ & + \sum_{\forall g}(-R_g^{+c} - P_g^{uc})\Omega_g^+ + \sum_{\forall g}(-R_g^{-c} + P_g^{uc})\Omega_g^- \\ & - \sum_{\forall k} P_k^{max} \overline{Z}_k N1_k (F_k^+ + F_k^-) + \sum_{\forall n} d_n L_n \\ & - \sum_{\forall k}(1 - \overline{Z}_k N1_k) M_k (S_k^+ + S_k^-) \\ \text{s.t. } & (4.36) - (4.40)\end{aligned} \tag{4.45}$$

4.6.2 Master Problem: Topology Selection

The master problem is a MIP problem and its objective is to determine the system topology. The master problem contains a topology selection formulation and combinatorial cuts. The master problem is represented by (4.46)-(4.48). For iteration $j \geq 1$,

$$\min \; 0 \tag{4.46}$$

$$\text{s.t. } 1 \leq \sum_{\overline{Z}_{k,l}=0} Z_k + \sum_{\overline{Z}_{k,l}=1} (1 - Z_k), \; \forall l \leq j \tag{4.47}$$

$$\sum_{\forall k}(1 - Z_k) \leq M \tag{4.48}$$

$$Z_k \in \{0, 1\}$$

At each iteration, the master problem finds a feasible solution and then passes Z_k to the subproblem as an input parameter. The solution Z_k will be evaluated for the worst-case scenario in the subproblem. If the master problem is infeasible, this states that all of the possible topologies are infeasible and there is no feasible switching action for the defined uncertainty set, as shown in stage 1 of Fig 4.5.

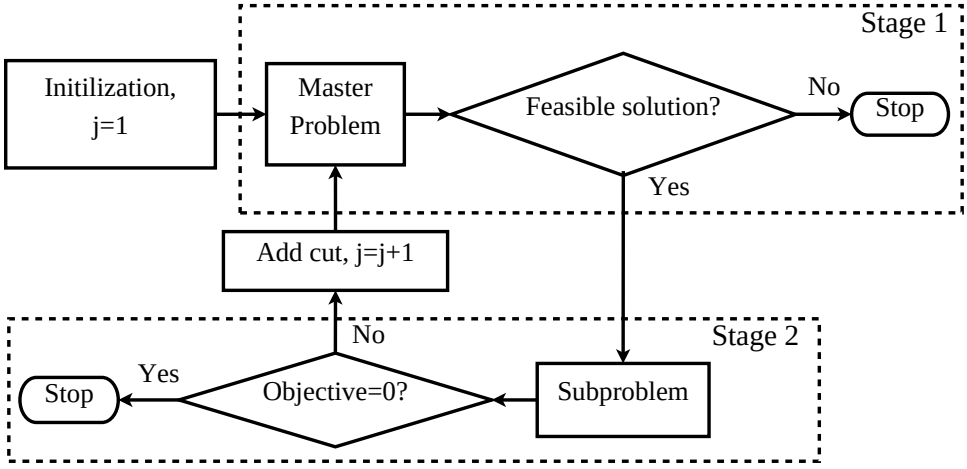

Figure 4.5: Flowchart for robust corrective topology control.

4.6.3 Subproblem: Worst-case Evaluation

The objective of the subproblem is to determine the worst-case demand associated with the topology (determined in the master problem). The subproblem is a MIP and presented in (4.35)-(4.44). If the subproblem is feasible and the objective is equal to zero, then it proves that, for a given topology, there is no system demand within the uncertainty set that will produce an infeasible OPF solution. In other words, the corresponding topology is feasible for the entire uncertainty set; hence, a robust solution is obtained. On the other hand, if the subproblem's objective is non-zero, then the corresponding topology is infeasible for a particular demand within the uncertainty set. Hence, that topology is discarded and a feasibility and/or combinatorial cut is applied to the master problem in form of (4.47). Equation (4.47) is known as a combinatorial cut, which prevents the master problem from choosing any prior binary Z_k solution that is known to be infeasible. The master problem is solved again and the process continues till the robust solution is found or all possible topologies are confirmed to be infeasible. The solution method for the robust topology control problem is summarized in Fig. 4.5.

4.7 Results

The computational study for robust corrective switching is performed on the IEEE 118-bus test case. The test case consists of 54 generators, 118 buses, and 186 transmission lines. The IEEE 118-bus test case given in [95] does not have generator information. Therefore, generator information from the Reliability Test System-1996 [95] is used. The fuel costs given in [22] are used to calculate generator operating costs. The basic unit commitment model presented in [13] is adopted. A 24-hour unit commitment problem is solved. The reserve requirement for the unit commitment problem is the sum of 5% of demand supplied by hydro generators and 7% of demand supplied by non-hydro units or the single largest contingency, whichever is greater. It is assumed that at least

50% of total required reserves will be supplied by spinning reserves and the rest will be supplied by non-spinning reserves. This assumption is in line with CAISO's guidelines for spinning reserve and non-spinning reserve [96]. The hour 16 solution of the unit commitment problem is used for deterministic as well as robust corrective switching analysis. The IEEE 118-bus test case in [95] does not have emergency transmission rating. Therefore, it is assumed that the emergency thermal rating for the transmission elements is 125% of the steady state operating limits.

4.7.1 Deterministic Corrective Switching

In the deterministic corrective switching analysis, the demand uncertainty is assumed to be zero. The switching action is determined with the static demand levels used in the unit commitment problem. It is observed that 10 transmission contingencies (out of 186) can only be alleviated if transmission switching is combined with generation re-dispatch, i.e., generation re-dispatch on its own cannot satisfy these 10 transmission contingencies. The generation re-dispatch allows each unit to change within 10 minutes of its ramping capability. This result is important because, traditionally, such contingencies are mitigated by expensive generation re-dispatch. Moreover, these 10 transmission contingencies have multiple corrective switching actions. The ability of the corrective switching algorithm to generate multiple solutions for a single contingency is critical from a system operations point of view. The corrective switching formulation is based on a DC framework. Therefore, the solution needs to be tested for AC feasibility and system stability requirements. Hence, the probability of having at least one AC feasible and stable corrective switching solution is higher if the corrective switching algorithm generates multiple corrective solutions.

It is also observed that the solution for corrective transmission switching will not always be 'to open the congested line', but frequently it will be 'to open a lightly loaded line'. This demonstrates that the commonly held assumption that congested lines are the top candidate lines for switching is not always correct. Furthermore, such examples demonstrate the need for systematic tools for topology control.

4.7.2 Robust Corrective Switching Analysis

For robust corrective switching analysis, $\pm 14.3\%$, i.e., $\pm 324.5MW$, demand uncertainty is assumed. For computational simplicity, the demand uncertainty is assumed only on 50% of the system MW demand involving roughly half of the load buses. It is also assumed that all of the system reserves are available within 10 minutes and the generators are allowed to change their outputs within each generators' 10 minutes ramp rate. Of the 186 transmission contingencies, 159 can be alleviated by dispatching reserves alone. While corrective switching is not required for these 159 contingencies, topology control can still be useful in response to these contingencies because it can reduce the need for a costly system re-dispatch; furthermore, the topology control algorithm provides multiple feasible switching solutions for these 159 transmission contingencies. The 7 transmission contingencies listed in Table 4.1 require corrective transmission switching actions in order to avoid load shedding, i.e., generation re-dispatch alone was not sufficient to respond to the contingencies. Note that these robust corrective switching solutions involve both corrective switching and generation re-dispatch.

The first column of Table 4.1 represents the transmission contingency and the second column represents the corresponding corrective switching actions. All 7 of these transmission switching contingencies can only be alleviated if corrective transmission switching is employed. For instance, a contingency on line 111 can only be mitigated by switching line 108 or 109 combined with

generation re-dispatch. No feasible solution is available with generation re-dispatch alone due to network congestion. The switching solutions for the other 6 transmission contingencies are documented in Table 4.1.

Table 4.1: Robust corrective switching solution with demand uncertainty.

Line Contingency	**Switching Solution(s)**	**Number of Deterministic Solutions**
63	64	3
111	108, 109	163
115	33, 34, 35, 38, 51, 78, 86, 112, 121, 132, 141	165
116	141	151
120	132	162
148	137, 138, 139, 140, 141, 143, 153, 157, 158, 159, 160, 161, 162, 163, 165, 166, 167, 168, 169, 173	163
154	139, 140, 153, 155, 157, 158, 159, 160, 161, 163,165, 167, 169, 173	166

The contingencies of line $111,\ 115,\ 148,$ and 154 have multiple robust corrective switching actions. Table 4.1 shows that there can be multiple switching solutions for a single contingency. Similarly, one switching action may alleviate multiple contingencies. For instance, the robust switching solution to open line 141 mitigated 3 transmission contingencies. This result shows the potential of robust corrective switching to generate multiple candidate switching solutions for a real-time dynamic security assessment tool to evaluate switching actions for real-time operations.

In the last column of Table 4.1, the number of deterministic corrective switching solutions, for a particular contingency, is presented. It shows that the number of possible deterministic corrective switching solutions is much more as compared to the number of robust solutions. However, the robust solutions guarantee solution feasibility over a wide range of operating states whereas the deterministic solutions do not guarantee solution feasibility if there is any change in the operating state. Therefore, the possibility of having a successful corrective action with the deterministic corrective switching solutions is far less than the potential success rates for the robust corrective switching solutions.

For a contingency on line 63, with the initial topology no feasible solution is obtained with a fixed demand. Hence, the unit commitment solution is not N-1 compliant. However, with the robust corrective switching framework, an N-1 feasible solution exists; furthermore, the robust corrective switching framework is able to produce an N-1 feasible solution that is robust against the demand uncertainty. This result is extremely important and powerful as we have proven that topology control can take a solution that is N-1 infeasible for a deterministic fixed demand and make it N-1 feasible even with a high level of demand uncertainty. Indeed, the assumption that transmission switching must degrade system reliability is false. Furthermore, in prior research, topology control has shown considerable operational benefits and cost savings [13]. The detail analysis for cost savings, obtained from robust corrective topology control methodology, is presented in Chapter 5.

The computational time for $\pm 14.3\%$ uncertainty set is about 10 minutes per contingency with a 2.93 GHz, Intel i-7 processor with 8 GB RAM. It is also observed that the computational time

increases with small increases in the uncertainty set. For instance, a 1% decrease in uncertainty causes a 13% drop in computational time.

4.8 Conclusion

In this chapter, three different corrective switching methodologies are presented: real-time, deterministic planning based, and robust corrective switching. Real-time corrective switching is very difficult to implement with today's technology due to a lack of computational power and the practical barriers of needing to ensure AC feasibility, voltage stability, and transient stability. Deterministic planning based corrective switching can be solved offline, but such an approach relies on predicting the operating state. Furthermore, the deterministic planning based methods cannot guarantee solution feasibility over a wide range of system states. The proposed method of robust corrective switching fills the technology gap between the real-time and the deterministic planning based corrective switching methodologies. The offline mechanism of robust corrective switching generates multiple solutions and can be implemented in real-time with the help of a real-time dynamic security assessment tool. As a result, the proposed robust corrective switching model provides a mathematical decision support tool that integrates topology control into every day operations by being able to guarantee robust solutions.

While deterministic corrective switching frameworks may suggest many potential switching solutions, the empirical results presented in this research show that many of these solutions will be infeasible for minor changes in the operating state. In contrast, the robust corrective switching scheme presented in this chapter guarantees solution feasibility for a wide range of system states, given a DCOPF formulation. In addition, the robust corrective switching formulation demonstrates the ability of generating multiple corrective switching actions for a particular contingency. Moreover, a single resulting corrective switching solution is capable of mitigating multiple contingencies.

Day-ahead unit commitment problems with proxy reserve requirements do not guarantee N-1 feasibility. Contingency analysis is used to determine whether there are contingencies that cannot be satisfied by the unit commitment solution. When this happens, unit commitment must be resolved or the operator will employ out-of-market corrections to obtain a feasible N-1 solution. The results have shown that robust corrective topology control can be used to reduce the occurrence of contingencies that are not satisfied by the re-dispatch capabilities of the unit commitment solution alone. Furthermore, the numerical results prove that topology control does not necessarily degrade system reliability; on the contrary, it can help the system to achieve N-1 feasibility even with uncertainty.

While transmission switching exists today, it is used to a limited extent; historical information or the operators' prior knowledge are the primary mechanisms to establish and implement corrective switching as opposed to using a mathematical framework to identify corrective switching actions. The electric grid is one of the most complex engineered systems to date. Relying on only prior observations to determine potential corrective switching actions limits our capability to harness the existing flexibility in the transmission network. Systematic procedures that are capable of capturing such complexities should be preferred over such limited methods. Furthermore, the hardware requirements to implement topology control (circuit breakers) already exist, leaving only the need to develop the appropriate decision support tools, which are low in cost, to obtain such benefits.

5. Renewable Integration with Robust Topology Control: Do-not-exceed Limits

5.1 Introduction

In recent years, the penetration of renewable resources in electrical power systems has increased. These renewable resources add more complexities to power system operations, due to their intermittent nature. As a result, operators must acquire additional reserves in order to maintain reliability. However, one persistent challenge is determining the optimal location of reserves and this challenge is exacerbated by the inability to predict key transmission bottlenecks due to this added uncertainty. This research presents robust corrective topology control as a congestion management tool to manage power flows and the associated renewable uncertainty. The proposed day-ahead method determines the maximum uncertainty in renewable resources in terms of do-not-exceed limits combined with corrective topology control. The day-ahead topology control formulation is based on the direct current optimal power flow; therefore, switching solutions obtained from these algorithms need to be tested for AC feasibility and system stability. All numerical results provided are based on the IEEE-118 bus test case with two different load profiles and wind forecasts.

As the penetration of stochastic resources (e.g., variable wind and solar power) increase, the challenge to maintain a continuous supply of electrical energy, at minimal cost, will increase in difficulty due to the increase in amount of semi-dispatchable and non-dispatchable resources. Traditionally, economic dispatch models, used in system operation, are deterministic and do not optimize system resources while explicitly accounting for the uncertain resources. In order to reduce operational costs, while maintaining reliability, uncertainty modeling plays an important role in the decision making process; by ignoring uncertainty, the operational decision can be suboptimal or even infeasible.

In general, most optimal dispatch models assign to conventional fossil-fuel power plants a fixed dispatch, i.e., a fixed operating point. While it is known that the plant is unlikely to stay at this fixed operating point over a long time period due to the changes in load and other resources, the assumption is adequate for the various optimal scheduling problems used at various time intervals (e.g., day-ahead, hour-ahead). However, it is problematic to make this assumption for semi-dispatchable renewable resources due to their inherent intermittent nature. Therefore, grid operators may instruct renewable power producers to stay within a desired dispatch range as opposed assuming, within their optimization problems, that these uncertain resources will be at a fixed operating point. Within the Independent System Operator of New England (ISONE), this dispatch range is known as a do-not-exceed (DNE) limit for intermittent renewable power producers. The DNE limit defines a continuous set of potential dispatch solutions for the renewable resource and the bounds of the DNE limit are meant to be set such that if the renewable resource stays within the specified DNE limits (i.e., the upper and lower bound), then the system will remain in a secure and reliable operating state. Such DNE limits are determined by constructing a robust optimization problem; the DNE limits are represented by an uncertainty set, which states that the uncertain resource can operate at any value within this continuous feasible set. Furthermore, the operator could also determine the maximum bounds for this uncertainty set by which the system can still absorb the variable production of the renewable resource without sacrificing system reliability.

The DNE limits will have both upper and lower bounds. Most of the time, a drop in renewable production is more critical than an increase in renewable production. However, there have

been situations where an oversupply of renewable resources can be detrimental to system operations and reliability as well. If the system operator is expecting a potential surge in renewable production, then the operator may dispatch additional units only to reduce their output in the approaching periods. Another way to handle this situation would be to allow for wind spillage. If wind spillage is possible, then over-generation is generally less of a concern than under-generation. The sudden decrease in renewable generation can cause serious operational issues and may require extreme corrective actions to avoid cascading failures or even blackout [97, 98]. Therefore, the results presented in this research are focused on determining lower bounds on renewable generation. However, the robust methodology, presented in this research, can be used to determine lower as well as upper bounds on intermittent resources.

Today, most corrective topology control actions are based on operators' prior knowledge. In [23, 99], a detailed review of current industrial practices for topology control actions are presented. Topology control has also been proposed to mitigate many power system related issues, such as voltage violations, line overloads [1–4], line losses and cost reduction [5–7], system security [8], or a combination of these [9, 10]. Topology control has also shown significant improvement in operational flexibility [99] and cost saving [13, 19, 20, 22, 23, 85].

Stochastic programming has been one common approach to model uncertainties. It typically assumes probability distributions for uncertain parameters or incorporates a large number of scenarios, which leads to computationally challenging optimization problems. The primary barrier to stochastic programming is the tradeoff between the computational challenge and the quality of the solution; to get a more accurate solution, it would be preferable to represent additional uncertainties but then this increases the model complexity, which makes it more difficult to obtain a quality solution.

Robust optimization has shown promising results in recent years to address issued associated with modeling uncertainty and decision making under uncertainty. In [62], a two-stage robust optimization technique is used to solve the unit commitment problem. Robust optimization deals with the data uncertainty and tries to find an optimal solution considering the worst-case uncertainty realization. The solution of the robust optimization problem is guaranteed to be optimal for a defined uncertainty set [78, 79, 99]. Since the optimal solution is a hedge against the worst-case realization, the solution is often conservative and probably expensive. For the application of power system reliability, such a robust policy is preferred due to the enormous costs of a potential blackout.

Topology control algorithms, presented in literature, are either based on ACOPF or DCOPF [10, 85, 99]. However, in an optimization framework, there is no systematic way to insure system stability with topology control. In prior literature, topology control actions combined with stability constraints are proposed [100, 101], but these methodologies were never tested on realistic test cases. Therefore, the solution obtained from topology control algorithms must be tested to insure that the topology control action will not cause cascading events or even a blackout. In [102], different stability studies are recommended for power system operation; they are classified based on nature and type of disturbance, and time span under consideration. Typically, stability studies are classified into three different categories- rotor angle stability, frequency stability, and voltage stability. In this research, all three stability studies are considered to study the effect of topology control action on system stability/reliability. The main contributions of this chapter are listed as follows:

1. A mathematical framework to determine do-not-exceed limits for renewable power producers is presented, which is similar to [103]. This mathematical framework utilizes robust optimization and a search algorithm is used to determine the lower bounds.

2. A robust corrective topology control program is used to determine single transmission switching actions in response to the renewable intermittency. The corrective transmission topology control actions essentially improve the deliverability of reserves by changing the network topology in order to reroute power flows on available branches.

3. A multi-stage (day-ahead and real-time) framework is proposed. At the day-ahead operational planning stage, DNE limits are determined for the system with and without topology control. The DNE limits with topology control provide the system operator more flexibility to manage the uncertain resources and the DNE limits without topology control can be used to define the trigger as to when it is necessary to implement the corrective topology control action in order to maintain transmission network limits. These day-ahead decisions are then passed to real-time tools that evaluate the proposed actions at the earlier time-stage to determine if they are still valid and, if not, propose updated corrective actions and DNE limits. This multi-stage approach is used to manage some of the computational complexities by taking part of the process to the day-ahead time stage and then to reconfirm the accuracy of the day-ahead time stage in real-time where fast computations are required.

4. A validation process is taken to ensure that the robust corrective topology control actions are AC feasible since the robust optimization framework is based on a linear approximation of the AC optimal power flow.

5. The topology control solutions, presented in this research, are studied for its effect on system stability. Different stability studies are carried out and the effects of the topology control actions on system stability are presented.

The rest of the chapter is structured as follows: The robust corrective topology control methodology to determine DNE limits is described in Section 5.2. The renewable generation uncertainty set modeling, used in this research, is presented in Section 5.3. The solution method for the nodal robust topology control (RTC) algorithm, to determine DNE limits, is presented in Section 5.4. The associated simulation results for the DNE limit algorithm are presented in Section 5.5. The analysis of robust topology control actions on system reliability, considering wind uncertainty, is presented in Section 5.6; results are also presented regarding a robust N-1 contingency analysis and AC feasibility. In Section 5.7, results related to stability studies associated with topology control actions are presented. Section 5.8 provides the conclusions.

5.2 Do-not-exceed Limits: Robust Corrective Topology Control Methodology

In a day-ahead unit commitment problem, conventional generators are dispatched at a fixed level, known as desired dispatch point (DDP); due to the intermittency in renewable resources, these resources are dispatched to a range of operating levels, known as a desired dispatch range or a do-not-exceed limit [103]. The DNE limits can also be viewed as the renewable resources' maximum

output range that the system can accommodate without sacrificing system reliability. These limits can be viewed as a maximum lower and upper bound on renewable generation.

ISONE has proposed to determine the DNE limits for wind resources in real-time and the proposed approach assumes that regulation reserve is used to compensate for the intermittency issues associated with the renewable resources [103]. In [103], a zonal approximation of the actual system is used as opposed to using the full network model with all high-voltage buses and transmission elements. For complex generation scheduling problems, such as security-constrained unit commitment (SCUC) or security-constrained optimal power flow, such approximations, for optimal power flow, are common. Due to the complexities of robust optimization, a zonal model is proposed by ISONE, which greatly reduces the complexity of the problem. The computational complexity of robust optimization for the DCOPF problem grows quickly when there are many individual uncertain variables; when using a nodal model, the uncertain variables will be the power injections at the various nodes (buses) where the wind farms are located. With a zonal approach, there is one uncertain variable for all of the renewable resources within that zone. Such an approach reduces the computational complexity but it also reduces the accuracy of the solution. Furthermore, incorporating more transmission lines and buses will further complicate the robust optimization framework.

This research proposed a modification to the DNE limit algorithm by incorporating corrective topology control into the algorithm to determine DNE limits and also extends the work of [99]. As shown by Fig. 5.1, the concept of corrective topology control is embedded within contingency analysis, as in [99], and this research proposes a new stage that will determine the DNE limits for uncertain resources at the day-ahead time stage. After solving the day-ahead SCUC problem, the market solution is checked to see if it is N-1 reliable; this chapter presents results pertaining to a robust N-1 contingency analysis study that incorporates corrective topology control where net injections are uncertain (load, renewables).

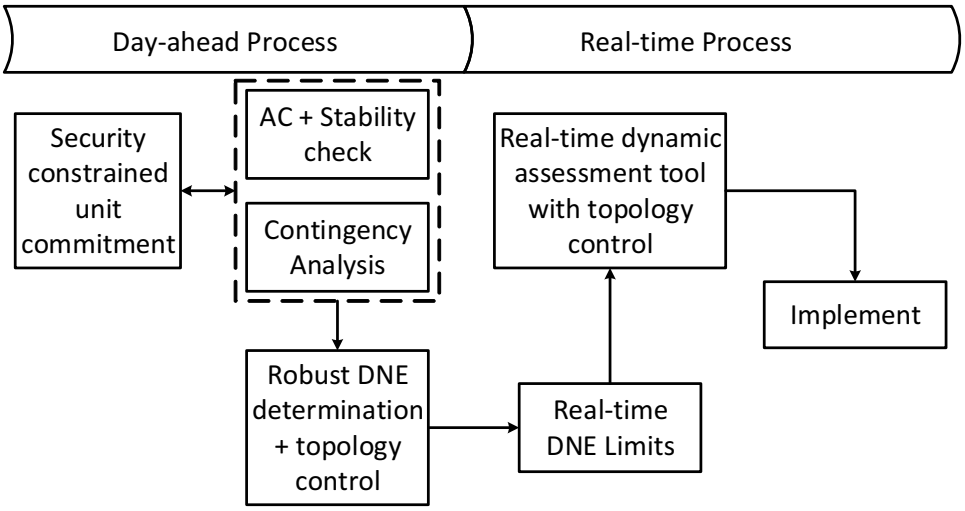

Figure 5.1: Process to determine do-not-exceed limits.

Once a robust N-1 solution is determined, the algorithm then solves for the DNE limits for the renewable power producers. The day-ahead robust DNE limits are determined by using a nodal

representation of the optimal power flow. The proposed algorithm will also determine the DNE limits with and without corrective topology control for the specified SCUC solution. The difference in these DNE limits identifies the situations when reserves are available in the system but they are not deliverable due to congestion. The differences in the DNE limits also identify the necessary triggers as to when to implement the corrective topology control action. When the expected uncertainty in renewable resources is more than the determined DNE limits, the operator can rerun the SCUC model to commit additional units in order to hedge against the resource uncertainty. Note that this DNE limit tool relies on a DC approximate power flow and, thus, it does not guarantee a robust AC power flow solution but it substantially improves the reliability of the day-ahead schedule by accounting for renewable uncertainty. This day-ahead tool will provide information for real-time operations, such as available ramping product and the proposed topology control actions. At present, there is no such systematic tool available to system operators to integrate renewable resources.

The final day-ahead schedule, which includes the DNE limits, the topology control actions, and the associated ramping product, is then passed to a real-time DNE limit tool, e.g., similar to what is proposed by ISONE [103]. The real-time DNE limit tool will compare and contrast the proposed schedule and actions against the operating state; since this tool needs to be fast, a zonal model is preferred. If the day-ahead protocols are not feasible, a new DNE limit will be determined based on the updated forecasts and the existing operating state. The final DNE limits and corresponding corrective actions are passed to a security assessment tool as well as to the renewable power producers. The real-time security assessment tool will pass to the operator potential corrective actions if a sizeable renewable deviation or contingency were to occur; such corrective actions may include activating reserves, as well as newly determined corrective topology control actions in case the previously proposed corrective actions are not sufficient, [18].

For this research, the focus is on the two boxes at the day-ahead time stage in Fig. 5.1 involving topology control: (a) robust contingency analysis with topology control and (b) robust nodal DNE limits with topology control. Further information regarding robust contingency analysis with topology control (TC) can be found in [99]. Fig. 5.2 provides additional information regarding the robust nodal DNE limits with topology control. The resulting SCUC solution and the renewable forecasts are fed into the first stage of the overall procedure. Robust optimization is used, with a DCOPF framework, to determine the DNE limits on a nodal basis for the renewable power producers. DNE limits with and without topology control will be determined. The proposed solution should be tested to ensure it is AC feasible and that the switching action does not cause any stability issues; for this work, we are only testing for AC feasibility. If the solution is not AC feasible, then a different topology control action will be determined. When there is no valid topology control action, either SCUC would be re-solved or the DNE limits would be determined without including topology control.

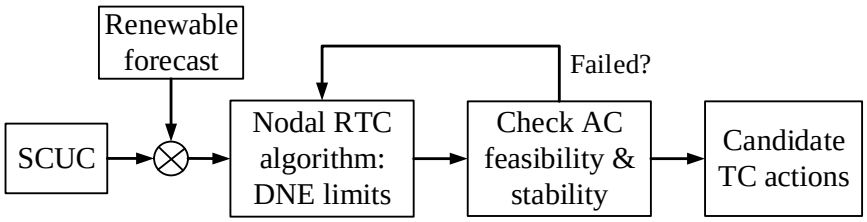

Figure 5.2: Robust do-not-exceed limits with topology control actions.

5.3 Uncertainty Modeling

Polyhedral uncertainty sets are used to capture the intermittency of renewable resources, as shown in (5.1); which can be divided to two parts, W_{low} and W_{high}, as shown in (5.2) and (5.3). The renewable resources (in this case, wind generation) are assumed to vary within these pre-determined lower and upper limits and the size of uncertainty set depends on the parameters D_w^- and D_w^+. Note that, in the process of determining DNE limits,D_w^- and D_w^+ are variables and determined outside of the robust framework as described in Section 4.6.

Furthermore, this uncertainty set definition is simple and more conservative than the uncertainty definition used in [62, 63, 78, 79]. The solution method presented here are independent of the assumed uncertainty definition; therefore, the presented technique can be easily modified for other uncertainty sets as shown in [62, 63, 78, 79].

$$W = \{P \in \mathbb{R}^w : P_w^{fix} D_w^- \leq P_w \leq P_w^{fix} D_w^+, \ \forall w\} \tag{5.1}$$

$$W_{low} = \{P \in \mathbb{R}^w : P_w^{fix} D_w^- \leq P_w \leq P_w^{fix}, \ \forall w\} \tag{5.2}$$

$$W_{high} = \{P \in \mathbb{R}^w : P_w^{fix} \leq P_w \leq P_w^{fix} D_w^+, \ \forall w\} \tag{5.3}$$

5.4 Solution Method: Nodal RTC Algorithm for DNE Limits

The robust topology control algorithm is a three-stage optimization problem: one master problem and two sub-problems [99], with an objective to find the optimal solution considering the worst-case scenario within the uncertainty set. However, it can be reformulated into a two-stage problem, as shown in (5.4) and (5.5), with a single master problem and a single sub-problem [99]. Note that, in classical robust optimization problem, as shown in (5.4) and (5.5), the uncertainty set, W, is fixed and known prior to solving the optimization problem. However, in nodal RTC DNE limit problem, the uncertainty set is unknown; in fact, it is a solution of DNE limit problem. Therefore, determining a robust DNE limit with topology control action is much harder problem and needs a more complex solution method as used in [63, 78, 99].

$$\min_{x \in \mathcal{X}} (c^T x + \min_{w \in W} b^T y) \tag{5.4}$$

$$\text{s.t. } Fx \leq f, Hy(w) \leq h, Ax + By(y) \leq a, Ey(w) = e. \tag{5.5}$$

A detailed formulation of a robust corrective topology control problem is presented in [99]; however, the uncertainty set definition used in [99] has been modified in this research, as shown in (5.1)-(5.3). The proposed solution method for nodal RTC algorithm to determine DNE limits

is an iterative process between a master problem and a sub-problem as shown in Fig. 5.3. Note that, the solution method presented below is to determine the lower bound of DNE limits. Similar procedure can be used to determine upper bound of DNE limits.

Initialization: It is assumed that the SCUC problem is solved prior to solving the nodal RTC algorithm. The solution of SCUC problem, such as generator status and associated dispatch, renewable generation, system demand, etc., is used as an input parameter to this algorithm.

Stage one: Stage one problem determines the system topology, which will be evaluated in the stage two of this solution method. In [99], the topology selection problem, a master problem, is a mixed integer programming (MIP) problem, which is computationally inefficient. Therefore, in this research, a sensitivity based greedy algorithm [18] is proposed. This algorithm suggests the topology control actions, in form of a rank list, which will be used as a candidate topology control action for stage two. If a feasible topology is obtained from the greedy algorithm (rank list), the resultant topology will be passed to stage two problem. If a rank list is exhausted, which indicates that there is no feasible topology control action available based on the incumbent SCUC solution and the chosen uncertainty set; therefore, at the next iteration, the uncertainty set will be updated by decreasing the parameter in (5.2).

Stage two: The sub-problem determines the worst-case renewable resource realization, for a chosen topology control action and generation dispatch. The formulation of the sub-problem is given in [99] with an updated uncertainty set definition presented in (5.1), which is determined outside of robust framework, as shown in Fig. 5.3. After solving the sub-problem, if a robust solution is obtained, this indicates that the chosen topology control satisfies the entire uncertainty set. At the next iteration, the uncertainty set will be updated by increasing the parameter in (5.2). If the sub-problem failed to obtain a robust solution, the resultant topology control action will be discarded and the next topology control action listed in the rank list will be tested.

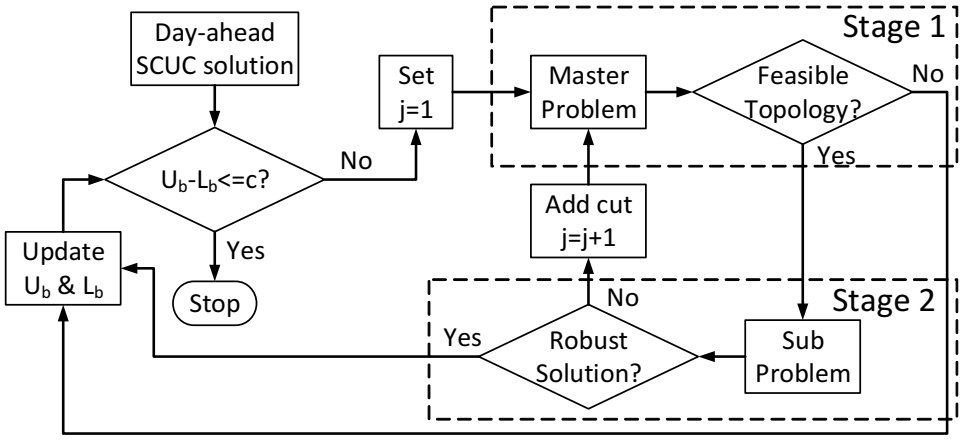

Figure 5.3: Solution method to determine DNE limits with robust corrective topology control.

The benefit of this solution method is that the stage two problem is independent of the stage one problem; therefore, it can be parallelize for solution speedup, which helps with scalability. Furthermore, for simplicity, a simple bisection method is used to update the uncertainty set.

5.5 Numerical Results: Robust DNE Limits

In this section, the robust nodal DNE limits with topology control algorithm is tested on the IEEE-118 bus test case. The branch data for the IEEE-118 bus test case is given [95]; however, the generation information for this test system is not available. Therefore, the generator mix of reliability test system 1996 (RTS) is used to create generator information for the IEEE-118 bus test case [95]. There are total 71 conventional generators and 9 wind injection locations, with peak demand of $4004MW$. For simulation purposes, two difference load profiles are used in this chapter: (a) IEEE-118 bust test case using RTS winter load profile given in [95] with wind profile case$\#12514$ for 20^{th} December 2005 from NERL western wind resource database [104], which will be noted as a traditional demand/wind profile and (b) California Independent System Operator (CAISO) duck chart [105].

A 24 hour SCUC is solved and the SCUC solution is used as a starting point for all the simulations presented in this research. The basic SCUC model and the fuel costs, given in [13], are used to calculate generator operating costs. The reserve requirements for the SCUC are modeled as sum of 5% of demand supplied by conventional generators and 10% of demand supplied by wind units or the single largest contingency, whichever is greater. On top of that, at least 50% of total required reserves will be supplied by spinning reserves and the rest will be supplied by non-spinning reserves. A similar assumption is cited in CAISO's guidelines for spinning reserve and non-spinning reserve [96].

The lower bounds of DNE limit for the CAISO's duck chart, with and without corrective topology control actions, are presented in Fig. 5.4. From Fig. 5.4 it is clear that, with corrective topology control action, during high wind periods, such as hours 1-3, 13-15, and 22-24, the lower bound of DNE limit with topology control actions can be increased by 200% as compared with DNE limits without corrective topology control action. In this case, due to higher congestion in initial topology, the generators ramping capabilities are not utilized to its limit. With topology control actions, the congestion within the system is reduced, which results in an increase in transfer capability across the network and subsequent DNE limits. Similarly, for the entire 24 hours, the DNE limits with topology control action can be increase by $\sim 30\%$ from the DNE limits determined without topology control actions. Note that, in this analysis, the number of topology control actions per hour are limited to 1.

In CAISO's duck chart, the peak demand occurs during hour 18 and hour 19, as shown in Fig. 5.4. In this case, from hour 16 to hour 18, the system demand increases by 29% and wind generation decreases by 22%. Therefore, to meet the system demand in peak hours, the slow start units will be committed during hour 13-14, resulting in the higher amount of operational reserves available in hours 13-14. Due to congestion within the network, this additional available generation could not be utilized to increase the DNE limits. In these situations, the topology control action shows great benefit to system operations as it helps to reduce congestion within the network, which results in increase in DNE limits.

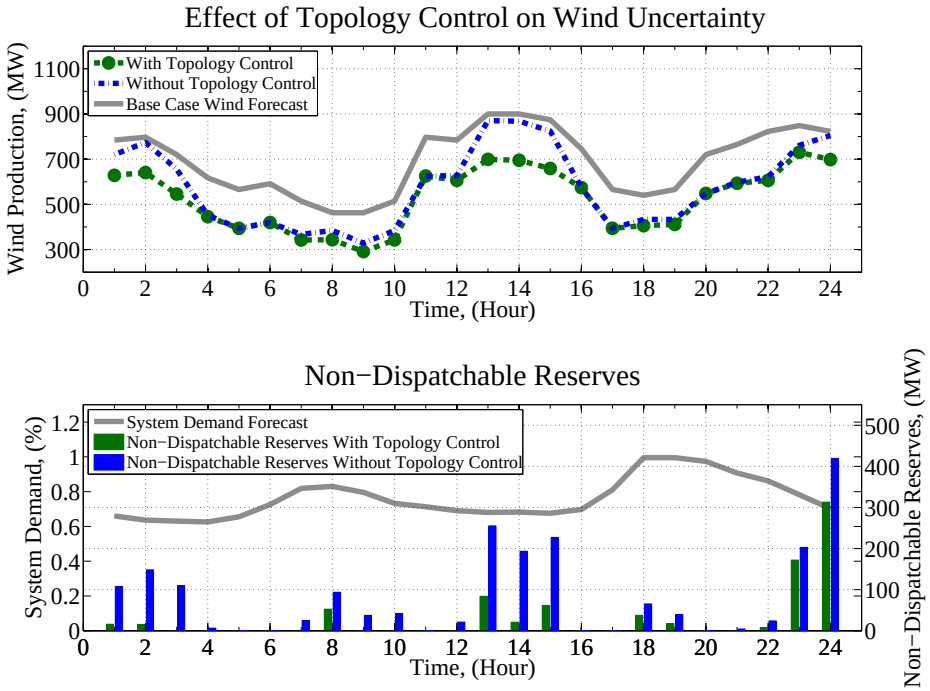

Figure 5.4: DNE limits with CAISO's duck chart and utilization of reserves.

In addition, when wind deviations are high, there seems to be less benefits from topology control. In these hours, the classical generators are forced to use their ramping capability to meet increased demand; therefore, the binding conditions in these cases are generators' ramping capability, not the power transfer limitations such as line congestion. In these cases, the DNE limits determined with single line switching does not report much benefit to renewable integration.

In the past, with topology control, significant savings were obtained for the IEEE 118-bus test case [85]. In this research, the cost benefits obtained with topology control actions, on renewable integration, are estimated. If the DNE limits obtained with topology control action are forced to be achieved without topology control, the operational cost would be increased by at least 6%, considering all the generators in the system are allowed to respond. To get this estimate, a robust unit commitment problem is solved with the uncertainty set obtained with topology control. Furthermore, if the original unit commitment status for the committed generator are assumed to be fixed and only non-committed generators are allowed to change its status, the operational cost increases by $\sim 14\%$. This result proves that topology control not only helps to integrate renewable resources, by increasing the DNE limits, but also provides substantial cost savings in system operations.

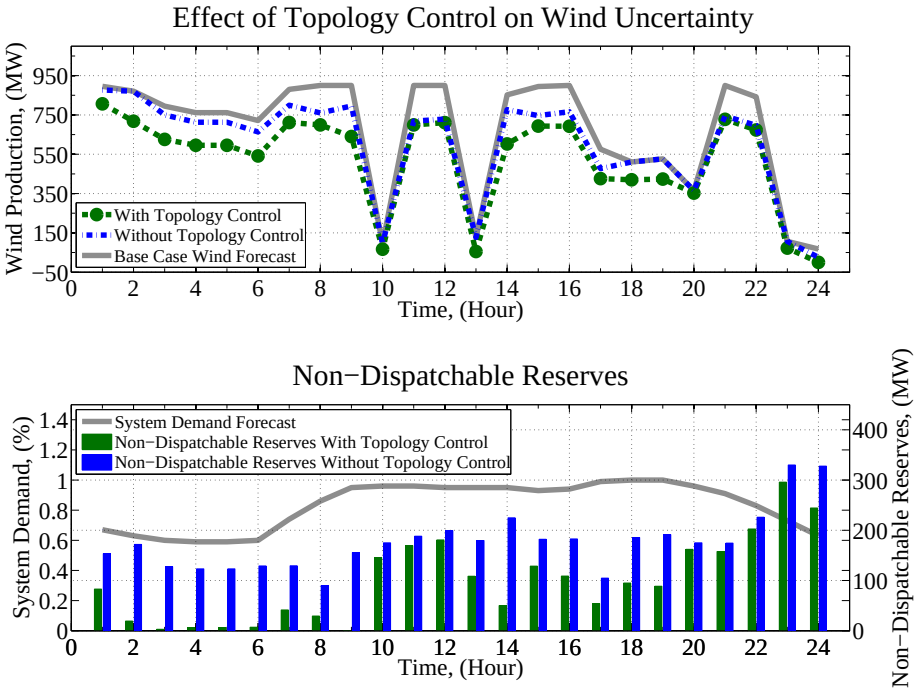

Figure 5.5: DNE limits with IEEE RTS forecasts and utilization of reserves.

The lower bound of DNE limit for the traditional demand/wind profile is presented in Fig. (5.5). In this case, the DNE limit obtained with topology control action are $\sim 100\%$ more than the DNE limit obtained without topology control action. In this particular test case, during the peak hour, without topology control, the DNE limits are close to zero. Furthermore, in these hours, a marginal change in renewable generation can cause system infeasibility. However, for the same operating condition, the robust topology control can give DNE limits of $\sim 17\%$. This results shows the criticality of topology control for renewable resource integration.

The computational time to determine DNE limits with master problem formulation given in [99] is about 10 min per DNE limit. However, with the topology control heuristics presented in [18], the number of iterations can be reduced by $\sim 80\%$, which will further improve the computational time with great extent.

5.6 Numerical Results: Robust Corrective Topology Control

The robust corrective topology control methodology for system reliability is presented in [99]. In this section, the detail analyses of this methodology under renewable uncertainties are presented. The unit commitment solution used in Section 5.5 is also used as an initial operating condition for all the studies presented in this section. Furthermore, the corrective topology control actions may or may not be combined with generator re-dispatch. However, for robust corrective topology control procedure, presented below, generator re-dispatch is taken into consideration.

5.6.1 Robust N-1 Analysis

To see the effect of higher renewable resource integration on N-1 reliability of the system, in this chapter, the robust corrective topology control N-1 analysis with wind uncertainty is presented. The basic model and solution method is the same as [99]. For analysis purposes, the wind uncertainty is assumed to be 20%. The N-1 analysis of the IEEE-118 bus test system with CAISO's duck chart demand and wind forecast are presented in Fig. 5.6. In this analysis contingencies, which can be mitigated by 10 minutes generators re-dispatch alone are not considered and are treated as a trivial case. The contingencies that can only be mitigated by corrective topology control action along with 10 minutes generator re-dispatch are considered in this analysis and are treated as a nontrivial cases.

The bar chart in Fig. 5.6 shows the number of nontrivial contingencies for a 24 hours period. During high wind generation and low demand periods, such as hours 1-2, 13-15, and 23-24, the numbers of contingencies requiring corrective topology control for N-1 reliability are much higher. In these hours, the system cannot survive in most of the N-1 contingencies with generator re-dispatch alone, if the forecasted renewable output deviates by 20% from its base value. Furthermore, during these hours of operations, the system has sufficient amount of reserves to overcome the single largest contingency; however, due to network congestion, these reserves cannot delivered with the initial topology. The corrective topology control actions essentially alters the power flow within the network so that the system reserves can be delivered to mitigate contingencies. In this analysis, only one corrective topology control action per contingency is considered. Similar conclusions are drawn with the IEEE-118 bus test system with a traditional demand/wind profile.

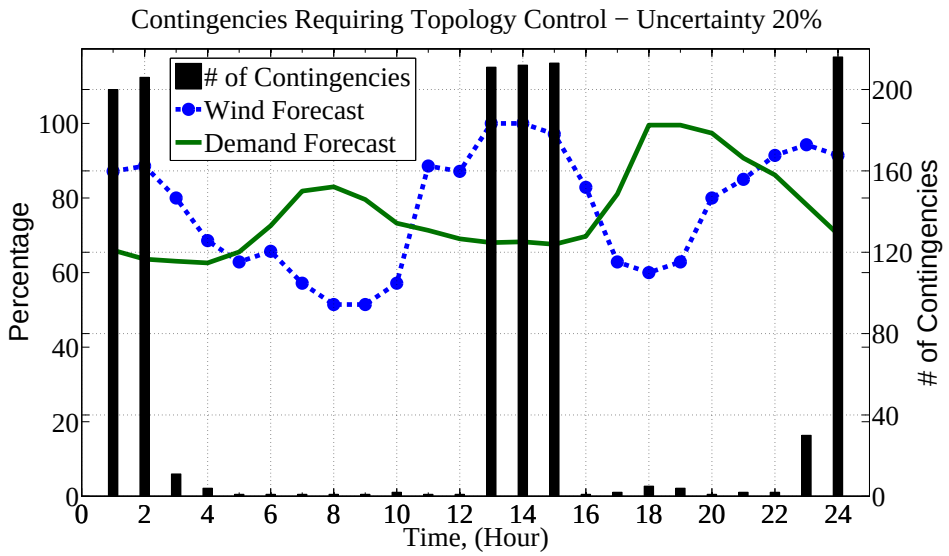

Figure 5.6: N-1 analysis with robust corrective topology control.

The computational time for these simulations on a 2.93 GHz, Intel i-7 processor with 8 GB RAM computer is about 5 seconds per iteration.

5.6.2 AC Feasibility of Topology Control Solution

The robust corrective topology control formulation used in [99] is based on a DC approximation. Therefore, a corrective topology control solution obtained from this algorithm must be tested for AC feasibility. The basic AC optimal power flow (ACOPF) formulation presented in [12] is used to check AC feasibility of the topology control solutions obtained from the robust topology control algorithm. The commercially available nonlinear solver KNITRO [106] is used to solve the AC feasibility problem. The DC solution obtained from a topology control algorithm, such as generator's real power output, line flows, etc., are used as a starting point for an AC feasibility test. Fig. 5.7 shows the base case bus voltages and the bus voltages with topology control action for an hour of peak demand (i.e. hour 18) with contingency of "loss of line $\#119$". Fig.5.7 shows that bus voltages do not change much with the corrective topology control action; in fact, with topology control, bus voltages are closer to unity (the ideal voltage scenario) compared with its pre-contingency state. The bus angle differences for the same base case condition and post-contingency simulation are presented in Fig. 5.8, which shows that bus angle differences do not change much with corrective topology control action. The maximum bus angle difference for this test case is about ± 15 degrees, which is less than its approximate stability limit of ± 30 degrees.

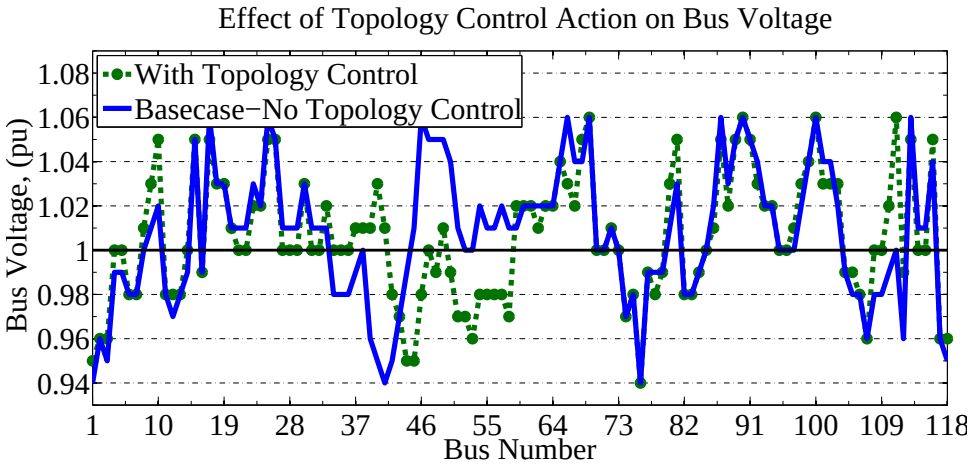

Figure 5.7: Bus voltages (in pu) with and without topology control action.

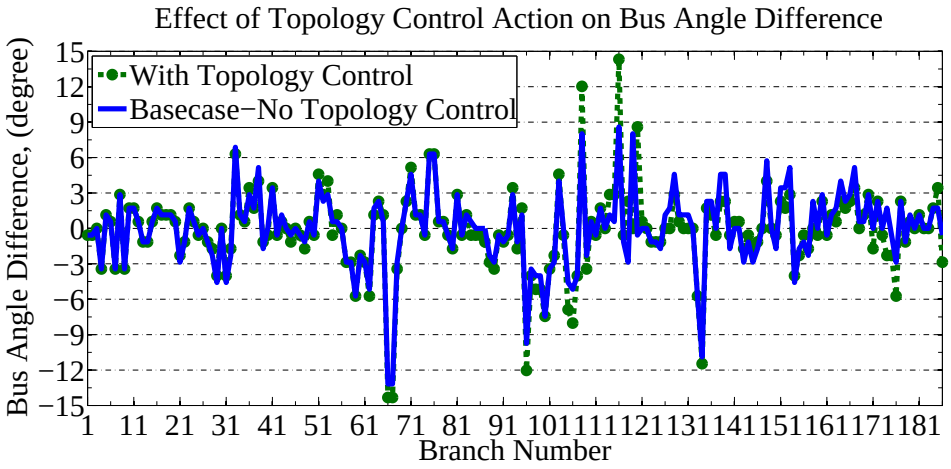

Figure 5.8: Bus angle difference (in degree) for all the transmission elements with and without topology control action.

To check overall AC feasibility of corrective topology control solutions, for the IEEE-118 bus test case with CAISO duck chart, more than 3000 topology control solutions are tested. Out of those 3000 DC robust solutions, $\sim 90\%$ of the topology control solutions obtained from a robust corrective switching algorithm produce AC feasible solutions. This result is very critical from system operations point of view, as this result fills the gap between the disconnected DC formulation and an AC operation. Similarly, with the IEEE-118 bus test system using traditional demand/wind profile, $\sim 85\%$ of robust DC topology control solutions provides an AC feasible corrective topology control solution on base case operating point.

The computational time for an AC feasibility test on a 2.93 GHz, Intel i-7 processor with 8 GB RAM computer is about 4 seconds per contingency.

5.7 Stability Study with Robust Corrective Topology Control Actions

In this section, topology control solutions, presented in Section 5.5, are tested for different stability studies. For discussion purposes, results associated with the peak load hour (hour 18) are presented in this research. The dynamic data for the IEEE-118 bus test case is not available; therefore, generator information from generators in the eastern interconnection are used to generate dynamic data. The dynamic data, for $1.5MW$ individual wind generator, given in [107], are used to model wind injection in this analysis.

Small signal eigenvalue studies are carried out on this test case, with dispatch solution, for hour 18. The real part of the smallest eigenvalue obtained from this study is ~ -112 and the real part of largest eigenvalue is ~ -0.01. This study shows that all the eigenvalues are negative and lie on the left hand side of the s-plain indicating that the given system is stable. This result shows that the given system is small signal stable and will remain stable for small perturbation in operating state. This analysis is carried out using SSAT tool [108].

To demonstrate the effect of topology control, on system reliability, scenario described in Table-5.1 are tested. The presented scenario represents the worst-case wind scenario for the given operating condition; the loss of wind represented by this scenario is equivalent to loss of $\sim 2\%$ of total generation. Note that, in the western interconnection, for many stability related studies, the worst-case scenario is the loss of two Palo Verde nuclear units [109], which is about 2% of total

online generation.

Table 5.1: Scenario to study the effect of topology control on system reliability.

t=10-12 sec.	Loss of wind generation (17%)
t=120 sec.	Topology control solution implemented (open line between bus#65-Bus#68)
t=150-750 sec.	Generators are dispatch based on ramping capability

The effect of topology control action on system frequency is presented in Fig. 5.9. Due to the sudden drop of wind generation, the system frequency drops below $59.8Hz$ and recovers to $\sim 59.88Hz$ using system inertia. After implementing the line switching action, the system frequency improves and reaches to $\sim 59.89Hz$. This small improvement in frequency happens because topology control action decrease the losses in the system. At t=150 sec., the generators are re-dispatched to overcome the loss of generation; in this analysis, 10 minutes ramping capability of generators are considered and it is assumed that the additional generation appears online after each one minute. After generation re-dispatch, at last, the frequency improves and settle downs to $\sim 59.97Hz$.

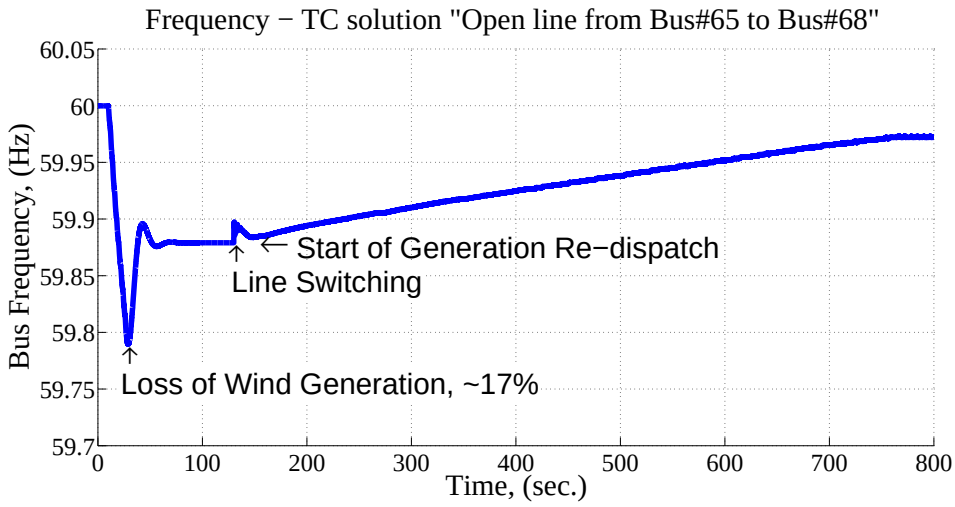

Figure 5.9: Effect of topology control action on system frequency.

The relative rotor angle of generators nearer to topology control action are presented in Fig. 5.10. The effect of loss of wind generation on generator's rotor angle is relatively smaller than the implementation of topology control action, as the loss of wind generation is not close of these buses. On other hand, the topology control action is close to these buses; therefore, the effect of loss of wind generation, on generators relative rotor angle, is smaller compared to topology control action. The real power supplied by these generators are also presented in Fig. 5.11.

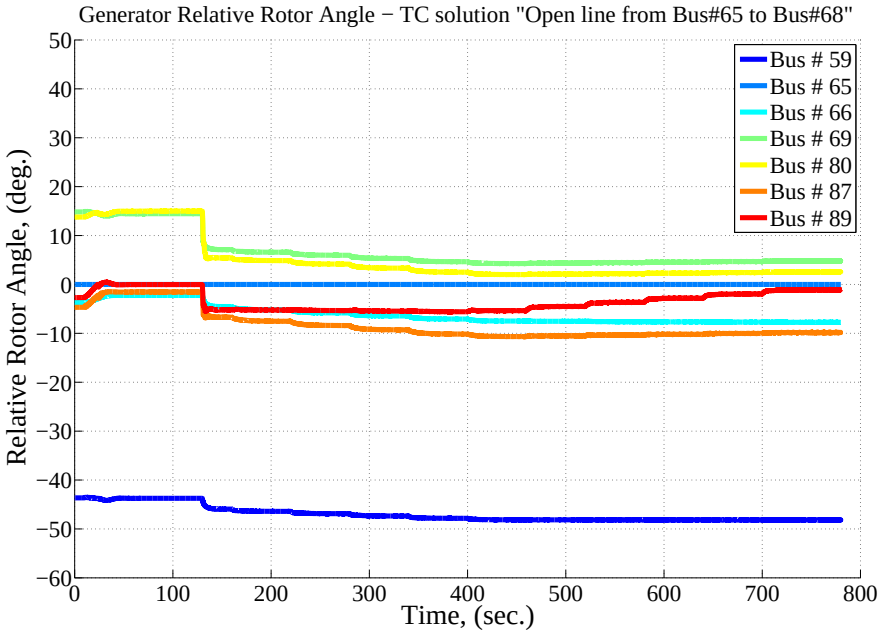

Figure 5.10: Generator Relative Rotor Angle - TC solution “Open line from Bus-65 to Bus-68”

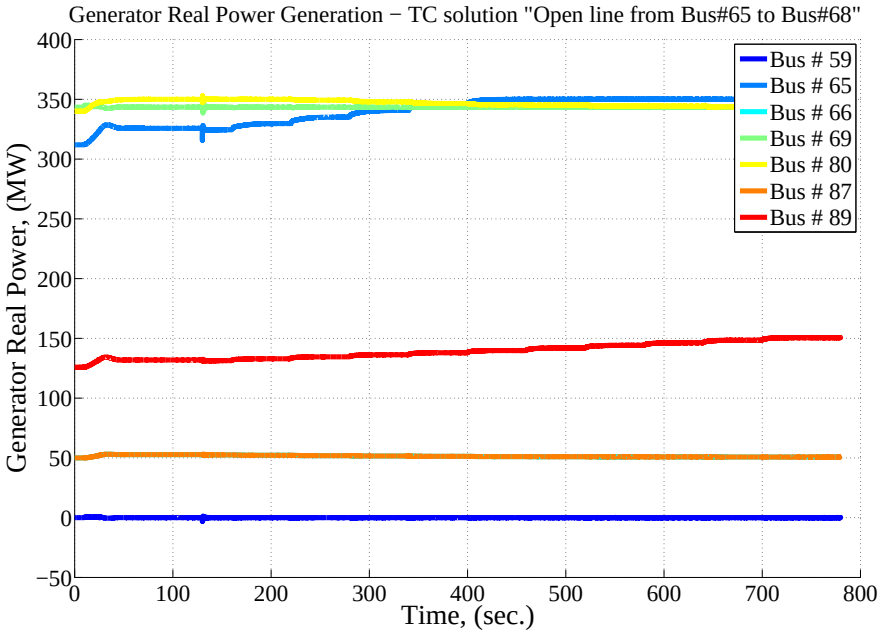

Figure 5.11: Generator Real Power Generation - TC solution “Open line from Bus-65 to Bus-68”

The effect of the topology control action on bus voltage stability is also studied. In the above scenario, the loss of wind on bus voltages are not significant; however, the topology control action alters the voltages on buses close to line switching action, as shown in Fig. 5.12. The magnitude of change in voltage is highest on buses that are connected to the switched line.

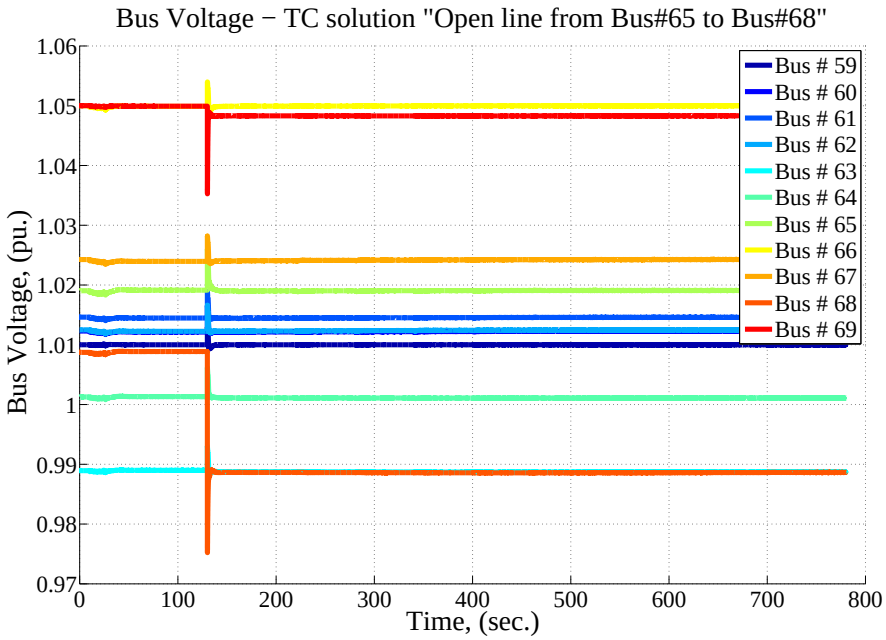

Figure 5.12: Bus Voltage - TC solution “Open line from Bus-65 to Bus-68”

5.8 Conclusion

The penetration of renewable resources in electrical power system is increased in recent years. This increase in intermittent renewable resources are forcing to alter the way bulk power systems are operated today. This research shows the usefulness of topology control actions for integration of renewable resources.

In case of renewable resource integration, the determination of DNE limits is critical; in this research, a systematic procedure to determine DNE limit is presented. With corrective topology control actions, the DNE limits can be increased by 30-100%, as compared with no topology control actions. At the same time, topology control actions can lower the operational cost by at least 6%. The robust topology control algorithm is based on a DCOPF; therefore, the topology control solutions obtained from this algorithm must be checked for AC feasibility; on the IEEE-118 bus test case, ∼85-90% of topology control solutions obtained from the robust topology control algorithm are AC feasible.

The intermittency in renewable resources add more complexity in system reliability. This chapter has demonstrated that topology control can help to achieve N-1 system reliability. Overall, with higher penetration of renewable resources within electrical power systems, the systematic implementation of topology control actions can provide significant operational benefits.

The stability studies, presented in this chapter, demonstrated that the solution obtained from the robust topology control algorithm can pass AC feasibility and stability tests. Furthermore, ∼66% of topology control solutions obtained from robust topology control algorithm pass the stability check. At the same time, these results show that topology control does not deteriorate the system stability; on contrary, topology control done properly can help to maintain stable operations.

6. Scalability of Topology Control Algorithms

6.1 Motivation

Robust topology control methodology, presented in Chapter 3, is tested on an IEEE-118 bus test case, which consists of 54 generators, 118 buses, and 186 transmission lines. This test system is much smaller than any realistic test case, for example, the PJM system is consists of 1375 generators, $62,556$ miles long transmission network and peak demand of $183,604$ megawatts [110]. Therefore, for any practical implementation, the robust topology control methodology must scale from IEEE-118 bus test case to much larger test system.

The master problem, presented in Chapter 4, Section 4.5, is a MIP problem with a combinatorial cut to determine the system topology. However, combinatorial cut is computationally inefficient, may lead to many iterations between the master problem and the sub-problem, which will increase the computational time and/or the master problem will become so big that it will be even infeasible to solve. To overcome this issue, topology control heuristic, presented in [18], is proposed to replace the master problem. The topology control heuristics is based on a sensitivity analysis and provides the topology control solutions in terms of a ranking list. This ranking list will be further used as a chosen topology control action and will be evaluated for its robustness properties in a sub-problem. The detail analysis of topology control heuristic is presented in Section 6.2, where accuracy and effectiveness of heuristic to identify correct topology control action is tested on 2383 bus Polish test system.

6.2 Performance of AC and DC Based Topology Control Heuristics

Traditionally, the transmission network is considered as a passive system and generation was optimized assuming a fixed transmission topology. The concept of dispatchable transmission was introduced in [19], which proposed a paradigm shift in the way the transmission topology is viewed. As a result, optimal topology control (OTC) was developed to harness the benefits of co-optimizing generation with transmission topology [20, 85]. Previous research shows that OTS would result in significant cost savings even under reliability constraints [13, 17]. Transmission switching has other applications, such as reliability improvement via corrective switching [99].

Binary variables representing the status of transmission lines make OTC a mixed-integer program problem. Real world power systems have thousands of transmission lines making the resulting OTC MIP a computationally expensive problem. Since the available computational time is limited, an MIP based implementation of OTC in day-ahead and real-time procedures is not practical. An alternative to solving the full MIP is the use of switching heuristics to obtain a good, suboptimal solution significantly faster. The MIP-heuristic introduced in [22] allows only one switching at a time, reducing the number of binary variables to one per iteration. This would significantly reduce the complexity of the problem. However, the formulation still requires mixed integer programming, which may still be too computationally challenging for certain applications that require fast solutions. There are other heuristics proposed in the literature, which only need the results of the original OPF. A DC-based heuristic is introduced in [90, 111], which ranks the lines based on their economic value. The lines value, or the congestion rent of a single line, is the price difference at the two ends of the line multiplied by the flow it carries [112]. The calculations are based on the results of a DCOPF. This will be referred to as the 'DC heuristic'. A similar heuristic is derived based on an ACOPF [113], which will be referred to as the 'AC heuristic'. In addition to

the real power value of the line, the AC heuristic takes into account the reactive power and losses. The results obtained from the heuristics in small scale test cases show that they perform relatively well [112].

In this section, these heuristics are tested to see if they perform well for a large-scale test case, the Polish system. The mathematical representations of the heuristics are presented briefly in the next section. The results suggest that the heuristics are not very different and the inclusion of losses and reactive power does not have a significant impact. This finding is in line with the conclusions made in [113], stating that the heuristics would be significantly different if the system was voltage constrained. The results also show that the best solutions are among the top twenty candidates identified by the heuristics. However, the correlation between the estimated and actual benefits from switching is not very strong.

6.2.1 Methodology

In this section, MATPOWER, a MATLAB based open sources power system simulation package, is used to solve the OPF problems [114, 115]. The detailed formulation and solution method for ACOPF and DCOPF problem is provided in [115]. Here, brief descriptions of AC as well as DCOPF formulations are presented. The ACOPF problem can be represented as shown in (6.1)-(6.10), with an objective function presented in (6.1). The upper bound on AC line flow equations are provided in (6.2), The real and reactive power flow across the transmission line k is represented by (6.3) and (6.4) respectively, the node balance constraints for real and reactive power are represented by (6.5) and (6.6). Note that the dual variables for node balance constraints, λ_{Pn} and λ_{Qn}, represent the active and reactive power locational marginal prices (LMP). Constraints (6.7)-(6.10) represent the lower and upper bounds on variables.

$$\min \sum_{\forall g} c_g P_g \tag{6.1}$$

$$\text{s.t. } P_k^2 + Q_k^2 \leq S_k^2, \forall k \tag{6.2}$$

$$P_k = V_m^2 G_k - V_m V_n (G_k \cos(\theta_m - \theta_n) + B_k \sin(\theta_m - \theta_n)), \forall k \tag{6.3}$$

$$Q_k = -V_m^2 B_k - V_m V_n (G_k \sin(\theta_m - \theta_n) - B_k \cos(\theta_m - \theta_n)), \forall k \tag{6.4}$$

$$\sum_{\forall k \in \delta(n)^+} P_k - \sum_{\forall k \in \delta(n)^-} P_k + \sum_{\forall g(n)} P_g = d_n, \forall n \tag{6.5}$$

$$\sum_{\forall k \in \delta(n)^+} P_k - \sum_{\forall k \in \delta(n)^-} P_k + \sum_{\forall g(n)} P_g = d_n, \forall n \tag{6.6}$$

$$P_g^{min} \leq P_g \leq P_k^{max}, \forall g \tag{6.7}$$

$$Q_g^{min} \leq Q_g \leq Q_k^{max}, \forall g \tag{6.8}$$

$$V_n^{min} \leq V_n \leq V_n^{max}, \forall g \tag{6.9}$$

$$\theta^{min} \leq \theta_n - \theta_m \leq \theta^{max}, \forall k \tag{6.10}$$

Using the ACOPF formulation presented, the sensitivity of the objective function to a marginal change in the status of a transmission line is calculated in [113]. This metric is used as a heuristic to estimate the benefits of switching the line. The heuristic is shown in (6.11),

$$LV_{AC} \;=\; P_{km}\lambda_{Pm} - P_{kn}\lambda_{Pn} + Q_{km}\lambda_{Qm} - Q_{kn}\lambda_{Qn}, \forall k \tag{6.11}$$

In this research, we refer to the method that ranks lines based on (6.11) as the AC Heuristic. The metric represents the economic value of the line, which equals the revenue collected from the sale of power at the importing end minus the cost of buying power at the exporting end, considering losses and reactive power. AC heuristic considers the negative of the line value, suggesting that a line with a larger negative economic value is a potential switching candidate. It is not expected that the heuristic estimates match the actual benefits accurately, because the change in the status of the line is not marginal.

With the well-known assumptions of DC power flow, the ACOPF formulated in (6.1)-(6.10) can be simplified to a DCOPF, in which there is no reactive power or network losses. Moreover, the power flow constraint can be approximated by a linear equation presented in (6.12). Under this set of assumptions, and with linear cost functions, the DCOPF becomes a linear program (LP). Because of the special properties of LP, LP-based DCOPF can be solved much faster than the original ACOPF.

$$P_k = B_k(\theta_n - \theta_m), \forall k \tag{6.12}$$

The same sensitivity is calculated with the DC set of assumptions in [90, 111]. The metric estimating the DC benefits of the line is presented in (6.13). We refer to the method ranking lines based on this metric as the DC heuristic. The DC estimation of the lines value is the same as the AC estimation, ignoring the reactive power and losses. It is concluded in [113] that the two heuristics may produce significantly different results if the system is voltage constrained.

$$LV_{DC} = P_k(\lambda_{Pm} - \lambda_{Pn}), \forall k \tag{6.13}$$

6.2.2 Simulation Studies

We test the two heuristics on the Polish test case provided by MATPOWER. The system has 2383 nodes, 327 generators, and 2896 transmission lines. We assume that all of the generators are on. The cost functions included in the dataset are linear, which matches the formulation presented in the previous section. In order to study the performance of the heuristics, we compare the actual benefit from the proposed switching action with the estimated benefit calculated by the heuristics. The actual switching benefit is the total cost difference between the case in which the transmission line is in the system, and the case in which it is taken out. We simulate the performance of the heuristics under three different settings:

1. DC Heuristic with DCOPF: a DCOPF is performed and all the primal and dual variables are taken from the DCOPF solution. The actual benefits are calculated through the total cost comparison of the two DCOPFs. The switching benefits are also estimated through the DC heuristic introduced in (6.13). A comparison between the actual and estimated benefits provides information on the performance of the DC heuristic with a DCOPF. Note that the solution to a DCOPF may or may not be AC feasible.

2. DC Heuristic with ACOPF: the dual and primal variables as well as the actual benefits are calculated through an ACOPF. The estimated switching benefits are obtained from the DC heuristic, which does not include losses or reactive power. Note that under this setting, despite using the DC heuristic, the power flow and active power LMP come from an ACOPF.

A comparison between the actual and estimated benefits provides information on the performance of the DC heuristic with an ACOPF.

3. AC Heuristic with ACOPF: the dual and primal variables are specified through an ACOPF algorithm. The actual switching benefits are also calculated by comparing the total cost obtained from the two ACOPFs. Under this setting, the benefits are estimated through the AC heuristic presented in (6.11). A comparison between the actual and estimated benefits provides information on the performance of the AC heuristic with an ACOPF.

Fig. 6.1 compares the benefits obtained by a single switching action with the estimated benefits calculated by the DC heuristic under setting 1. Fig. 6.2 shows the performance of an algorithm based on the DC heuristic using a DCOPF for the first twenty switching candidates. The dashed line specifies the maximum possible benefit from the switching identified by an ACOPF while the dotted line shows the maximum possible benefits of switching using a DCOPF. The results show that the algorithm is not able to find the best switching action in the first twenty candidates it proposes. Five out of twenty proposed candidates are beneficial actions when tested with a DCOPF. However, there exist only two candidates that provide ACOPF beneficial switching actions. In electricity markets today, all the procedures are based on DCOPF due to the computational complexity of ACOPF. However, operators need to make sure that the solution is AC feasible. This is often done via out of market correction (OMC) mechanisms [116]. Our results suggest that switching candidates identified by the solution of a DCOPF may not be AC feasible or may not be beneficial even though DCOPF identifies them to be beneficial.

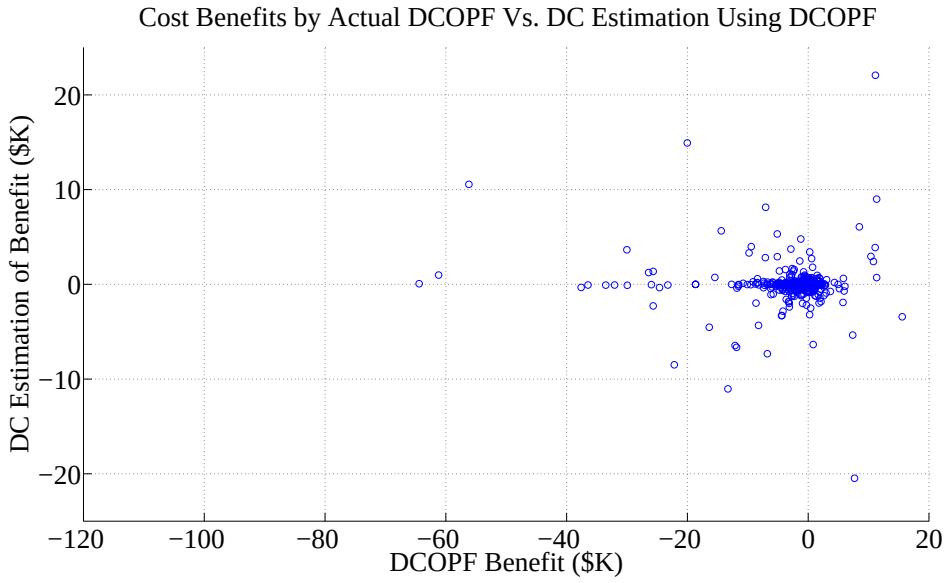

Figure 6.1: The benefits identified by DCOPF versus the DC heuristic estimation of the benefits using DCOPF.

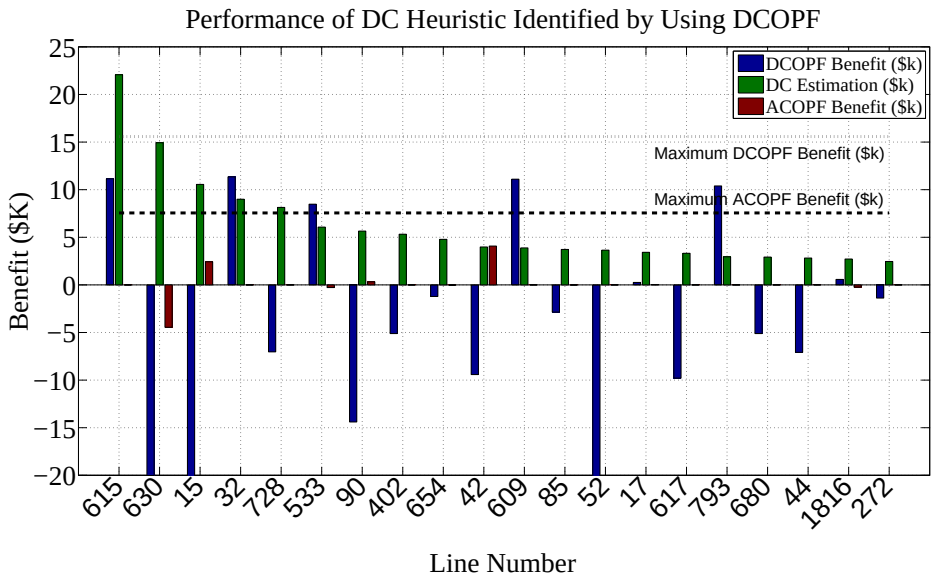

Figure 6.2: Performance of the DC heuristic for the first twenty lines identified by the heuristic using DCOPF.

Fig. 6.3 and 6.4 show the same results under setting 2 where ACOPF is used instead of DCOPF. The results suggest that the algorithm is able to identify the best switching action among its first twenty proposed candidates. Six out of twenty proposed actions are beneficial. Note that the only difference between settings 1 and 2 is the fact that ACOPF solution is used under setting 2 for both actual and estimated benefit calculation. However, under both settings the DC heuristic presented in (6.13) is employed. The difference between the results comes from the fact that the dispatch and prices are different when AC power flow constraints are taken into account in the optimal power flow problem.

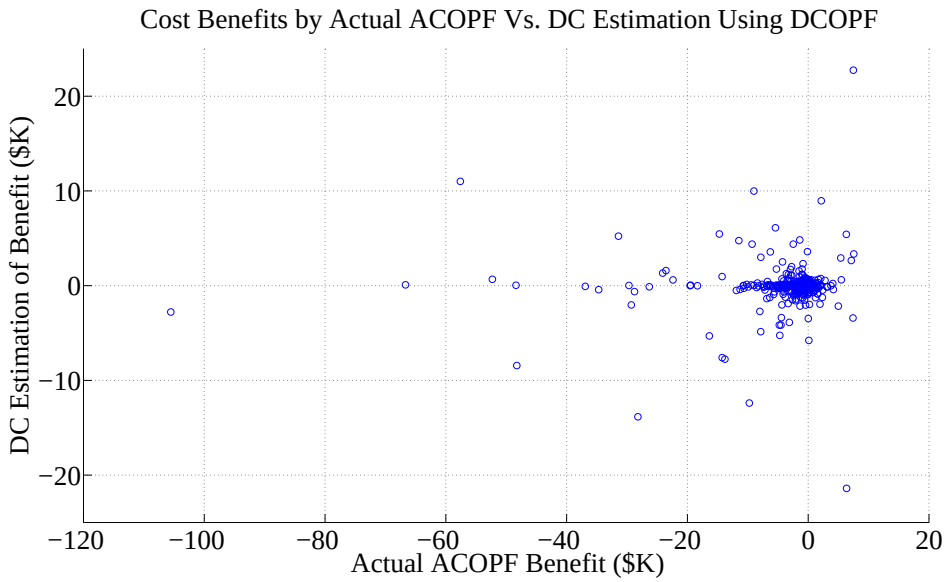

Figure 6.3: The actual benefits obtained by ACOPF versus the DC heuristic estimation of the benefits using ACOPF.

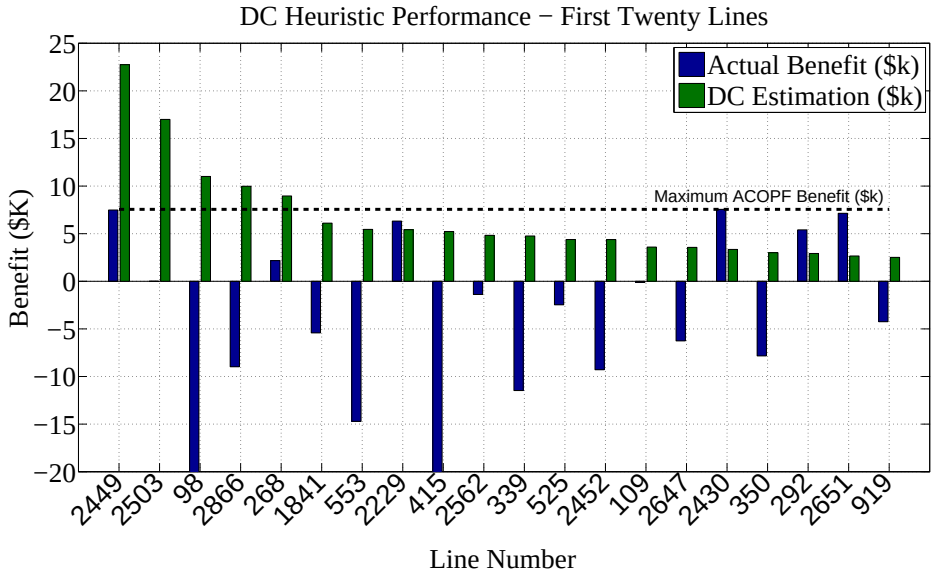

Figure 6.4: Performance of the DC heuristic for the first twenty lines identified by the heuristic using ACOPF.

Fig. 6.5 and 6.6 show the results under setting 3 where the AC heuristic is used with ACOPF solution. The results are very similar to those of setting 2 with six beneficial solutions among the first twenty proposed actions.

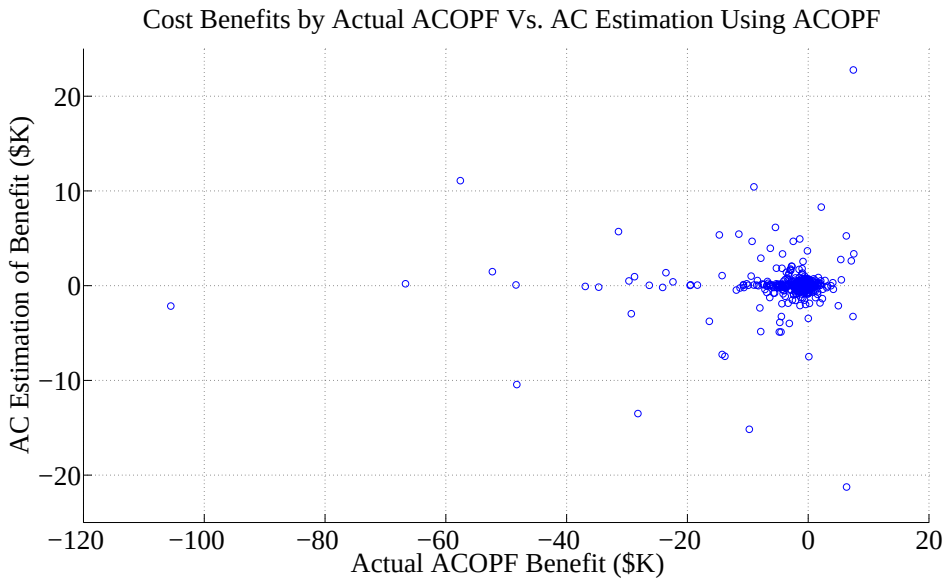

Figure 6.5: The actual benefits obtained by ACOPF versus the AC heuristic estimation of the benefits using ACOPF.

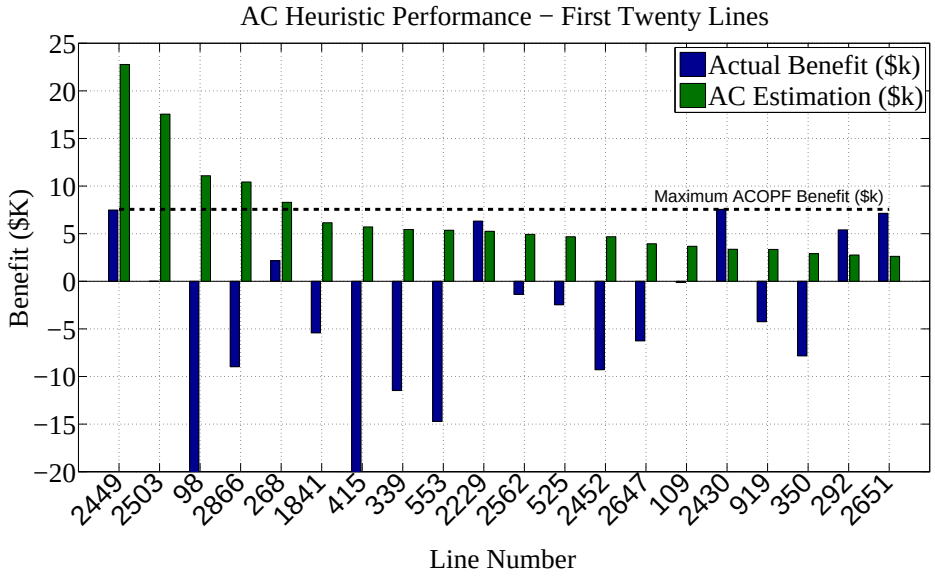

Figure 6.6: Performance of the AC heuristic for the first twenty lines identified by the heuristic using ACOPF.

The results obtained under settings 2 and 3 show that AC and DC heuristics produce very similar results when the ACOPF solution is used. Under both settings, six out of twenty proposed actions were beneficial and the algorithm was able to identify the best switching action. The only

difference was a slight change in the candidates order. Such results were expected and are in line with the conclusions of [113], which suggests the results to be similar when the system is not heavily voltage constrained. Nevertheless, the results obtained under setting 1, where the DCOPF solution is used for heuristic calculations, are substantially different from those of settings 2 or 3. The difference appears both in the suggested switching candidates and the benefits.

As was stated before, in electricity markets today, ACOPF solutions are not generally available similar to setting 1. Our results show that the studied heuristics do not provide consistent results when they are based on the DCOPF solution compared to a more realistic ACOPF. The more realistic benefits, ACOPF based benefits, as well as the proposed candidates are different than those based on a DCOPF.

6.2.3 Conclusion

Due to the computational complexity of the OTC problem, different heuristics are used to obtain fast sub-optimal solutions. The heuristics are often tested on small scale systems and the scalability of their application is not well understood. We studied the performance of two such fast heuristics on the Polish system. The heuristics were studied under three different settings: DC heuristic with DCOPF, DC heuristic with ACOPF, and AC heuristic with ACOPF. Our results suggest that the AC and DC heuristics are not very different when they are based on the solution to ACOPF. However, the heuristics do produce different results if they are based on DCOPF solutions. Our results suggest that DCOPF based solutions obtained for OTC may not perform well under realistic system conditions modeled by an ACOPF. Since the market procedures are based on DCOPF, not ACOPF, and AC feasibility is achieved via OMC routines, implementation of ACOPF based heuristics would not be straightforward.

7. Robust Minimax Regret Unit Commitment

7.1 Introduction

Increasing utilization of intermittent wind power has been a challenging issue for a system operator in making day-ahead unit commitment decisions. For instance, there does not exist a day-ahead unit commitment decision that is optimal with regard to every possible outcome of the real-time wind power generation. Meanwhile, wind power is often considered to be more volatile and harder to predict than demand or natural water inflows in a power system in the short term. Accordingly, for daily operations, the system operator faces a high risk (i.e., the loss to which one is exposed because of uncertainties) of real-time load imbalance. To manage this risk, the system operator defines different types of reserves. In addition, several electric power markets in the U.S. execute reliability unit commitment after the closure of the day-ahead market, and evaluate the generation needs for the next operating day (see, e.g., [117]). Reliability unit commitment ensures that there is sufficient generation capacity in the proper locations to reliably serve the load. From the methodology point of view, stochastic and recently introduced robust optimization approaches are shown to be effective to solve the unit commitment problem with uncertain wind power output (see, e.g., [52], [118], [119] and [120]).

Stochastic optimization approaches have been studied extensively during the last several years. In the early 90's, multistage stochastic programming formulations were proposed and an augmented Lagrangian decomposition framework was studied to solve the problem efficiently (see, e.g., [47], [48], [49], and [50]), targeting load uncertainty for vertically integrated utility companies. Recently, significant research progress has been made in the application of stochastic programming approaches to the deregulated electricity markets (see, e.g., [51], [52] and references therein). The basic idea of stochastic programming in solving the unit commitment problem for Independent System Operators (ISOs) is to formulate the day-ahead unit commitment as the first-stage problem and the real-time economic dispatch as the second-stage problem, with the objective of minimizing the total expected cost. Stochastic programming can also help consumers decide optimal bidding strategies. For instance, readers are referred to its application in generating supply curves [121], and its contribution in hedging strategies in the wholesale market [122]. Most recently, stochastic programming approaches have been used to combine the slow-start generator commitment in day-ahead and fast-start generator commitment in real-time operations (see, e.g., [53] and [54]), estimate the contribution of demand flexibility in replacing operating reserves [55], and solve stochastic security-constrained unit commitment models (see, e.g., [56], [57], [58], and [59]). Besides these applications, chance-constrained two-stage stochastic programming has been studied to ensure high utilization of wind power output [60], and the parallel computing (see, e.g., [61]) implementation under a cloud computing or high performance computing environment has increased the capacity to solve large-scale two-stage stochastic power system optimization problems. From all of the above papers, it can be observed that stochastic optimization has been an effective approach to solve the unit commitment problem with uncertainty, especially with the objective of minimizing the total expected cost (e.g., using the expected cost as the risk measure). However, there are still challenges. For instance, for most stochastic optimization approaches, scenarios are generated based on a certain probabilistic distribution, and a large sample size is usually considered to increase the accuracy of the obtained solution. Thus, the challenges include: 1) how to derive the precise probabilistic distribution of an uncertain parameter that has an intermittent na-

ture (e.g., wind output) and accordingly generate the scenarios, and 2) how to solve the large-sized extensive formulation (see, e.g., [123]).

To address the challenges of the stochastic optimization approaches, robust optimization approaches have been proposed (see, e.g., [41, 124], and [43]). For some instances (see, e.g., [125]), robust optimization involves a comparatively low computational burden, as compared to the stochastic optimization (scenario-based) approach, because it does not need to enumerate a large number of scenarios. In the robust optimization approach, the worst-case cost is used as the risk measure. Instead of using a probabilistic distribution, the uncertain factor such as wind power output is assumed to be within an uncertainty set. This approach searches a solution that can ensure system robustness under the worst-case scenarios. Recently, a robust optimization approach has been studied for contingency-constrained unit commitment with n-K security criterion in [126]. In that study, a robust integer programming formulation is proposed and a corresponding reformulation approach is developed to solve the problem. Besides [126], robust optimization approaches have been proposed to solve other related problems, which include a robust optimization approach for planning the transition to plug-in hybrid electric vehicles for Ontario, Canada [127], a robust optimization approach to build hourly offering curves for a price-taking producer [125], a two-stage robust optimization approach to solve the unit commitment problem under wind power output uncertainty [120], and an adaptive robust optimization approach to solve the unit commitment problem under nodal net injection uncertainty [128].

Robust optimization approaches provide an effective way to improve system robustness because the minimax criterion for the robust optimization approach aims at optimizing the problem under the worst-case scenarios. However, the solutions of the robust optimization approaches are often considered to be very conservative and the total cost tends to be very high. Hence, in this research, we propose using the minimax regret criterion (e.g., using regret as the risk measure), an alternative subjective decision rule in decision theory, which is less conservative and meanwhile can provide the same robustness guarantee, as compared to the minimax criterion. Note here that recently studies also use other risk measures such as the conditional value at risk (CVaR) (see, e.g., [129] and [130]), and it is indicated in [125] that managing risk through robust optimization and through stochastic programming incorporating risk measures (e.g., CVaR) is equivalent under certain assumptions. In this research, we focus our study on the regret risk measure. In decision theory, regret is measured by the deviation, in terms of the total costs, between the current solution without knowing the uncertain parameters and the perfect-information solution, i.e., the action we would have taken had we known which scenario would occur. By applying the minimax regret criterion, we aim at obtaining a solution that minimizes the worst-case regret over all possible scenarios while ensuring system robustness. In practice, regret is a common subjective decision rule that is naturally used by many decision makers. As mentioned in [131] and [132] (cf. Section 2.3 in [131]), it has been shown that the behavior of some economic agents could be better predicted using a minimax regret criterion in the presence of uncertain yields (e.g., uncertain wind power output in this research).

We now explain the minimax regret, robust optimization, and stochastic optimization approaches by a simple example shown in Table 7.1. In this example, there are two possible scenarios (S1 and S2), each with a certain probability (S1 with probability 0.10 and S2 with probability 0.90) of happening. There are three possible decisions (A, B, and C) before the two possible scenarios (S1 and S2) are realized with the estimated cost listed. For instance, suppose that we commit to decision A. If S1 happens (with probability 0.10), then we have to pay $100. Since a smarter deci-

Table 7.1: An example on decision making under uncertainty

		Decision		
Scenario	Probability	A	B	C
S1	0.10	\$100	\$50	\$60
S2	0.90	\$20	\$50	\$30
Expected Cost		\$28	\$50	\$33
Maximum Cost		\$100	\$50	\$60
Maximum Regret		\$50	\$30	\$10

sion could have been made (by committing to B), in which case the cost is \$50, we have a regret of \$100-\$50=\$50. Instead if S2 happens, since we have made the best decision, we have zero regret (the cost \$20 of decision A is less than those of B and C). Hence, the maximum regret with respect to decision A is $\max\{\$50, \$0\}$=\$50. We list the maximum regrets for all the decisions in Table 7.1, as well as their maximum (e.g., for A: $\max\{\$100, \$20\} = \$100$; for B: $\max\{\$50, \$50\} = \$50$; for C: $\max\{\$60, \$30\} = \$60$) and expected costs (e.g., for A: $0.10 \cdot \$100 + 0.90 \cdot \$20 = \$28$; for B: $0.10 \cdot \$50 + 0.90 \cdot \$50 = \$50$; for C: $0.10 \cdot \$60 + 0.90 \cdot \$30 = \$33$), corresponding to robust and stochastic optimization approaches respectively. By comparison, it is clear that we have different optimal decisions under different criteria: the stochastic optimization approach chooses decision A, which overlooks the less likely but risky scenario (S1); the robust optimization approach (minimax criterion) selects decision B, which picks the lowest maximum cost at a cost of the highest expected cost; the minimax regret criterion commits to decision C, which performs reasonably well under the other criteria, and excels in terms of regrets. In previous research, the minimax regret concepts have been applied in risk-constrained power system planning problems, to model multiobjective tradeoff (see, e.g., [65], [66], and [67]), to handle the uncertainty that emerges in market competition [68], to serve as an alternative of the probabilistic choice approach [69], and to mitigate the vulnerability against intentional attacks while meeting budgetary limits [70]. For a comprehensive survey and more examples on the minimax regret criterion, readers are referred to [64] and [131].

In this research, we propose the minimax regret approach to solve the unit commitment problem under wind power output uncertainty, and compare its performance to the robust optimization and stochastic optimization approaches. To ensure fairness in the comparison, we compare both the worst-case regret value and the expected total cost, among the three approaches. Our case studies under various data settings show that our proposed minimax regret approach can provide robust and less conservative unit commitment solutions which outperform those obtained from the other two approaches in terms of regrets. Meanwhile, the total expected cost for our proposed approach is only sightly greater than the stochastic optimization approach. More specifically, compared to the robust optimization approach, our proposed approach is less conservative while maintaining robustness. As compared to the stochastic optimization approach, our proposed approach sacrifices a little in terms of the total expected cost, and significantly increases system robustness. Note here that our proposed minimax regret approach is almost distribution-free, maintaining the same advantage as the robust optimization approach, as compared to the stochastic optimization (scenario-based) approach. Therefore, the proposed approach can serve as an alternative to the commonly accepted stochastic optimization approach for the reliability unit commitment practice at ISOs to help obtain a unit commitment decision that leads to the minimum regret under the

worst-case scenario while keeping the system robust under wind power output uncertainty.

The remaining part of this research is organized as follows. Section 7.2 describes the mathematical formulation of the two-stage minimax regret unit commitment problem. Section 7.3 presents a Benders' decomposition framework to solve the problem. In the framework, both feasibility and optimality cuts are developed. Section 7.4 compares the performances of the minimax regret, the robust optimization, and the stochastic optimization approaches. Finally, Section 7.5 concludes our study.

7.2 Mathematical Formulation

For a fixed wind power output r, $\mathcal{Q}(r)$ is the optimal objective value of the following mixed-integer program:

$$\min_{y,o,s,x,v} \sum_{t=1}^{T} \sum_{i\in\mathcal{G}} \Big(\mathrm{SU}_i o_{it} + \mathrm{SD}_i s_{it} + f_{it}(x_{it}) \Big) \tag{7.1}$$

$$\text{s.t. } -y_{i(t-1)} + y_{it} - y_{ik} \le 0, \forall i \in \mathcal{G}, \forall t, \quad k \in \{t, t+1, \cdots, \mathrm{MU}_i + t - 1\} \tag{7.2}$$

$$y_{i(t-1)} - y_{it} + y_{ik} \le 1, \forall i \in \mathcal{G}, \forall t, \quad k \in \{t, t+1, \cdots, \mathrm{MD}_i + t - 1\} \tag{7.3}$$

$$-y_{i(t-1)} + y_{it} - o_{it} \le 0, \forall i \in \mathcal{G}, \forall t \tag{7.4}$$

$$y_{i(t-1)} - y_{it} - s_{it} \le 0, \forall i \in \mathcal{G}, \forall t \tag{7.5}$$

$$Q_i y_{it} \le x_{it} \le U_i y_{it}, \forall i \in \mathcal{G}, \forall t \tag{7.6}$$

$$x_{it} - x_{i(t-1)} \le (2 - y_{i(t-1)} - y_{it})\overline{\mathrm{RU}}_i + (1 + y_{i(t-1)} - y_{it})\mathrm{RU}_i, \forall i \in \mathcal{G}, \forall t \tag{7.7}$$

$$x_{i(t-1)} - x_{it} \le (2 - y_{i(t-1)} - y_{it})\overline{\mathrm{RD}}_i + (1 - y_{i(t-1)} + y_{it})\mathrm{RD}_i, \forall i \in \mathcal{G}, \forall t \tag{7.8}$$

$$\sum_{n=1}^{N} \Big(\sum_{i\in\mathcal{G}_n} x_{it} + r_{nt} \Big) = \sum_{n=1}^{N} d_{nt}, \ \forall t \tag{7.9}$$

$$-K_{ij} \le \sum_{n=1}^{N} L_{ij}^{n} \Big(\sum_{\ell\in\mathcal{G}_n} x_{\ell t} + r_{nt} - d_{nt} \Big) \le K_{ij}, \quad \forall (i,j) \in \mathcal{A}, \forall t \tag{7.10}$$

$$y_{it}, o_{it}, s_{it} \in \{0,1\}, \forall i \in \mathcal{G}, \forall t \tag{7.11}$$

where $f_{it}(x_{it})$ represents the fuel cost function, which is a nondecreasing quadratic function and expressed as $f_{it}(x_{it}) = a_i y_{it} + b_i x_{it} + c_i (x_{it})^2$, constraints (7.2) (respectively constraints (7.3)) describe the minimum up (respectively minimum down) time restrictions, constraints (7.4) (respectively constraints (7.5)) describe the start-up (respectively shut-down) operations, constraints (7.6) describe the upper and lower limits of the power output of generator i if it is on in time period t, constraints (7.7) (respectively (7.8)) describe the ramping-up and start-up (respectively ramping-down and shut-down) ramp rate limit restrictions as described in [133], constraints (7.9) ensure the power grid flow balance, and constraints (7.10) describe the transmission capacity limit restrictions

as described in [134] and [135]. Note here that the fuel cost function $f_{it}(\cdot)$ can be approximated by a piecewise linear function (see, e.g., [120]). Under this approximation, the above program can be reformulated as a mixed-integer linear program. For notational brevity, we group the binary decision variables to be y, $y \in \mathbb{B}^q$ with $\mathbb{B} = \{0, 1\}$. Moreover, we group the continuous decision variables to be x, $x \in \mathbb{R}^m_+$. The corresponding abstract unit commitment model for a fixed wind power output r is shown as follows:

$$\mathcal{Q}(r) = \min_{(y,x)\in\mathcal{M}(r)} c(y) + f(x), \tag{7.12}$$

$$\text{where } \mathcal{M}(r) = \Big\{(y, x) \in \mathbb{B}^q \times \mathbb{R}^m_+ : Ay \le b, \tag{7.13}$$

$$Gx + Dr \le d, \tag{7.14}$$

$$Wy + Hx \le h\Big\}. \tag{7.15}$$

In the above formulation, A, G, D, W and H are given matrices, and b, d, and h are given vectors of parameters. Functions $c(y)$ and $f(x)$ represent the transition and dispatching costs, respectively. Constraint (7.13) represents the minimum up/down time constraints, and the start-up and shut-down operations. Constraint (7.14) collects the power flow balance constraints and the transmission capacity limits. Constraint (7.15) describes the upper and lower bounds of power output of generators, and the ramping-up/-down rate limit restrictions.

In practice, for ISOs, the unit commitment and economic dispatch is a two-stage decision process. In the first stage (e.g., day-ahead market), the commitment schedule y is determined without the knowledge of real-time wind power. The dispatching amount x is a recourse in the second stage (e.g., real-time market) after the wind power is observed.

For the uncertain wind power output parameter r, we assume it is unknown and is within an uncertainty set $\mathcal{R}$. In this research, we consider a parametric polyhedral uncertainty set $\mathcal{R}$ defined below (cf. [136]):

$$\mathcal{R} = \Big\{r : \quad R^\ell_{nt} \le r_{nt} \le R^u_{nt}, \forall n \in \mathcal{N}, \forall t, \tag{7.16}$$

$$\sum_{n=1}^{N} w_{nt} r_{nt} \ge \bar{w}_t, \forall t, \tag{7.17}$$

$$\sum_{n=1}^{N}\sum_{t=1}^{T} w_{nt} r_{nt} \ge \bar{w}_0\Big\}, \tag{7.18}$$

where the indices n and t represent buses and discretized time periods. Constraints (7.16) restrict wind power r_{nt} for each time period t at each bus n between a lower bound R^ℓ_{nt} and an upper bound R^u_{nt}. Constraints (7.17) describe the lower bound for the total weighted wind power of all the buses in each single period t, where w_{nt} represents the weight of r_{nt}. Similarly, constraints (7.18) describe the lower bound for the total weighted wind power of all the buses in the whole operational time interval. Note that the parameters in $\mathcal{R}$ can be easily obtained from historical data. For instance, we can set R^ℓ_{nt} and R^u_{nt} equal to the .05 and .95-quantiles of the wind power forecast, respectively, and we can similarly obtain the values of $\bar{w}_t$ and $\bar{w}_0$. For example, if $w_{nt} = 1, \forall n, \forall t$,

we can set $\bar{w}_t$ equal to the .40-quantile of the total wind power forecast in time period t, and $\bar{w}_0$ equal to the .20-quantile of the total wind power forecast in the whole operational time interval.

In this research, we study the minimax regret model. For a fixed first-stage decision y, the maximum regret $\text{Reg}(y)$ is defined as

$$\text{Reg}(y) := \max_{r\in\mathcal{R}}\Big\{\min_{x\in\mathcal{M}(y,r)}\{c(y)+f(x)\} - \mathcal{Q}(r)\Big\}, \tag{7.19}$$

where $\mathcal{M}(y,r)$ is the feasible region of economic dispatch amount x given fixed wind power r and schedule y, i.e., $\mathcal{M}(y,r) = \{x \in \mathbb{R}^m_+ : (7.14), (7.15)\}$. In this definition, the term $\min_{x\in\mathcal{M}(y,r)}\{c(y)+f(x)\}$ evaluates the minimum total cost by adjusting the dispatch amount for a given unit commitment decision y, and $\mathcal{Q}(r)$ represents the minimum perfect-information total cost by deciding the unit commitment and dispatch amount after the uncertain wind power amount is realized to be r for this scenario (see (7.12) for comparison). Thus, $\text{Reg}(y)$ evaluates the worst-case regret over all the possible realizations of wind power r within the uncertainty set. In this research, we minimize $\text{Reg}(y)$ by making the best first-stage decision y, i.e.,

$$\begin{aligned}
\text{(MRP)}\quad z^{\text{MRP}} = \min_{y}\ & \text{Reg}(y) && && (7.20)\\
\text{s.t.}\ & Ay \le b, && && (7.21)\\
& \mathcal{M}(y,r) \neq \emptyset, && \forall r\in\mathcal{R} && (7.22)\\
& y \in \mathbb{B}^q. && && (7.23)
\end{aligned}$$

We call the above formulation Minimax Regret Problem (MRP). Constraints (7.22) are the feasibility constraints of y. Specifically, in the unit commitment problem, they are the security restrictions that for all realizations of the wind power in the uncertainty set, there are feasible second stage dispatching solutions.

To illustrate the differences, we present the robust optimization model, denoted as (RO), and the traditional two-stage stochastic programming formulation (SP) for comparison. (RO) contains the same constraint set as the one in (MRP) and a different objective function in the form $z^{\text{RO}} = \min_y \text{Val}(y)$, where $\text{Val}(y)$ is defined as the worst-case cost, instead of the worst-case regret, i.e., $\text{Val}(y) := \max_{r\in\mathcal{R}}\Big\{\min_{x\in\mathcal{M}(y,r)}\{c(y)+f(x)\}\Big\}$. The abstract (SP) can be described as follows:

$$\begin{aligned}
\text{(SP)}\quad \min_{y,x}\ & c(y) + \sum_{s\in S} p_s f(x_s) && && \\
\text{s.t.}\ & Ay \le b, && && \\
& (y, x_s) \in \mathcal{M}(r_s), && \forall s\in S && (7.24)\\
& y \in \mathbb{B}^q, x_s \in \mathbb{R}^m_+, && \forall s\in S &&
\end{aligned}$$

where S is the set of scenarios and p_s is the probability of the scenario $s \in S$. We treat all the wind power scenarios in the set S equally, i.e., we let $p_s = 1/N$ if a total of N random samples are generated. Decision variables x_s and parameters r_s are the dispatching decision and wind power amount in scenario s, respectively. Constraints (7.24) are the collection of constraints (7.14) and (7.15) for each scenario $s \in S$. A major difference between (MRP) (i.e., equations (7.20)-(7.23))

and (SP) is the objective. (MRP) strives to minimize the maximum deviation from the total cost based on the perfect-information solution whereas (SP) strives to minimize the total expected cost.

7.3 Solution Methodology

In this section, we develop a Benders' decomposition framework to solve the minimax regret problem (MRP) (i.e., equations (7.20)-(7.23)). First, we describe how to obtain a reformulation of (MRP), upon which we can apply a Benders' decomposition framework. We also formulate the master problem and subproblem in this framework. Second, we describe the detailed algorithm by deriving both feasibility and optimality cuts in the Benders' decomposition framework. Third, we describe lower and statistical upper bounds that can be generated by our proposed algorithm.

7.3.1 Reformulation of the objective function

To solve the minimax regret problem (MRP), we first reformulate the objective function $\text{Reg}(y)$ (i.e., equation (7.19)) by combining the inner optimization problems as follows:

$$\text{Reg}(y) = c(y) + \max_{r\in\mathcal{R}}\Big\{\min_{x\in\mathcal{M}(y,r)}\{f(x)\} - \mathcal{Q}(r)\Big\} \tag{7.25}$$

$$= c(y) + \max_{r\in\mathcal{R}}\Big\{\min_{x\in\mathcal{M}(y,r)}\{f(x)\}- \min_{(\bar{x}_r,\bar{y}_r)\in\mathcal{M}(r)}\{c(\bar{y}_r) + f(\bar{x}_r)\}\Big\} \tag{7.26}$$

$$= c(y) + \max_{r\in\mathcal{R}}\Big\{\max_{(\lambda,\mu)\in\mathcal{H}(y,r)}\{\mu^\top(h - Wy)+ \lambda^\top(d - Dr)\} - \min_{(\bar{x}_r,\bar{y}_r)\in\mathcal{M}(r)}\{c(\bar{y}_r) + f(\bar{x}_r)\}\Big\} \tag{7.27}$$

$$= c(y) + \max_{(r,\lambda,\mu,\bar{x}_r,\bar{y}_r)\in\mathcal{R}\times\mathcal{H}(y,r)\times\mathcal{M}(r)}\Big\{\mu^\top(h - Wy)+ \lambda^\top(d - Dr) - c(\bar{y}_r) - f(\bar{x}_r)\Big\}, \tag{7.28}$$

where (7.25) takes the constant $c(y)$ out of the inner problem, (7.26) follows the definition of $\mathcal{Q}(r)$, (7.27) takes the Lagrangian dual (where λ and μ are dual variables for constraints (7.14) and (7.15) respectively, and $\mathcal{H}(y,r)$ represents the feasible region of the dual problem), and (7.28) combines all the maximization operators. Note here that r is a decision variable in (7.26), and $(\bar{x}_r, \bar{y}_r)$ represents the perfect information solution corresponding to r. Note also we have taken advantage of strong duality of linear programs in (7.27), as we model the fuel cost $f(x)$ as a convex piecewise linear function. We let (SUB) represent the embedded maximization problem in equation (7.28),

$$\text{(SUB)} \quad \max_{\mu,\lambda,r,\bar{x}_r,\bar{y}_r} \ \mu^\top(h - Wy) + \lambda^\top(d - Dr) - c(\bar{y}_r) - f(\bar{x}_r) \tag{7.29}$$

$$\text{s.t. } r \in \mathcal{R}, \tag{7.30}$$

$$(\lambda, \mu) \in \mathcal{H}(y, r), \tag{7.31}$$

$$(\bar{x}_r, \bar{y}_r) \in \mathcal{M}(r). \tag{7.32}$$

We notice that the optimal objective value of (SUB) is a function of y, and we denote it as $z^{\text{SUB}}(y)$. Furthermore, we can observe that $z^{\text{SUB}}(y)$ is a convex function of variable y, because it can be represented as the maximum of linear functions of variable y as shown in equation (7.29).

Based on the above explanation, we can rewrite (MRP) (i.e., equations (7.20)-(7.23)) as follows, denoted as (MMR).

$$
\begin{aligned}
(\text{MMR}) \quad \min_{y,\theta} \quad & c(y) + \theta && (7.33)\\
\text{s.t.} \quad & Ay \le b, && (7.34)\\
& \mathcal{M}(y,r) \neq \emptyset, \ \ \forall r \in \mathcal{R}, && (7.35)\\
& \theta \ge \mu^\top (h - Wy) + \lambda^\top (d - Dr) \\
& \quad - c(\bar{y}_r) - f(\bar{x}_r), \\
& \forall (r, \lambda, \mu, \bar{x}_r, \bar{y}_r) \in \mathcal{R} \times \mathcal{H}(y,r) \times \mathcal{M}(r), && (7.36)\\
& y \in \mathbb{B}^q, && (7.37)
\end{aligned}
$$

where θ is an auxiliary variable representing $z^{\text{SUB}}(y)$. Accordingly, to solve (MRP), we can solve the equivalent formulation (MMR). To solve (MMR), we can apply the Benders' decomposition framework, where we first solve a relaxation of (MMR) by relaxing all the constraints (7.35) and (7.36), and then gradually adding them back if they are violated by the solution obtained in the current iteration. Therefore, the initial master problem before we add in any cuts in the Benders' decomposition framework is (MMR) without constraints (7.35) and (7.36). In the algorithm framework, we denote this initial master program as $(\text{MMR})_0$. Note here that one way of finding violated constraints (7.36) in the traditional Benders' decomposition is to solve (SUB) (i.e., equations (7.29)-(7.32)) to global optimality. However, in this research (SUB) is a bilinear mixed integer program because of the term $\lambda^\top r$ and the binary decision variable $\bar{y}_r$. Therefore, the convexity for the subproblem in the traditional Benders' decomposition does not hold here. Meanwhile, noting that (SUB) is typically very hard to solve, we do not solve it to optimality like in the traditional Benders' decomposition. Instead, we build Benders' cuts by utilizing feasible solutions to (SUB), as introduced in detail in Section 7.3.2.

7.3.2 Algorithm framework

We consider both feasibility and optimality cuts in our Benders' decomposition framework as described in [137] (cf. pages 412-414). In this subsection, we first describe how to obtain the feasibility and optimality cuts for the Benders' decomposition framework. Then, we derive lower and statistical upper bounds for the problem and summarize the algorithm.

Feasibility cuts. We call $y \in \mathbb{B}^n$ feasible if $\mathcal{M}(y,r) \neq \emptyset$ for each $r \in \mathcal{R}$. We now develop a cutting plane to cut off the infeasible solutions. First, we construct, for given $\hat{y} \in \mathbb{B}^n$ and $\hat{r} \in \mathcal{R}$, the following feasibility check problem, based on constraints (7.14) and (7.15):

$$
\begin{aligned}
(\text{FC}) \quad \theta^{\text{FC}} = \min_{x,w,z \ge 0} \quad & e^\top w + e^\top z \\
\text{s.t.} \quad & Gx - w \le d - D\hat{r}, && (\lambda_{\text{FC}})\\
& Hx - z \le h - W\hat{y}, && (\mu_{\text{FC}})
\end{aligned}
$$

where the vector e represents the vector with all components 1 in appropriate dimensions, and λ_{FC}

and μ_{FC} are the corresponding dual variables. It is clear that $\theta^{\text{FC}} > 0$ if and only if $\mathcal{M}(\hat{y}, \hat{r}) = \emptyset$. Using the strong duality of linear programming problems, we know that these conditions are further equivalent to $\hat{\lambda}_{\text{FC}}^\top (d - D\hat{r}) + \hat{\mu}_{\text{FC}}^\top \big(h - W\hat{y}\big) > 0$, where $\hat{\mu}_{\text{FC}}$ and $\hat{\lambda}_{\text{FC}}$ are the optimal dual variables to (FC). Hence, for a given $(\hat{y}, \hat{\theta})$ obtained from (MMR), if $\theta^{\text{FC}} > 0$, the cutting plane

$$\big(\hat{\mu}_{\text{FC}}^\top W\big) y \geq \hat{\lambda}_{\text{FC}}^\top (d - D\hat{r}) + \hat{\mu}_{\text{FC}}^\top h \tag{7.38}$$

can be added into (MMR) to cut off the infeasible $\hat{y}$.

Optimality cuts. We develop optimality cuts to cut off the current master program solution $(\hat{y}, \hat{\theta})$ by solving the corresponding subproblem (SUB) (i.e., equations (7.29)-(7.32)) to local optimality. Suppose that we have obtained a feasible solution $(\hat{\lambda}, \hat{\mu}, \hat{r}, \bar{x}'_r, \bar{y}'_r)$ to (SUB) with objective value $\hat{\theta}'$. If $\hat{\theta}' > \hat{\theta}$, then we can simply add the following constraint into (MMR) to cut off solution $(\hat{y}, \hat{\theta})$:

$$\theta \geq -\big(\hat{\mu}^\top W\big) y + \Big(\hat{\mu}^\top h + \hat{\lambda}^\top (d - D\hat{r}) - c(\bar{y}'_r) - f(\bar{x}'_r)\Big). \tag{7.39}$$

Separation procedure (finding violated cuts). Given $(\hat{y}, \hat{\theta})$, we now discuss how to find violated feasibility/optimality cuts, which we call the separation procedure:

1. Initialize $\hat{r}$ equal to its mean value $\bar{R} \in \mathcal{R}$ and $(\bar{x}'_r, \bar{y}'_r) \in \mathcal{M}(\hat{r})$.

2. Define the value functions

$$\begin{aligned} \theta_1(\hat{r}, \bar{x}'_r, \bar{y}'_r) = & \max_{(\lambda,\mu)\in\mathcal{H}(y,r)} \Big\{ (h - W\hat{y})^\top \mu + (d - D\hat{r})^\top \lambda \Big\} \\ & - c(\bar{y}'_r) - f(\bar{x}'_r), \end{aligned} \tag{7.40}$$

$$\begin{aligned} \theta_2(\hat{\lambda}, \hat{\mu}) = & \max_{(r,\bar{x}_r,\bar{y}_r)\in\mathcal{R}\times\mathcal{M}(r)} \Big\{ -(\hat{\lambda}^\top D) r - c(\bar{y}_r) - f(\bar{x}_r) \Big\} \\ & + \hat{\mu}^\top (h - W\hat{y}) + \hat{\lambda}^\top d. \end{aligned} \tag{7.41}$$

3. Initialize $\theta_1 \leftarrow 0$ and $\theta_2 \leftarrow 1$.
   While $(\theta_1 \neq \theta_2)$ Do

   (i) Solve (FC) and obtain a θ^{FC}. If $\theta^{\text{FC}} > 0$, we have found a violated feasibility cut in the form of (7.38) and stop; otherwise, go to (ii).

   (ii) Solve (7.40) to optimality. Let $\theta_1 = \theta_1(\hat{r}, \bar{x}'_r, \bar{y}'_r)$, and denote the optimal solution to be λ^* and μ^*. Update $\hat{\lambda} \leftarrow \lambda^*$ and $\hat{\mu} \leftarrow \mu^*$.

   (iii) Solve (7.41) to optimality. Let $\theta_2 = \theta_2(\hat{\lambda}, \hat{\mu})$, and denote the optimal solution to be r^*, $\bar{x}^*_r$ and $\bar{y}^*_r$. Update $\hat{r} \leftarrow r^*$, $\bar{x}'_r \leftarrow \bar{x}^*_r$ and $\bar{y}'_r \leftarrow \bar{y}^*_r$.

   End While

4. If $\theta_1 > \hat{\theta}$, we have found a violated optimality cut in the form of (7.39).

Note that in the separation procedure, we are applying a bilinear heuristic (cf. [138]) to obtain a local optimal solution to (SUB) (i.e., equations (7.29)-(7.32)), which is a bilinear integer program and can stop in finite steps. Hence, the while loop in Step 3 takes at most finite steps (for

a formal proof, see Proposition 2.3 in [138]). Therefore, we can find a violated cut or decide that no feasibility/optimality cuts can be added in finite steps. Note also that the proposed Benders' decomposition framework terminates in a finite number of steps, i.e., it calls the separation procedure for finite times. This is because variable y admits a finite set of values and from (7.39) it follows that different θ requires different y, so θ can only admit a finite number of values during the progress of the algorithm.

Lower and statistical upper bounds. Since the bilinear programming heuristics cannot guarantee an optimal objective value for the subproblem, accordingly our Benders' decomposition algorithm cannot be guaranteed to converge to the optimal solution of the original minimax regret problem. Instead, what we obtained by employing the separation procedure, is a lower bound (LB) for the original problem. The reason is that by not solving the subproblem to optimality, we might not be able to add all constraints (7.36) in the master program when needed. Thus, we might finally solve a relaxation of (MMR), which provides us a lower bound due to the minimization objective. Now we describe how we can obtain a statistical upper bound (UB) (i.e., UB is a statistical estimate of the worst-case regret) for the original problem by Monte Carlo simulation. To obtain UB, we first fix the unit commitment decision y to be the optimal solution to a relaxed (MMR) in the Benders' decomposition algorithm, and then generate a large number of random wind power output scenarios to evaluate the regrets for the given commitment decision y under different wind power output scenarios. For each wind power sample r, to find the worst-case regret for a given UC solution, we go through the separation procedure displayed in Fig. 7.2 (except for the last step, i.e., comparing the values θ_1 with $\hat{\theta}_K$ and building optimality/feasibility cuts). That is, we generate the random scenario r as the starting point of the separation procedure, and look for the worst-case regret by solving the bilinear subproblem (SUB) to local optimality. Then we update UB by $\max\{\text{UB}, \theta_1\}$, where θ_1 is obtained from the separation procedure. Note here that this requires solving a collection of linear programs and mixed-integer programs. Finally, we assign the largest regret to UB. Hence, UB also serves as a real-time test of worst-case regret for the UC decision we have made. In addition, in this research, we use the Weibull distribution to help generate the random wind power output. We assume that r_{nt} is within the interval $[R^{\ell}_{nt}, R^{u}_{nt}]$ with the mean $\bar{R}_{nt}$ and the standard deviation $(R^{u}_{nt} - R^{\ell}_{nt})/4$. Also, we require the generated wind power output $r \in \mathcal{R}$, as defined in (7.16)-(7.18). In case that the generated sample r does not satisfy equations (7.17)-(7.18), we randomly choose indices n and t to increase the r_{nt} value to R^{u}_{nt} until equations (7.17)-(7.18) are satisfied. Note here that it is also possible to incorporate the actual wind time series (e.g., real wind power data in the past weeks) in the set of wind power scenarios. We summarize the Benders' decomposition algorithm and statistical upper bound calculation in Algorithm BD and Figs. 7.1 and 7.2. In every step of Algorithm BD, $(\text{MMR})_K$ represents (MMR) with the first K Benders' cuts. Finally, we remark that Algorithm BD can provide exact lower bounds and statistical upper bounds for (MMR). Our statistical upper bounds do not guarantee theoretical exactness but can converge to exact upper bounds as the sample size increases in the Monte Carlo simulation.

7.4 Computational Results

In this section, we present numerical experiments of Algorithm BD on a modified IEEE 118-bus power system. Specifically, we apply three methodologies on this system, namely (a) minimax regret, (b) robust, and (c) stochastic optimization approaches. For the minimax regret approach, we employ Algorithm BD. For the robust optimization approach, we implement the methods proposed

Algorithm BD

1. Initialization. Set the iteration number $K \leftarrow 0$. Model (MMR)$_0$ is assigned with only constraints (7.34) and (7.37).
2. Solve the current model (MMR)$_K$ and obtain the optimal solution $(\hat{y}_K, \hat{\theta}_K)$.
3. Employ separation procedure to find a violated feasibility/optimality cut and add the cut to (MMR)$_K$. Denote the updated formulation as (MMR)$_{K+1}$ and update $K \leftarrow K + 1$. Go to 2. If no cuts found, go to 4.
4. Return the optimal solution $(\hat{y}_K, \hat{\theta}_K)$ and the optimal value LB.
5. Obtain UB by Monte Carlo simulation with $\hat{y}_K$.

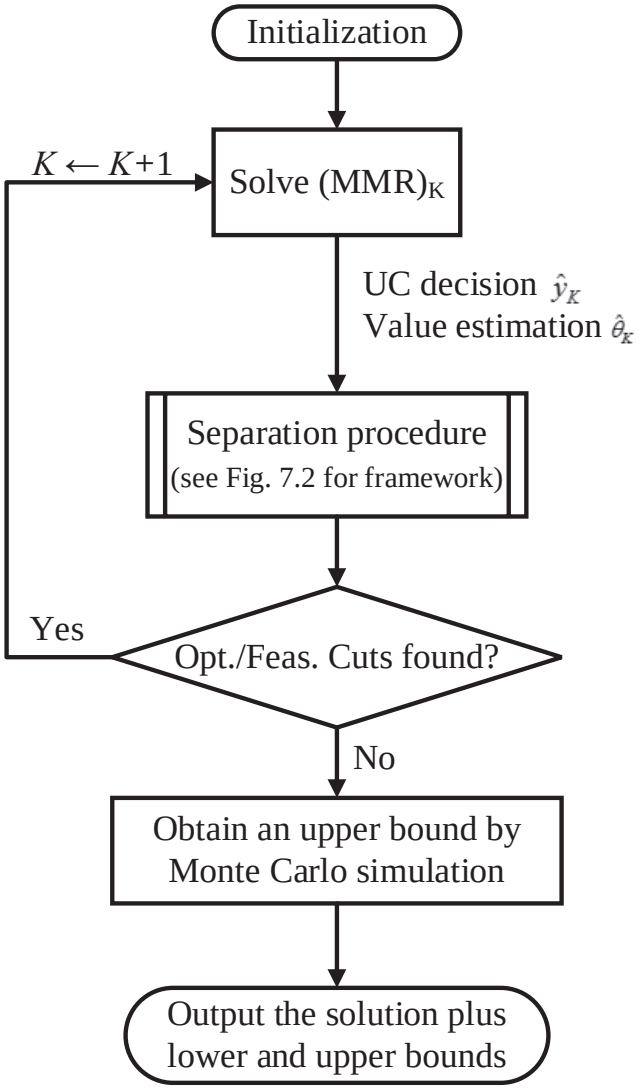

Figure 7.1: Framework of Benders' decomposition algorithm

in [136] for comparison. For the stochastic optimization approach, among algorithms to solve two-stage stochastic UC problems (e.g., see [139] and [53], among others), we apply the sample average approximation (SAA) algorithm proposed in [140] for comparison. All the experiments

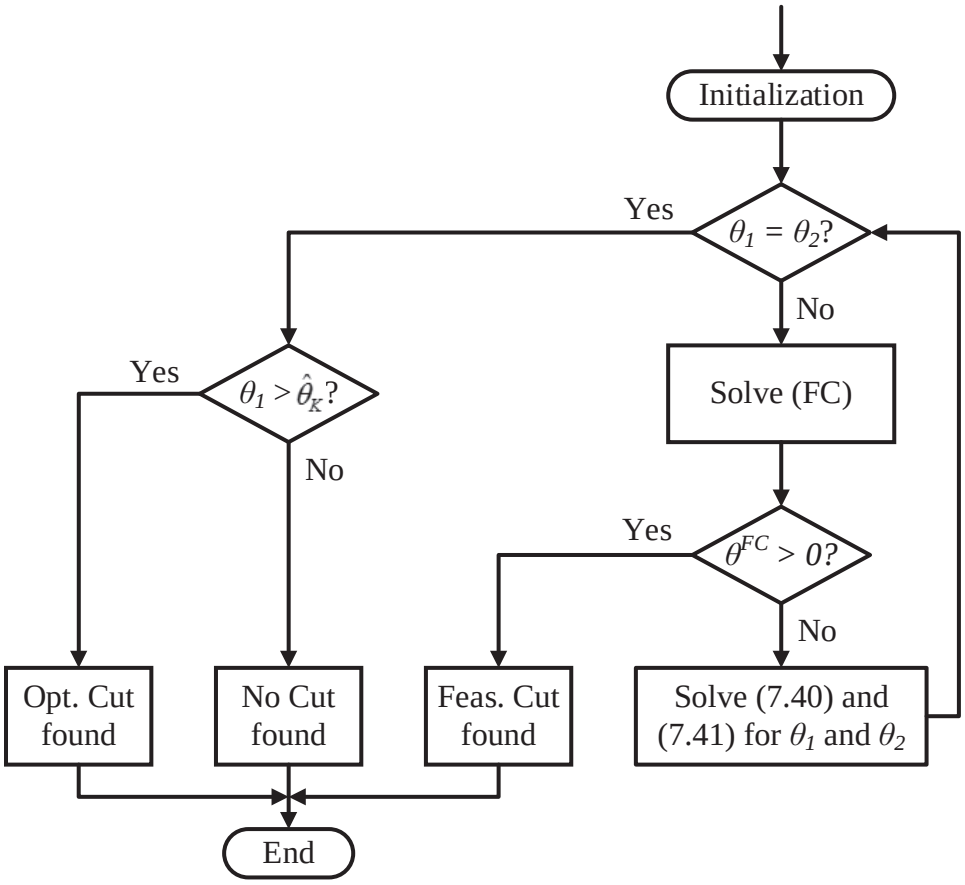

Figure 7.2: Framework of the separation procedure

were implemented by using CPLEX 12.1, at Intel Quad Core 2.40GHz with 8GB memory. We set the time limit to be one hour and the unit penalty cost to be \$7947/MWh (cf. [120]) in the Monte Carlo simulation.

The IEEE 118-bus system consists of 118 buses, 33 thermal generators, and 186 transmission lines. The operational time interval is 24 hours. In order to construct the uncertainty set, we let $\bar{R}_{nt}$ denote the forecasted wind power, and let $R^u_{nt} = 1.2\bar{R}_{nt}$, $R^\ell_{nt} = (1 - \text{Lower}\%)\bar{R}_{nt}$, $\bar{w}_t = (1 - \text{Budget}\%) \sum_{n=1}^{N} \bar{R}_{nt}$, and $\bar{w}_0 = (1 - \text{Overall}\%) \sum_{t=1}^{T} \sum_{n=1}^{N} \bar{R}_{nt}$. In this experiment, we first compare the optimal solutions obtained from different approaches under a given data setting to explore the insights of different approaches. Then we run numerical experiments to compare the worst-case regret and the expected total cost of the optimal solutions obtained by different methodologies under various data settings by adjusting the values of Lower%, Budget%, and Overall%. To verify the effectiveness of the proposed algorithm, we provide the following lower and statistical upper bounds on regrets:

(1) Lower bound LB of the minimax regret problem: The objective value obtained from Algorithm BD, i.e., by using the bilinear heuristics to solve the minimax regret UC problem.

(2) Statistical upper bound UB of the minimax regret problem: As shown in Section 7.3.2, we provide a statistical bound derived by Monte Carlo simulation. Besides, UB also serves as

a real-time economic dispatch with known wind power output information to calculate the worst-case regret.

(3) Statistical upper bound R_{rob} of the maximum regret obtained by the robust optimization approach: For this case, R_{rob} represents the worst-case regret incurred by the robust optimal solution. To obtain R_{rob}, we first fix y to be the robust optimal solution, and then generate a large number of random scenarios to estimate the worst-case regret as we did in obtaining UB.

(4) Statistical upper bound R_{sto} of the maximum regret obtained by the stochastic optimization approach: In this case, R_{sto} evaluates the worst-case regret incurred by the stochastic optimal solution. To obtain R_{sto}, we first fix y to be the stochastic optimal solution, and then generate a large number of random scenarios to estimate the worst-case regret as we did in obtaining UB and R_{rob}.

(5) The expected total cost A_{reg} obtained by the minimax regret approach: In this case, A_{reg} evaluates the average performance of the minimax regret optimal solution. To obtain A_{reg}, we first fix y to be the minimax regret optimal solution, and then generate a large number of random scenarios to estimate the total costs incurred by the given solution y under different wind power output scenarios. Finally, we assign the average of the total costs to A_{reg}.

(6) The expected total cost A_{rob} obtained by the robust optimization approach: In this case, A_{rob} evaluates the average performance of the robust optimal solution. To obtain A_{rob}, we first fix y to be the robust optimal solution, and then generate a large number of random scenarios to estimate the expected total costs as we did in obtaining A_{reg}.

(7) The expected total cost A_{sto} obtained by the stochastic optimization approach: In this case, A_{sto} evaluates the average performance of the stochastic optimal solution. To obtain A_{sto}, we first fix y to be the stochastic optimal solution, and then generate a large number of random scenarios to estimate the expected total costs as we did in obtaining A_{reg}.

Along with the computational results, we verify the effectiveness of the proposed algorithm and compare the worst-case regrets and the expected total cost of the solutions obtained from different methodologies by evaluating the following gaps:

(1) Opt. Gap $= (\text{UB} - \text{LB})/\text{LB} \times 100\%$. It estimates the optimality gap of the minimax regret solution obtained from Algorithm BD.

(2) Rob. Gap $= (R_{rob} - \text{UB})/\text{UB} \times 100\%$. It estimates the difference of worst-case regrets between the robust optimal solution and the minimax regret solution.

(3) Sto. Gap $= (R_{sto} - \text{UB})/\text{UB} \times 100\%$. It estimates the difference of the worst-case regrets between the stochastic optimal solution and the minimax regret solution.

(4) Reg. Inc. $= (A_{reg} - A_{sto})/A_{sto} \times 100\%$. It estimates the increase of the expected total cost incurred by the minimax regret optimal solution, as compared to the stochastic optimal solution.

(5) Rob. Inc. $= (A_{rob} - A_{sto})/A_{sto} \times 100\%$. It estimates the increase of the expected total cost incurred by the robust optimal solution, as compared to the stochastic optimal solution.

The computational results and the gap estimates are presented in Tables 7.2-7.5 and Fig. 7.3. In these experiments, we first compare the optimal solutions obtained from the three different approaches under the data setting Lower%=20%, Budget%=4% and Overall%=36% (see Table 7.2 and Fig. 7.3). Then, we run a group of sensitivity analyses by adjusting Lower% within the range $[10\%, 40\%]$ and Budget% within the range $[4\%, 40\%]$, while Overall% is fixed at 36% (see Tables 7.3 and 7.4). In another group of sensitivity analysis, we fix Lower% at 40% and allow Budget% and Overall% to vary within the intervals $[10\%, 40\%]$ and $[4\%, 40\%]$, respectively. We obtain similar results which are therefore not reported for brevity.

Table 7.2: Optimal solutions obtained from the three different approaches, with Lower%=20%, Budget%=4%, and Overall%=36%

Time	# Online Generators			Total Capacity (MW)			Nominal
Period	Sto	Reg	Rob	Sto	Reg	Rob	Load (MW)
1	14	14	14	4290	4290	4290	2246.03
2	14	14	14	4290	4290	4290	2117.69
3	14	14	14	4290	4290	4290	1861.00
4	14	14	14	4290	4290	4290	1283.45
5	14	14	14	4290	4290	4290	1604.31
6	14	14	15	4290	4290	4390	1925.17
7	16	16	16	4590	4590	4590	2246.03
8	16	16	18	4590	4590	4790	2502.72
9	17	17	19	4690	4690	4890	2631.07
10	17	17	19	4690	4690	4890	2823.59
11	17	17	19	4690	4690	4890	2855.67
12	17	17	19	4690	4690	4890	2695.24
13	17	17	19	4690	4690	4890	2566.90
14	17	17	19	4690	4690	4890	2438.55
15	17	18	19	4690	4790	4890	2823.59
16	17	18	19	4690	4790	4890	2887.76
17	17	18	19	4690	4790	4890	2727.33
18	18	19	19	4790	4890	4890	2855.67
19	18	19	19	4790	4890	4890	3016.10
20	18	19	19	4790	4890	4890	3144.45
21	18	19	19	4790	4890	4890	3208.62
22	18	19	19	4790	4890	4890	2887.76
23	18	18	19	4790	4790	4890	2791.50
24	17	17	19	4690	4690	4890	2631.07

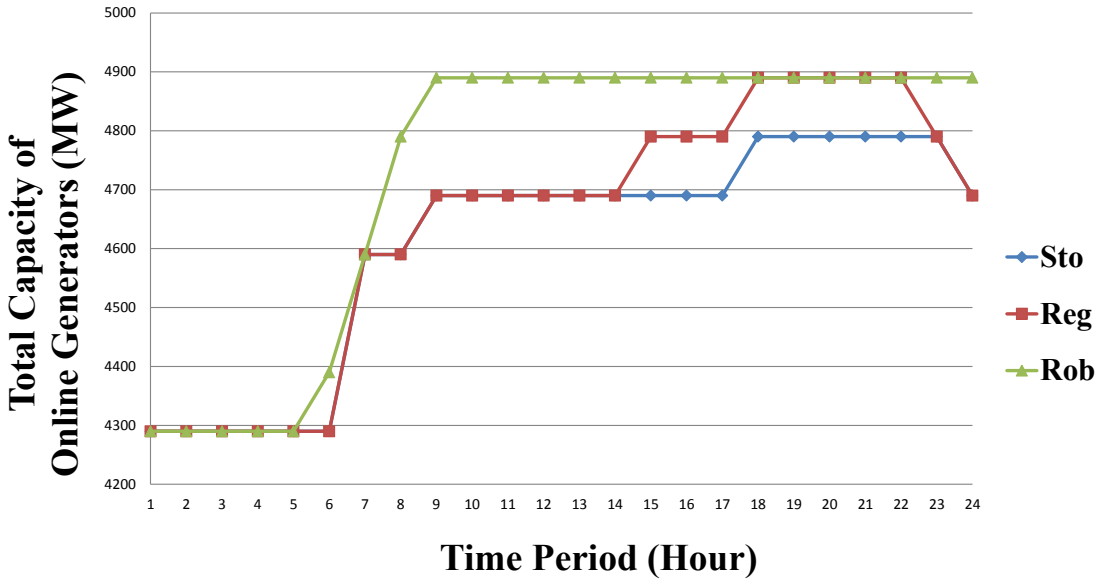

Figure 7.3: Comparison of the total capacity of the online generators

From Table 7.2 and Fig. 7.3, we observe that the robust optimal solution is the most conservative and the stochastic optimal solution is the least conservative in terms of both the number of online generators and the total generation capacity. The optimal solution obtained from the minimax regret approach lands somewhere in between the robust and stochastic optimal solutions. For example, when the net forecast load (difference of the forecasted load and the forecasted wind power) peaks in time periods 18-22, the minimax regret optimal solution agrees with the robust one, while in the remaining time periods, it runs in between the robust and stochastic optimal solutions (e.g., in time periods 15-17) or even equal to the stochastic one. Note here that in time periods 18-22, the stochastic optimal solution is infeasible for some Monte Carlo simulation scenarios due to lack of generation capacity.

From Table 7.3, we first observe that statistically our algorithm can provide a feasible solution in all the instances, inferred from the fact that both LB and UB values are significantly lower than the surging R_{sto} values in Table 7.4. Second, we notice that in most instances, Algorithm BD solves the UC problem to within a 1% optimality gap before touching the one-hour time limit. This indicates that the proposed algorithm can provide a solution that is very close to the optimal one within a reasonable amount of time. Hence, our algorithm suffices to solve reasonable size problems and find near-optimal solutions. Besides, the small optimality gaps confirm that the UB listed in Table 7.3 is a reasonable estimate of the worst-case regret of the minimax regret solution. Noting that UB is a statistical upper bound of the worst-case regret for a given UC solution, in the following, we use UB as a benchmark to compare the worst-case regrets obtained from different approaches.

The worst-case regrets obtained from the three different approaches are listed and compared in Table 7.4. From this table, we observe that UB is strictly less than R_{rob} and R_{sto} in all the instances. For the robust optimization approach, we find that it provides feasible solutions in all the instances

Table 7.3: Computational results for an IEEE 118-bus system with various Lower% and Budget% - minimax regret approach

			Budget			
			4	16	28	40
Lower	10	LB	1275	1267	1267	1267
		UB	1275	1278	1278	1278
		Opt. Gap (%)	0.01	0.86	0.86	0.86
		Time (s)	3468.16	3068.14	3068.14	3068.14
	20	LB	2102	3055	3377	3377
		UB	2117	3083	3386	3386
		Opt. Gap (%)	0.73	0.93	0.26	0.26
		Time (s)	3353.83	3173.75	3599.13	3599.13
	30	LB	2878	4441	4435	5386
		UB	2893	4445	4459	5530
		Opt. Gap (%)	0.52	0.11	0.54	2.68
		Time (s)	3396.56	3069.52	3489.92	3599.89
	40	LB	3030	5446	5458	6687
		UB	3030	5530	5496	6738
		Opt. Gap (%)	0.00	1.54	0.70	0.75
		Time (s)	2119.85	3082.97	3045.23	2921.33

while the robust gaps are not negligible. For the stochastic optimization approach, we see that it provides feasible solutions to the UC problem when the wind power uncertainty is restricted (e.g., when Lower% $\leq 30\%$ or Budget% $\leq 4\%$ in Table 7.4), while the stochastic optimal solutions become infeasible when the wind power uncertainty gets larger (e.g., when Lower% $= 40\%$ in Table 7.4), which contributes to the surging worst-case regrets. By comparing UB with R_{rob} and R_{sto}, we observe that the regrets can stem from both over-conservatism and infeasibility. On one hand, the robust optimization approach can provide robust UC solutions, but might be over-conservative in that it underlines the scenarios with large absolute costs (but not those with high regrets), and so implicitly commits more units. In contrast, the minimax regret approach avoids being overly pessimistic on the extreme cases by addressing the regrets explicitly, and thus performs less conservatively. On the other hand, the UC solutions provided by the stochastic optimization approach might become unreliable as the wind power uncertainty becomes significant. A possible explanation for this observation is that it is not easy for the stochastic UC to accommodate the "ramp events", which refer to dramatic changes in wind plant power output in a short period of time caused by big shifts in wind speed, due to, e.g., a fast-moving weather front [141]. Under this case, the wind power can drop from a very high value to near zero and vice versa and it can cause severe impacts to the power system. The reasons are as follows: (a) the "ramp events" are hard to predict since they might come from complicated weather conditions; (b) the "ramp events" are usually unlikely to happen, and hence less possible to be picked out through typical sampling algorithms for stochastic UC. Consequently, as the magnitude of the "ramp events" increases, stochastic UC provides less robust solutions. On the contrary, minimax regret and robust optimization approaches provide robust UC solutions, because those "ramp events" can be conveniently

Table 7.4: Computational results for an IEEE 118-bus system with various Lower% and Budget% - worst-case regrets comparison

			Budget			
			4	16	28	40
Lower	10	UB	1275	1278	1278	1278
		R_{rob}	2244	1509	1509	1509
		R_{sto}	1336	1340	1340	1340
		Rob. Gap (%)	76.00	18.09	18.09	18.09
		Sto. Gap (%)	4.82	4.83	4.83	4.83
	20	UB	2117	3083	3386	3386
		R_{rob}	2517	3582	4764	4764
		R_{sto}	2533	235690	270362	270362
		Rob. Gap (%)	18.90	16.19	40.71	40.71
		Sto. Gap (%)	19.61	7544.24	7885.42	7885.42
	30	UB	2893	4445	4459	5530
		R_{rob}	3255	4948	5627	5898
		R_{sto}	3491	727549	1374106	1664217
		Rob. Gap (%)	12.49	11.31	26.20	6.66
		Sto. Gap (%)	20.66	16266.96	30715.99	29992.67
	40	UB	3030	5530	5496	6738
		R_{rob}	4195	6410	7418	9386
		R_{sto}	5619	1100992	1973001	4005551
		Rob. Gap (%)	38.44	15.91	34.96	39.30
		Sto. Gap (%)	85.45	19808.89	35797.98	59350.88

captured by defining appropriate uncertainty sets. To sum up, the robust optimization approach is over-conservative and hence sacrifices the regret for system robustness; the stochastic optimization approach can provide satisfactory solutions under restricted uncertainty scenarios, but might become vulnerable in face of the "ramp events". Finally, the minimax regret approach can provide robust UC solutions in various uncertainty scenarios, and meanwhile prevent over-conservatism.

The expected total costs obtained from the three different approaches are listed and compared in Table 7.5. From this table, we first observe that A_{sto} is strictly less than A_{reg} and A_{rob} in all the instances, which confirms that the stochastic optimization approaches can provide the best UC solution in terms of the expected total cost. Second, we can observe that the increase of the expected total cost, if we employ the minimax regret approach, is not large. Indeed, the increased values by the minimax regret approach (denoted by Reg. Inc.) shown in Table 7.5 is less than 1% for all the instances. The robust optimization approach performs the worst (denoted by Rob. Inc.). However, it is still less than 2% in all the instances. Hence, we can conclude that the price of robustness is limited in this experiment. That is, we can increase system robustness, with a reasonable increase of the expected total cost, by employing the alternative approach such as the minimax regret approach. Finally, due to the observation that the increased value by the minimax regret approach is less than that by the robust optimization approach in most instances, the minimax regret approach is less conservative than the robust optimization approach, and can be applied to

increase system robustness with a smaller increase of the expected total cost.

Table 7.5: Computational results for an IEEE 118-bus system with various Lower% and Budget% - expected total cost comparison

			Budget			
			4	16	28	40
Lower	10	A_{reg}	1210397	1210520	1210520	1210520
		A_{rob}	1210501	1201278	1201278	1201278
		A_{sto}	1208485	1198661	1198661	1198661
		Reg. Inc. (%)	0.16	0.99	0.99	0.99
		Rob. Inc. (%)	0.17	0.22	0.22	0.22
	20	A_{reg}	1211643	1211725	1212986	1212986
		A_{rob}	1215168	1215260	1216236	1216236
		A_{sto}	1210934	1210944	1210949	1210949
		Reg. Inc. (%)	0.06	0.06	0.17	0.17
		Rob. Inc. (%)	0.35	0.36	0.44	0.44
	30	A_{reg}	1211954	1220400	1220318	1221371
		A_{rob}	1218692	1222001	1228323	1228500
		A_{sto}	1211079	1212817	1218103	1218621
		Reg. Inc. (%)	0.07	0.63	0.18	0.23
		Rob. Inc. (%)	0.63	0.76	0.84	0.81
	40	A_{reg}	1222215	1225807	1224903	1226850
		A_{rob}	1232798	1228238	1241572	1246943
		A_{sto}	1211166	1221040	1222750	1226766
		Reg. Inc. (%)	0.91	0.39	0.18	0.01
		Rob. Inc. (%)	1.79	0.59	1.54	1.64

7.5 Conclusion and Future Research

In this research, we proposed an innovative approach to solve unit commitment problems under uncertainty. First, we provided an uncertainty set description that can capture the "ramp events" in wind power output randomness, and our proposed minimax regret approach can provide robust while less conservative UC solutions. Second, with the consideration of regret under each scenario, our proposed approach avoids over-conservatism by minimizing the worst-case regret value. Third, we developed an iterative algorithmic framework which can derive tight lower and statistical upper bounds of the minimax regret. The statistical upper bounds do not guarantee theoretical exactness, but can converge to exact upper bounds as the sample size increases in the Monte Carlo simulation. Finally, our computational results verified the effectiveness of our proposed approach. In future research, we will study large-scale problems involving hundreds of generators and thousands of transmission lines when such data are available. Accordingly, we will develop efficient heuristic and decomposition algorithms and implement the algorithms in high performance computing facilities. Finally, we will extend our minimax regret model to incorporate the n-k security criteria.

8. Data Driven Two-Stage Robust Unit Commitment

8.1 Introduction

Increasing uncertainties in the power grid are continuously challenging the current procedure of the power production scheduling due to the high penetration of intermittent renewable resources in the grid and increasing uncertainty from price response demands. The electric power, as a special type of commodity, requires high reliability to guarantee the delivery. Independent System Operators (ISO) traditionally solve a unit commitment (UC) problem to determine the production schedule of the thermal generators for the next 24 hours with minimal total cost, which is referred as day-ahead UC problem. In practice, when the real situation, including load and supply of intermittent resources, is deviating from the expectation as well as generator and transmission outages, the dispatch quantities of the generators are adjusted accordingly by system operators in real time. Such corrective actions may result in significant cost increases as well as unmet demand referred as load shedding. Therefore, a "robust" UC solution is highly desired to be able to efficiently adaptive to different scenarios.

Traditional methods of addressing uncertainty within the UC problem involve committing substantial amounts of spinning and non-spinning reserves to meet any deviations from the expected forecasts. The requirements for spinning reserve are frequently set by deterministic criteria. For example, reserve requirements may be given by: a multiple (usually 1.5 to 2 times) of the largest active generator capacity; a percentage of the peak forecasted load; as well as the 3+5 rule (3% of hourly forecasted load + 5% of hourly forecasted wind power). Much research has been performed in determining appropriate levels of spinning reserves based on various deterministic criteria, [142–144], as well as by incorporating various probabilistic information [145, 146]. These approaches are not guaranteed to maintain system feasibility or to provide system feasibility in a cost efficient manner.

Stochastic programming programming has been introduced to solve the UC problem with a set of scenarios . In stochastic formulations, a set of scenarios are identified. Two stage or multi-stage stochastic programs were studied to adaptively adjust the dispatch solutions when the reality reveals, while determining the unit commitment solutions before the realization of the uncertainties. In a stochastic programming formulation, the corrective solutions for all the scenarios are explicitly modeled and the objective is to minimize the expected cost over all the scenarios. Due to the difficulty of determining exact probability distribution of uncertainty parameters or the complexity of the explicit representation, the sampling average approximation (SAA) method has been widely adapted. The SAA method guarantees the convergence of the optimal solution while the sample size is large enough. However, the large number of samples impose additional computational challenges of the stochastic programming formulations.

Robust optimization is an alternative model to determine the solution under uncertainties. Unlike stochastic programming, robust optimization typically model the uncertainty parameters in a predefined uncertainty set. The objective of robust optimization formulation is to ensure that the solution will be feasible for all possible realization in the uncertainty set and to minimize the worst case commitment and operational cost. The high feasibility requirements in the robust optimization align with the high reliability standard of the power system. Therefore, there are a lot of practice of implementing robust models in the power systems, including unit commitment problem, capacity expansion, and optimal power flow. These work have shown the potential of robust optimization

approaches in the power system application. Most of the work focus on the algorithm developments of the robust formulations for particular problems with a given uncertainty set. Since many of the deterministic formulations of the power system problems are linear or mixed integer linear formulation, polyhedral uncertainty sets are the popular ones to be adopted. The determination of the uncertainty sets is not commonly discussed in the literature. In the robust optimization literature, there are works shown that there are connections with the risk measures with probability constraints. However, there are no much of the guidelines of how these uncertainty sets should be constructed unless from the computational point of view. Recently, A note by Guan and Wang [147] described genetic rules of selecting uncertainty set. Again, these are from statistic study to ensure of the feasibility without consideration of optimality.

One close related discussion is from probability constraints in stochastic programming literature. The probability constraints ensure that the solution will be feasible with a given probability threshold. It has been shown that even for a single linear constraint, the feasible region of probability constraints is not convex. Convex approximation of the uncertainty sets are examined and coherent risk measures are used to approximate the feasible set. One may consider that the feasible solution of robust optimization solution is a solution that satisfies the probability constraints. The corresponding uncertainty set is a set that describes the confidence set of the uncertain parameters. In this chapter, we study two types of polyhedral uncertainty sets that are constructed from historical or simulated data. We propose two types methods to estimate the parameters used in the uncertainty sets based on historical data.

The remainder of this chapter is organized as follows. Section 8.2 provides a description of the nominal and robust UC formulations and a structural description of the uncertainty sets used to represent the demand and wind uncertainties. Section III describes our solution methodology where we adopt a heuristic benders decomposition algorithm described in [136]. In Section IV we give two data-driven uncertainty set formulations for providing probabilistic guarantees on the feasibility of the commitment schedule under demand and wind generator capacity uncertainty. In Section V we provide test results to demonstrate the performance of each uncertainty set. Finally, Section VI concludes our study.

8.2 Mathematical Formulation

A typically formulation of the nominal UC problem is given below. The objective function, given by equation (8.1), is to minimize the sum of the commitment and dispatch costs necessary to satisfy the expected demand forecast. Equation(8.2) represents the startup/shutdown relationships while equations (8.3) and (8.4) represent the generator minimum up/down time requirements. Equations (8.6)-(8.7) give the bounds for the generator startup, shutdown, and commitment status variables. The node balance constraints are given by equations (8.8)-(8.9) and line flow constraints are given by equation (8.10). Equations (8.11) and (8.12) represent the minimum/maximum generation capacity for standard generators and wind generators respectively. The ramp rate constraints are given by equations (8.13) and (8.14). Equations (8.15) and (8.16) describe the limits of generators to provide spinning reserve while equation (8.17) provides the total system requirements for spinning reserve. Equations (8.18) and (8.19) simply fix the demand and wind capacity variables to their expected forecast levels. In this formulation, the wind power is considered dispatchable, which is limited by the available capacity. In certain situation, it can be treated as non-dispatchable, which is commonly model as negative load.

Nominal UC Model

Objective function:

$$z^N := \min \sum_{t\in T}\sum_{g\in G}(c_g^{SU}v_{g,t} + c_g^{NL}u_{g,t} + c_g^v p_{g,t}) \tag{8.1}$$

Constraints:

$$v_{g,t} - w_{g,t} = u_{g,t} - u_{g,t-1}, \qquad \forall g,t; \tag{8.2}$$

$$\sum_{s=t-UT_g+1}^{t} v_{g,s} \le u_{g,t}, \quad \forall g, t \in \{UT_g, ..., T\}, \tag{8.3}$$

$$\sum_{s=t-DT_g+1}^{t} w_{g,s} \le 1 - u_{g,t}, \quad \forall g, t \in \{DT_g, ..., T\}, \tag{8.4}$$

$$0 \le v_{g,t} \le 1, \qquad \forall g,t, \tag{8.5}$$

$$0 \le u_{g,t} \le 1, \qquad \forall g,t, \tag{8.6}$$

$$u_{g,t} \in \{0,1\}, \qquad \forall g,t, \tag{8.7}$$

$$\sum_{g\in G(n)} p_{g,t} + \sum_{w\in W(n)} p_{w,t} - d_{n,t} = p_{n,t}^{Net}, \qquad \forall n,t, \tag{8.8}$$

$$\sum_{n\in N} p_{n,t}^{Net} = 0, \qquad \forall t, \tag{8.9}$$

$$-F_k^{Max} \le \sum_{n\in N} PTDF_k^n p_{n,t}^{Net} \le F_k^{Max}, \qquad \forall k,t, \tag{8.10}$$

$$P_g^{Min} u_{g,t} \le p_{g,t} \le P_g^{Max} u_{g,t}, \qquad \forall g,t, \tag{8.11}$$

$$0 \le p_{w,t} \le P_{w,t}^{Cap}, \qquad \forall w,t, \tag{8.12}$$

$$p_{g,t} - p_{g,t-1} \le (2 - u_{g,t-1} - u_{g,t})R_g^{SU} + (1 + u_{g,t-1} - ug,t)R_g^{+}, \qquad \forall g,t \tag{8.13}$$

$$p_{g,t-1} - p_{g,t} \le (2 - u_{g,t-1} - u_{g,t})R_g^{SD} + (1 - u_{g,t-1} + ug,t)R_g^{-}, \qquad \forall g,t \tag{8.14}$$

$$p_{g,t} + r_{g,t} \le P_g^{Max} u_{g,t} \qquad \forall g,t \tag{8.15}$$

$$0 \le r_{g,t} \le R_g^E \qquad \forall g,t \tag{8.16}$$

$$\sum_{g\in G} r_{g,t} \ge r_t \qquad \forall t, \tag{8.17}$$

$$d_{n,t} = \bar{d}_{n,t}, \qquad \forall n,t, \tag{8.18}$$

$$P_{w,t}^{Cap} = \bar{P}_{w,t}^{Cap}, \qquad \forall w,t, \tag{8.19}$$

In this chapter, we use a three-stage robust UC model to describe the system. The model formulation is given below. The objective function, given by equation (20), is to minimize the sum of the commitment costs and the worst-case dispatch costs over the uncertainty sets $\mathcal{D}$ and $\mathcal{W}^{Cap}$. The constraints in $\chi(u, d, P^{Cap})$ describe the third stage dispatch problem for commitment decision u, demand d, and wind generator capacity P_w^{Cap}.

Robust UC Model

Objective function:

$$z^R = \min_{u,v,w} \left\{ \sum_{t\in T}\sum_{g\in G}(c_g^{SU} v_{g,t} + + c_g^{NL} u_{g,t}) + \max_{d,P^{Cap}} \min_{p\in\chi(u,d,P^{Cap})} \sum_{t\in T}\sum_{g\in G} c_g^v p_{g,t} \right\} \tag{8.20}$$

Constraints: (8.2)-(8.7),

$$d \in \mathcal{D},$$
$$P_w^{Cap} \in \mathcal{W}^{Cap}$$

where $\chi(u, d, P^{Cap}) = \{p : (8.8) - (8.14)$. Note here we omit the reserve constraints in the robust formulation since the uncertain load and wind supply are modeled explicitly using the uncertainty sets.

In this work, we adopt a polyhedral uncertainty set description of the form presented in [136]. To describe the demand uncertainty set we use $\bar{D}_{nt}$, D_{nt}^l, and D_{nt}^u to denote the nominal values, lower bounds, and upper bounds for the demand at node n and time t. Correspondingly we use $\bar{P}_{wt}$, P_{wt}^l, and P_{wt}^u to denote the nominal values, lower bounds, and upper bounds for the wind generation capacity for wind generator w at time t. We also apply budgetary constraints restricting the maximum total demand and the minimum total wind generator capacity for each time period t as well as across the entire planning horizon to control the conservativeness of the uncertainty set, which will be determined in the later sections from historical data. The uncertainty set formulations for the demand, $\mathcal{D}$, and wind generator capacity, $\mathcal{W}^Cap$, are given as follows.

$$\mathcal{D} = \left\{ \begin{array}{ll} d: & D_{nt}^l \le d \le D_{nt}^u, \ \ \forall n \in N, t \in T, \\ & \sum\limits_{n\in N} \pi_{nt}^\tau d_{nt} \le \bar{\pi}_t^D, \ \ \forall t \in T, \\ & \sum\limits_{t\in T}\sum\limits_{n\in N} \pi_{nt}^0 d_{nt} \le \bar{\pi}_0^D \end{array} \right\}, \tag{8.21}$$

$$\mathcal{W}^{Cap} = \left\{ \begin{array}{ll} P^{Cap}: & P_{wt}^l \le P_{wt}^{Cap} \le P_{wt}^u, \ \ \forall w \in W, t \in T, \\ & \sum\limits_{w\in W} \pi_{wt}^\tau P_{wt}^{Cap} \ge \bar{\pi}_t^W, \ \ \forall t \in T, \\ & \sum\limits_{t\in T}\sum\limits_{w\in W} \pi_{wt}^0 P_{wt}^{Cap} \ge \bar{\pi}_0^W. \end{array} \right\}. \tag{8.22}$$

To solve the Robust UC model, we first analyze the solution to the second-stage problem for a given commitment decision. Given a specified UC decision, u, we define the objective function value of the second-stage problem to be $z(u)$, which is the worst case dispatch cost over the uncertainty set. To determine the value of $z(u)$ we dualize the constraints in $\chi(u, d, P^{Cap})$ to obtain a single-stage representation of the maximum dispatch cost of the UC decision u over the uncertainty sets $\mathcal{D}$ and $\mathcal{W}^{Cap}$.The resulting dispatch cost formulation is given below.

Dispatch Cost Model

Objective function:

$$z(u) = \max \sum_{t\in T}\sum_{g\in G} f_g(u_g, \gamma^+_{g,t}, \gamma^-_{g,t}, \xi_{g,t}, \zeta_{g,t}) + \sum_{k\in K} F^{Max}_k(\tau^-_{k,t} - \tau^+_{k,t}) + \sum_{n\in N} d_{n,t}\eta_{n,t} - \sum_{w\in W} P^{Cap}_{w,t}\alpha_{w,t} \tag{8.23}$$

Constraints:

$$\gamma^+_{g,t} - \gamma^-_{g,t} + \xi_{g,t+1} - \xi_{g,t} + \zeta_{g,t} - \zeta_{g,t+1} + \eta_{nt,} = c_g, \qquad \forall g, t, \tag{8.24}$$

$$-\alpha_{w,t} + \eta_{n,t} \leq 0, \qquad \forall w, t \tag{8.25}$$

$$\beta_t + \eta_{n,t} + \sum_{k\in K} PTDF^{n(g)}_k(\tau^+_{k,t} - \tau^-_{k,t}) = 0, \qquad \forall g, t \tag{8.26}$$

$$\gamma^+_{g,t}, \gamma^-_{g,t}, \xi_{g,t}, \zeta_{g,t} \geq 0, \qquad \forall g \in G, t \in T \tag{8.27}$$

$$\tau^+_{k,t}, \tau^-_{k,t} \geq 0 \qquad \forall k \in K, t \in T \tag{8.28}$$

$$\alpha_{w,t} \geq 0, \qquad \forall w \in W, t \in T, \tag{8.29}$$

$$d \in \mathcal{D}, P^{Cap} \in \mathcal{W}^{Cap} \tag{8.30}$$

where

$$\begin{aligned} f_g(u_g, \quad & \gamma^+_{g,t}, \gamma^-_{g,t}, \xi_{g,t}, \zeta_{g,t}) = P^{Min}_g u_{g,t}\gamma^+_{g,t} - P^{Max}_g u_{g,t}\gamma^-_{g,t} - \left[(1 + u_{g,t-1} - u_{g,t})R^+_g \right. \\ & \left. + (2 - u_{g,t-1} - u_{g,t})R^{SU}_g\right] \xi_{g,t} - \left[(1 - u_{g,t-1} + u_{g,t})R^-_g + (2 - u_{g,t-1} - u_{g,t})R^{SD}_g\right] \zeta_{g,t}. \end{aligned}$$

The decision variables $\eta_{n,t}$, β_t, $\tau^{\pm}_{k,t}$, $\gamma^{\pm}_g$, $\alpha_{w,t}$, $\xi_{g,t}$, and $\zeta_{g,t}$ are the dual variables corresponding to constraints (8.8) - (8.14). The objective function is given by equation (8.23) and the dual constraints for the traditional generator variables, wind generator variables, and the nodal net injection, $p_{g,t}$, $p_{w,t}$, and $p^{Net}_{n,t}$, are given by equations (8.24)-(8.26). Note that the objective function of the dispatch cost formulation is a bilinear function due to the product of the dispatch dual variables (η, α, τ), with the demand, wind generator capacity, and nodal net injection variables (d, P^{Cap}_w). Thus, the dispatch cost problem is NP-hard in general. Algorithms providing exact and near-optimal solutions are discussed in [136]. In this chapter, we adopt the heuristic Benders decomposition framework as given by [136] for the tractable application to large-scale systems. A detailed description of the algorithm is presented in Section 8.3.

8.3 Solution Methodology

Due to the bilinear form of the objective function in the dispatch cost problem it can be very computationally intensive to obtain an exact solution to the Robust UC model. This difficulty increases dramatically when the Robust UC model is applied to large-scale systems which form the core of electrical energy systems in the United States.

To maintain applicability of the Robust UC model to large-scale systems we adopt a heuristic Benders decomposition framework from [136] which consists of a master UC problem that iteratively adds feasibility and optimality cuts to obtain a near-optimal solution to the Robust UC model.

The remainder of this section is organized as follows. In Subsection 8.3.1, we discuss the representation of the Robust UC model within the Benders decomposition framework. In Sub-

sections 8.3.2 and 8.3.3 we address the feasibility and optimality of the UC decision respectively. Subsection 8.3.4 outlines the Benders decomposition algorithm that we employ in this paper.

8.3.1 Decomposition of the Robust UC Model

The Robust UC model is decomposed into three components: a master UC problem, and two dispatch cost subproblems, subproblem 1 and subproblem 2.

The master problem is a UC problem that characterizes the commitment stage of the Robust UC model. The master problem formulation is given below.

Master Problem

Objective function:

$$z^M = \min_{u,v,w} \left\{ \sum_{t\in T} \sum_{g\in G} (c_g^{SU} v_{g,t} + + c_g^{NL} u_{g,t}) + z(u) \right\} \tag{8.31}$$

Constraints:
(8.2)-(8.7),

$$\sum_{t\in T} \sum_{g\in G} \sigma_{gt}^{rf} u_{g,t} \leq \bar{\sigma}_r^f, \qquad \forall r = 1, .., R \tag{8.32}$$

$$z(u) - \sum_{t\in T} \sum_{g\in G} \sigma_{gt}^{so} u_{g,t} \geq \bar{\sigma}_s^o, \qquad \forall s = 1, .., S \tag{8.33}$$

The objective function of the master problem, given by equation (8.31), is to minimize the sum of the commitment cost and the estimate for the worst-case dispatch cost corresponding to the UC decision u, given by the variable $z(u)$. Specifically, $z(u)$ represents a lower bound on the worst-case dispatch cost corresponding to the UC decision u. Equations (8.32) and (8.33) represent the feasibility and optimality cuts that are added to the master problem respectively. We describe the procedure for generating the feasibility and optimality cuts in Subsections 8.3.2 and 8.3.3 respectively.

As stated in the last section, it is difficult to determine exact feasibility and optimality of a given UC decision due to the bilinear terms in objective function of the dispatch cost problem. To remove these bilinearities, we decompose the dispatch cost problem into two subproblems: Subproblem 1 and Subproblem 2, in which the dispatch dual variables $(\gamma, \xi, \zeta, \tau, \eta, \alpha, \beta)$, and the demand and wind generator capacity (d, P_w^{Cap}), are fixed respectively. The formulations are given below.

Subproblem 1

Objective:

$$\begin{aligned} z_1(u, d, P_w^{Cap}) = \quad & \max \sum_{t\in T} \sum_{g\in G} f_g(u_g, \gamma_{g,t}^+, \gamma_{g,t}^-, \xi_{g,t}, \zeta_{g,t}) + \sum_{k\in K} F_k^{Max}(\tau_{k,t}^- - \tau_{k,t}^+) \\ & + \sum_{n\in N} d_{n,t}\eta_{n,t} - \sum_{w\in W} P_{w,t}^{Cap} \alpha_{w,t} \end{aligned} \tag{8.34}$$

Constraints: (8.24)-(8.26),

$$\begin{aligned} \gamma^+_{g,t}, \gamma^-_{g,t}, \xi_{g,t}, \zeta_{g,t} \geq 0, & \qquad \forall g \in G, t \in T \\ \tau^+_{k,t}, \tau^-_{k,t} \geq 0 & \qquad \forall k \in K, t \in T \\ \alpha_{w,t} \geq 0, & \qquad \forall w \in W, t \in T. \end{aligned}$$

Subproblem 2

Objective:

$$\begin{aligned} z_2(u, \gamma, \xi, \zeta, \tau, \eta, \alpha, \beta) = \quad & \max \sum_{t \in T} \sum_{g \in G} f_g(u_g, \gamma^+_{g,t}, \gamma^-_{g,t}, \xi_{g,t}, \zeta_{g,t}) + \sum_{k \in K} F^{Max}_k(\tau^-_{k,t} - \tau^+_{k,t}) \\ & + \sum_{n \in N} d_{n,t}\eta_{n,t} - \sum_{w \in W} P^{Cap}_{w,t}\alpha_{w,t} \end{aligned} \tag{8.35}$$

Constraints: (8.24)-(8.26),

$$d \in \mathcal{D}, P^{Cap} \in \mathcal{W}^{Cap}$$

8.3.2 Feasibility of the UC Decision

We now address the feasibility of the third-stage problem $\min_{p \in \chi(u,d,P^{Cap})} \sum_{t \in T} \sum_{g \in G} c^v_g p_{g,t}$ with respect to given values for the UC decision, u, demand d, and wind generator capacity P^{Cap}. The solution space for subproblem 1, given by equations (8.24)-(8.26), defines a non-empty feasible region. For example, a solution with $\gamma_{g,t} = c_g$ and all other variables are zeros is a feasible solution. Additionally,since the objective function of the third-stage problem is linear and equations (21)-(26) defining the uncertainty sets D and W^{Cap} define bounded regions, from duality theory, the infeasibility condition of the third-stage problem is equivalent to the unboundedness of subproblem 1.

We thus determine the feasibility of the third-stage problem by determining whether the optimal solution to subproblem one is finite, i.e. whether $z_1(u, d, p^{Cap}_w) < \infty$. Subproblem 1 is unbounded if and only if there exists an extreme ray solution $(\gamma, \xi, \zeta, \tau, \eta, \alpha, \beta)$ such that

$$\sum_{t \in T} \sum_{g \in G} f_g(u_g, \gamma^+_{g,t}, \gamma^-_{g,t}, \xi_{g,t}, \zeta_{g,t}) + \sum_{k \in K} F^{Max}_k(\tau^-_{k,t} - \tau^+_{k,t}) + \sum_{n \in N} d_{n,t}\eta_{n,t} - \sum_{w \in W} P^{Cap}_{w,t}\alpha_{w,t} > 0.$$

We determine the existence of such extreme ray solutions through the optimal solution of the feasibility subproblem given below.

Feasibility Subproblem

Objective function:

$$\begin{aligned} z_f(u, d, p^{Cap}_w) = \quad & \max_{\gamma, \xi, \zeta, \tau, \eta, \alpha, \beta} \Big(\sum_{t \in T} \sum_{g \in G} f_g(u_g, \gamma^+_{g,t}, \gamma^-_{g,t}, \xi_{g,t}, \zeta_{g,t}) + \sum_{k \in K} F^{Max}_k(\tau^-_{k,t} - \tau^+_{k,t}) \\ & + \sum_{n \in N} d_{n,t}\eta_{n,t} - \sum_{w \in W} P^{Cap}_{w,t}\alpha_{w,t} \Big) \end{aligned} \tag{8.36}$$

Constraints:

$$\gamma^+_{g,t} - \gamma^-_{g,t} + \xi_{g,t+1} - \xi_{g,t} + \zeta_{g,t} - \zeta_{g,t+1} + \eta_{nt,} = 0, \ \ \forall g, t \tag{8.37}$$

(8.25)-(8.30),

$$\gamma^+_{g,t}, \gamma^-_{g,t}, \xi_{g,t+1}, \xi_{g,t} \leq 1, \forall g, t \tag{8.38}$$

$$\tau^+_{k,t}, \tau^-_{k,t} \leq 1, \forall k, t \tag{8.39}$$

$$\alpha_{w,t} \leq 1, \forall w, t \tag{8.40}$$

$$-1 \leq \eta_{n,t} \leq 1 \forall n, t \tag{8.41}$$

$$-1 \leq \beta_t \leq 1 \forall t. \tag{8.42}$$

Note that in this model, we restricted the feasible region in a unit box to avoid unboundedness. Specifically, a given UC decision u is feasible with respect to demand d and wind generator capacity P^{Cap} if $z_f(u, d, p^{Cap}_w) = 0$. Otherwise, if $z_f(u, d, p^{Cap}_w) > 0$, we add the feasibility cut

$$\sum_{t\in T}\sum_{g\in G} f_g(u_g, \gamma^+_{g,t}, \gamma^-_{g,t}, \xi_{g,t}, \zeta_{g,t}) + \sum_{k\in K} F^{Max}_k(\tau^-_{k,t} - \tau^+_{k,t}) + \sum_{n\in N} d_{n,t}\eta_{n,t} - \sum_{w\in W} P^{Cap}_{w,t}\alpha_{w,t} \leq 0 \tag{8.43}$$

to the master problem, where $(\gamma, \xi, \zeta, \tau, \eta, \alpha, \beta)$ is the optimal solution to the feasibility subproblem corresponding to the demand d and wind generator capacity P^{Cap}. We outline the feasibility cutting-plane sub-algorithm below.

Feasibility Cutting-Plane Subalgorithm

1. Initialization. Given UC solution u, demand d, and wind generator capacity P^{Cap}_w
2. Solve the feasibility subproblem and store the solution $z_f(u, d, p^{Cap}_w)$;
3. If $z_f(u, d, p^{Cap}_w) = 0$: Then the commitment schedule u is feasible with respect to demand d and wind generator capacity P^{Cap};

Else if $z_f(u, d, p^{Cap}_w) > 0$: Then add the feasibility cut (8.43) to the master problem.

8.3.3 Optimality of the UC decision

As stated in section 8.3 an exact solution to the dispatch cost problem is very computationally intensive to obtain. However, from (27) we know that for all feasible solutions $(\gamma, \xi, \zeta, \tau, \eta, \alpha, \beta, p^{Cap}_w)$ of the dispatch cost problem we have

$$z(u) \geq \sum_{t\in T}(\sum_{t\in T}\sum_{g\in G} f_g(u_g, \gamma^+_{g,t}, \gamma^-_{g,t}, \xi_{g,t}, \zeta_{g,t}) + \sum_{k\in K} F^{Max}_k(\tau^-_{k,t} - \tau^+_{k,t}) + \sum_{n\in N} d_{n,t}\eta_{n,t} - \sum_{w\in W} P^{Cap}_{w,t}\alpha_{w,t}) \tag{8.44}$$

Thus, adding constraints of this form constitute valid inequalities for the master problem. However, there are exponential number of feasible extreme point solutions to the dispatch cost problem and constraints of this form are not guaranteed to provide tight bounds on the value of the dispatch cost function $z(u)$, i.e. for many feasible solutions $(\gamma, \xi, \zeta, \tau, \eta, \alpha, \beta, p^{Cap}_w)$ the inequality in (8.44) are not strict. We adopt the following cutting-plane heuristic from [136] to selectively generate valid inequalities to be added to the master problem.

Optimality Cutting-Plane Subalgorithm

1. Initialization. Given a feasible UC solution u, demand d, and wind generator capacity P_w^{Cap}
2. Solve subproblem 1 and store the solution $z_1(u, d, p_w^{Cap})$.
3. Solve subproblem 2 and store the solution $z_2(u, \gamma, \xi, \zeta, \tau, \eta, \alpha, \beta)$.
4. If $z_1(u, d, p_w^{Cap}) \neq z_2(u, \gamma, \xi, \zeta, \tau, \eta, \alpha, \beta)$: Go to step 2. Else: Go to step 5.
5. If $z(u) < z_1(u, d, p_w^{Cap}) = z_2(u, \gamma, \xi, \zeta, \tau, \eta, \alpha, \beta)$, generate the valid optimality cut (8.44) and add the cut to the master problem.

8.3.4 Outline of the Benders Decomposition Algorithm

The heuristic Benders decomposition algorithm used in this paper is outlined below. A flowchart depiction of the algorithm is given by Figure 8.1.

Benders Decomposition Heuristic Algorithm

1. Solve the master problem and store the solution z^M and the dispatch cost estimate $z(u)$.
2. Call the feasibility cutting-plane subalgorithm for UC decision u.
3. If a feasibility cut was generated then go to step 1; else: Go to step 4.
4. Call the optimality cutting-plane subalgorithm for UC decision u.
5. If an optimality cut was generated: go to step 1; Else: End with UC decision u.

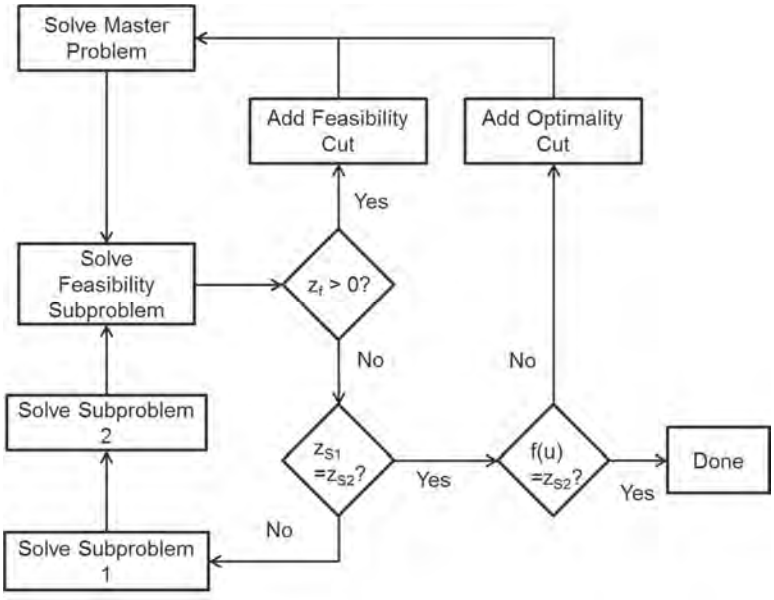

Figure 8.1: Flowchart representation for the Benders Decomposition Heuristic Algorithm.

8.4 Construction of Uncertainty Sets

We now present two polyhedral uncertainty set formulations for providing probabilistic guarantees on the feasibility of the commitment schedule under demand and wind generator capacity uncertainty. Both uncertainty set formulations make use of historical data for demand and wind generator capacity and are of the form given by equations (8.21) and (8.22).

In Subsection 8.4.1 we present an uncertainty set formulation that takes advantage of asymptotic results of random variable summations derived from the central limit theorem (CLT). In Subsection 8.4.2 we present a new method for determining optimal hyperplanes to describe the uncertainty set.

8.4.1 Central Limit Theorem Uncertainty Set Formulation

From probability theory we know that the sum of random variables converges in distribution to a normally distributed random variable according to the central limit theorem. Additionally, for a normally distributed random variable X with mean μ and standard deviation ρ, we have $P\{(X - \mu)/\rho z_\alpha\} = \alpha$, where z_α is the standardized score for the standard normal distribution.

Using these results we can determine the $\bar{\pi}$ values contained in equations (8.21) and (8.22), such that the probability of violation is within a specified value. Specifically, we determine the $\bar{\pi}$ coefficients as follows:

$$\begin{aligned}
\bar{\pi}_t^D &= \bar{D}_t + s_t^d z_\alpha, \\
\bar{\pi}_t^W &= \bar{p}_t^w + s_t^w z_\alpha, \\
\bar{\pi}_0^D &= \bar{D}_0 + s_0^d z_\alpha, \\
\bar{\pi}_0^W &= \bar{p}_0^w + s_0^w z_\alpha.
\end{aligned}$$

The π coefficients contained are given by the inverse of the standard deviation estimate:

$$\begin{aligned}
\pi_{nt}^\tau = \pi_{nt}^0 &= \frac{1}{s_{nt}^d}, \\
\pi_{wt}^\tau = \pi_{wt}^0 &= \frac{1}{s_{wt}^w}.
\end{aligned}$$

We now discuss two methods for determining the upper and lower limits of the demand and wind generator capacity variables. Under assumptions of normality we can determine the bounds through the use of the relevant z-score values as follows:

$$\begin{aligned}
D_{nt}^l &= \bar{D}_{nt} - s_{nt}^d z_{\alpha/2}, \\
p_{wt}^l &= \bar{p}_{wt} - s_{wt}^w z_{\alpha/2}, \\
D_{nt}^u &= \bar{D}_{nt} + s_{nt}^d z_{\alpha/2}, \\
p_{wt}^u &= \bar{p}_{wt} + s_{wt}^w z_{\alpha/2}.
\end{aligned}$$

If large deviations from normality are present within the data, we can let the upper and lower bounds be given by the $\alpha/2$,$(1 - \alpha/2)$ percentile values from the historical data.

8.4.2 Percentile Uncertainty set Formulation

We now present a method for generating optimal hyperplane coefficients such that $(1 - \alpha)\%$ of the historical data is contained in the uncertainty set. Let H represent the set of historical data.

For each data point $h \in H$ we represent the overall percentiles sums by ϵ_h^0 and the percentile sums for time period t by ϵ_h^t. The lower and upper bounds for the uncertainty set variables are given by the $\alpha/2$ and $(1-\alpha/2)$ percentiles of the historical data for the variable. The formulation for the demand hyperplane coefficients is given below. The formulation for the wind uncertainty set is determined similarly.

Percentile Uncertainty Set Formulation

Objective function:

$$\min \sum_{h \in H} [(\epsilon_h^0 - (1-\alpha))^+ + \sum_t (\epsilon_h^t - (1-\alpha))^+] y_h \tag{8.45}$$

Constraints:

$$\sum_n \pi_{nt}^\tau d_{nt}^h \leq \bar{\pi}_t^d, \forall t, h, \text{ such that } \epsilon_h^t \leq 1-\alpha \tag{8.46}$$

$$\sum_n \pi_{nt}^\tau d_{nt}^h - z_h \leq \bar{\pi}_t^d, \forall t, h, \text{ such that } \epsilon_h^t \leq 1-\alpha \tag{8.47}$$

$$\sum_t \sum_n \pi_{nt}^\tau d_{nt}^h \leq \bar{\pi}_0^D, \forall h, \text{ such that } \epsilon_h^0 \leq 1-\alpha \tag{8.48}$$

$$\sum_t \sum_n \pi_{nt}^\tau d_{nt}^h - z_h \leq \bar{\pi}_0^D, \forall h, \text{ such that } \epsilon_h^0 \leq 1-\alpha \tag{8.49}$$

The objective function for the percentile uncertainty set, given by equation (8.45), is to minimize the inclusion of historical data points with either overall or time period percentile values larger than $(1-\alpha)$. Equations (8.46) and (8.48) require that the historical data with time period and overall percentile values smaller than $(1-\alpha)$ are contained in the uncertainty set respectively. Equations (8.47) and (8.49) provide indicators for data points with time period and overall percentile values larger than $(1-\alpha)$ that are contained in the uncertainty set respectively.

8.5 Numerical Experiments

In this section we test the performance of three methods for generating UC decisions: (i) the CLT uncertainty set, (ii) the percentile uncertainty set, and (iii) a deterministic reserve method. The deterministic reserve method, with total reserve requirements equal to twice the output of the largest generator, serves as a baseline for comparing the CLT and percentile uncertainty sets with respect to managing the effects of uncertainty. All tests are performed on the IEEE RTS96 model, which consists of 73 buses, 99 generators, and 117 lines; the problem is formulated as a day-ahead UC problem with 24 periods. The optimization is performed using IBM ILOG CPLEX version 12.5.

The simulated historical data consists of $100,000$ demand and wind capacity data points that are generated from a normal distribution. The standard deviation of the demand is equal to 10% of the expected value of the demand while the wind standard deviation is equal to the expected value. The demand and wind data are correlated both spatially and temporally. The spatial correlation for the demand and wind is 0.9 while the time correlation for the demand and wind is 0.99 and 0.7 respectively.

We test four uncertainty set types over three levels of probabilistic constraint and a deterministic reserve method to serve as a baseline for comparison. For each method the average cost and number of infeasibilities is determined using a sample of 500 scenarios generated from the same distribution as the historical data. We test the effectiveness of CLT and percentile uncertainty sets with $(0 + t)$ and without (0) the inclusion of the knapsack constraints over each time period. The results for $p = 0.9$, $p = 0.95$, and $p = 0.99$ are given in tables I,II, and III respectively.

Table 8.1: Computational performance for $p = 0.9$

	Worst case bound (M$)	Average cost (M$)	Number of infeasible cases	Time to obtain UC solutions (s)
CLT 0	4.40	3.23	50	408
CLT 0+t	3.91	2.96	0	721
Percentile 0	4.26	3.00	1	686
Percentile 0+t	3.67	2.98	71	911
Reserve	N/A	3.44	102	8

Table 8.2: Computational performance for $p = 0.95$

	Worst case bound (M$)	Average cost (M$)	Number of infeasible cases	Time to obtain UC solutions (s)
CLT 0	4.39	3.26	60	430
CLT 0+t	3.93	2.92	0	703
Percentile 0	4.30	3.01	13	694
Percentile 0+t	3.71	2.95	28	611
Reserve	N/A	3.44	102	8

Table 8.3: Computational performance for $p = 0.99$

	Worst case bound (M$)	Average cost (M$)	Number of infeasible cases	Time to obtain UC solutions (s)
CLT 0	4.47	3.25	11	324
CLT 0+t	4.19	3.05	2	478
Percentile 0	4.71	3.22	0	362
Percentile 0+t	3.85	3.07	2	665
Reserve	N/A	3.44	102	8

In this experiment, we observe that the performance of the CLT and percentile uncertainty sets were superior to the deterministic reserve method with respect to managing the effects of uncer-

tainty at the expense of increased time requirements to obtain the UC solution. The CLT uncertainty set was found to have scenario cost savings averaging 10.03% over the reserve method with an average of a 79.9% percent decrease in the number of infeasible scenarios. The percentile uncertainty set exhibited similar performance benefits over the reserve method. The average scenario cost savings improved by 11.67% with an 81.21% decrease in the number of infeasible scenarios. Additionally, the time required to obtain the UC solution was increased by an average of 32.27% for the percentile uncertainty set compared to the CLT uncertainty set.

The inclusion of knapsack constraints on each time period was found to be beneficial to both the CLT and percentile uncertainty sets while increasing the time required to obtain the UC solution. Both uncertainty sets exhibited reductions in the worst case and average scenario costs. The knapsack constraints on each time period improved the worst case bound by an average of 8.53% for the CLT uncertainty set and 15.30% for the percentile uncertainty set. The average scenario cost was reduced by an average of 7.38% for the CLT uncertainty set and 2.39% for the percentile uncertainty set. The effect of the inclusion of knapsack constraints on each time period on the number of infeasible scenarios differed between the CLT uncertainty set and the percentile uncertainty set: substantially reducing the number of infeasible instances for the CLT uncertainty set but increasing the number of infeasibilities for the percentile uncertainty set. The average percent increase in the time required to obtain the UC solution was 62.58% for the CLT uncertainty set and 34.85% for the percentile uncertainty set.

8.6 Conclusion

In this chapter, two methods for generating uncertainty sets, the CLT uncertainty set and the percentile uncertainty set, are analyzed using two polyhedral uncertainty set structures. The performance of each uncertainty set was compared against a deterministic reserve method with respect to managing the effects of uncertainty. Both the CLT uncertainty set and the percentile uncertainty set demonstrated superior performance over the deterministic reserve method with respect to the average scenario cost and the number of infeasible scenarios. The time required to obtain the UC solutions was significantly larger compared to the deterministic reserve method however. The inclusion of knapsack constraints on each time period was found to be beneficial to both the CLT and percentile uncertainty sets however the CLT uncertainty set benefitted more than the percentile uncertainty set. Further studies are required to determine the effectiveness of the CLT and percentile uncertainty sets using correlated data for load and wind uncertainties.

9. Conclusion

9.1 Conclusion

In the report, robust optimization techniques are applied to two power grid problems: topology control and unit commitment.

First, topology control is an integral part of power system operations. Today, most of the topology control actions are determined based on operators' past knowledge about the system or other ad-hoc methods. Relying on only prior observations to determine potential corrective topology control action limits the capability to harness the existing flexibility in the transmission network. Systematic procedures that are capable of capturing such complexities should be preferred over these limited methods. Furthermore, the hardware requirements to implement topology control (circuit breakers) already exist, leaving only the need to develop the appropriate decision support tools, which are low in cost, to obtain such benefits.

In this research, three different corrective topology control methodologies are presented: real-time, deterministic planning based, and robust corrective topology control. Real-time corrective topology control is very difficult to implement with today's technology due to a lack of computational power and the practical barriers of needing to ensure AC feasibility, voltage stability, and transient stability. Deterministic planning based corrective topology control can be solved offline, but such an approach relies on predicting the operating state. Furthermore, the deterministic planning based methods cannot guarantee solution feasibility over a wide range of system states. The proposed method of robust corrective topology control fills the technology gap between the real-time and the deterministic planning based corrective topology control methodologies. The offline mechanism of robust corrective topology control algorithm generates solutions, which can be implemented in real-time with the help of a real-time dynamic security assessment tool. As a result, the proposed robust corrective topology control model provides a mathematical decision support tool that integrates topology control into every day operations by being able to guarantee the robustness of solutions.

While deterministic corrective topology control frameworks may suggest many potential switching solutions, the empirical results presented in this research show that many of these solutions will be infeasible for minor changes in the operating state. In contrast, the robust corrective switching scheme guarantees solution feasibility for a wide range of system states, given a DCOPF formulation. In addition, the robust corrective topology control formulation demonstrates the ability of generating multiple corrective switching actions for a particular contingency. Moreover, a single resulting corrective switching solution is capable of mitigating multiple contingencies.

Day-ahead unit commitment problems with proxy reserve requirements do not guarantee N-1 feasibility. Contingency analysis is used to determine whether there are contingencies that cannot be satisfied by the unit commitment solution. When this happens, unit commitment must be resolved or the operator will employ out-of-market corrections to obtain a feasible N-1 solution. The results have shown that robust corrective topology control can be used to reduce the occurrence of contingencies that are not satisfied by the re-dispatch capabilities of the unit commitment solution alone. Furthermore, the numerical results proved that the topology control does not necessarily degrade system reliability; on the contrary, it can help the system to achieve N-1 feasibility even with uncertainty.

The penetration of renewable resources in electrical power system is increased in recent years.

This increase in intermittent renewable resources are forcing to alter the way bulk power systems are operated today. This research shows the usefulness of topology control actions for integration of renewable resources, in terms of determining DNE limits. For renewable resource integration the determination of DNE limits is critical; in this research, a systematic procedure to determine DNE limit is presented. With corrective topology control actions, the DNE limits can be increased by 30-100%, as compared with no topology control actions. At the same time, topology control actions can lower the operational cost by at least 6%. The robust topology control algorithm is based on a DCOPF; therefore, the topology control solutions obtained from robust algorithm must be checked for AC feasibility. On the IEEE-118 bus test case, $\sim$$85$-$90\%$ of topology control solutions obtained from the robust topology control algorithm are AC feasible.

The stability studies, presented in this research, demonstrated that the solution obtained from the robust topology control algorithm can pass AC feasibility and stability tests. Furthermore, 30 topology control solutions, obtained from robust topology control algorithm, are tested for stability check and out it $\sim$$66\%$ of topology control solutions passes the stability check.

The robust topology control algorithm, presented in this report, is tested on small test case. To scale this algorithm, from a smaller test case to a real life test system, the sensitivity analysis bases topology control heuristic is proposed. The proposed heuristic has shown adequate ability to create a rank list to determine the potential topology control solution, which can be tested for robustness properties.

Second, the two-stage robust formulation is applied to the unit commitment problem with alternative objective function, maximum regret. The motivation of such objective is to avoid overly conservative solutions from traditional absolute worst-case robust objective. Wind uncertainty is modeled in this application since it is aligned with the motivation of utilizing as much wind as possible while ensuring the reliability of the power system. Bender's decomposition is proposed to solve the robust model. In this work, an uncertainty set description capturing the ramp events in wind power output randomness. With the consideration of regret under each scenario, the proposed approach avoids over-conservatism by minimizing the worst-case regret value. The iterative algorithmic framework developed can derive tight lower and statistical upper bounds of the minimax regret. The statistical upper bounds do not guarantee theoretical exactness, but can converge to exact upper bounds as the sample size increases in the Monte Carlo simulation. The computational results verified the effectiveness of the proposed approach.

With the more adoption of robust optimization in the power grid problems, a key question of how to construct the uncertainty set as an input of the robust models needs an answer. This work uses the two-stage unit commitment problem as an example to study the impacts of different types of uncertainty sets constructed from historical data and given confidence level. The uncertainty set construction is closely related to chance constraint programming problems. In this work, simulated historical data are used to construct the uncertainty sets with different predetermined confidence levels. The computational results suggest that more detailed uncertainty sets by including facets describing individual time periods provide better solution in robustness and cost effectiveness.

9.2 Proposed Future Research

9.2.1 Scalability of Robust Topology Control Problem - Zonal vs. Nodal Approach

Robust topology control methodology, presented in Chapter 3, is tested on an IEEE-118 bus test case, which consists of 54 generators, 118 buses, and 186 transmission lines. This test system is much smaller than any realistic test case, for example, the PJM system is consists of $1,375$ generators, $62,556$ miles long transmission network and peak demand of $183,604$ megawatts [110]. Therefore, for any practical implementation, the robust topology control methodology must be scaled from the smaller test case, such as a IEEE-118 bus test case, to a much larger test system.

To overcome this scalability issue, in literature, a zonal approach is used over the nodal approach. With a zonal approach, instead of modeling details of each node within the zone, all the nodes (within the zone) are represented by a single node/zone. For instance, in [62], the entire ISONE system is presented into a 4 zone system with transmission lines connecting between these zones. The benefit of zonal approach over the nodal approach is that it simplifies the problem to a great extent. Instead of solving a system consisting of a few thousand buses and a few thousand lines, the problem is simplified to a few buses and a few branches. This simplification reduces the computational complexities and improves the computational time. However, a zonal approach is based on the following critical assumptions.

With the zonal approach, each zone is considered as a single node; it is assumed that in each zone there is no congestion within the zone and any contingency within the zone can be mitigated by using the resources within the zone. Furthermore, it is assumed that a contingency within the zone will not affect the flows on line connecting between the two zones. This assumption indicates that within each zone there is sufficient reserves, which can be delivered, upon need, to mitigate contingency. However, in [148], the authors show that intra zonal congestion can be critical. If there is a congestion within the zone, it is possible that for a particular contingency, reserves are not delivered, and may lead to system failure. Therefore, determining system zones are critical for reliable system operations.

For DNE limits, the choice of modeling approach affects the quality of solution. With a nodal approach, more accurate results can be obtained, compared with the zonal approach; however, solving the nodal model can be computationally cumbersome and may have longer computational time. On the contrary, zonal approach can be computationally efficient; however, the solution obtained from the zonal approach can be less accurate, or even infeasible, due to over model simplification. Furthermore, the DNE limits, the maximum uncertainty in renewable resources, determined based on the zonal approach and the nodal approach may not be the same. There is still an open question about how to determine nodal uncertainty (uncertainty in renewable resources at each renewable injection node) from the DNE limits determined using zonal approach. Therefore, the future work will involve investigation in zonal DNE limits compared with nodal DNE limits.

9.2.2 Stability Studies

In Chapter 5, the effect of topology control on system stability under deviation of renewable resources are studied. This analysis is performed at peak demand levels with relatively low wind generation. However, there are many other operating conditions, which require stability studies to understand the effect of topology control on renewable integration. For instance, in general,

during nights, the system demand is lower and wind generation is higher; in these hours, the effect of topology control on system stability might be different from the peak loading condition. During the low demand and high wind generation periods, only the base load units are committed along with low inertia wind generation; hence, during these hours the system inertia is much lower than the peak loading hour. Therefore, in this case, the effect of loss of renewable resources with topology control action on system stability must be studied.

References

[1] G. Granelli, M. Montagna, F. Zanellini, P. Bresesti, R. Vailati, and M. Innorta, "Optimal network reconfiguration for congestion management by deterministic and genetic algorithms," *Elect. Power Syst. Res*, vol. 76, no. 6-7, pp. 549–556, Apr. 2006.

[2] A. A. Mazi, B. F. Wollenberg, and M. H. Hesse, "Corrective control of power system flows by line and bus-bar switching," *IEEE Trans. Power Syst.*, vol. 1, no. 3, pp. 258–264, Aug. 1986.

[3] W. Shao and V. Vittal, "Bip-based opf for line and bus-bar switching to relieve overloads and voltage violations," in *Proc. 2006 IEEE Power Syst. Conf. and Expo.*, Nov. 2006.

[4] A. G. Bakirtzis and A. P. S. Meliopoulos, "Incorporation of switching operations in power system corrective control computations," *IEEE Trans. Power Syst.*, vol. 2, no. 3, pp. 669–675, Aug. 1987.

[5] R. Bacher and H. Glavitsch, "Loss reduction by network switching," *IEEE Trans. Power Syst.*, vol. 3, no. 2, pp. 447–454, May 1988.

[6] S. Fliscounakis, F. Zaoui, G. Simeant, and R. Gonzalez, "Topology influence on loss reduction as a mixed integer linear programming problem," *IEEE Power Tech. 2007*, pp. 1987–1990, July 2007.

[7] G. Schnyder and H. Glavitsch, "Security enhancement using an optimal switching power flow," *IEEE Trans. Power Syst.*, vol. 5, no. 2, pp. 674–681, May 1990.

[8] ——, "Integrated security control using an optimal power flow and switching concepts," *IEEE Trans. Power Syst.*, vol. 3, no. 2, pp. 782–790, May 1988.

[9] R. Bacher and H. Glavitsch, "Network topology optimization with security constraints," *IEEE Trans. Power Syst.*, vol. 1, no. 4, pp. 103–111, Nov. 1986.

[10] W. Shao and V. Vittal, "Corrective switching algorithm for relieving overloads and voltage violations," *IEEE Trans. Power Syst.*, vol. 20, no. 4, pp. 1877–1885, Nov. 2005.

[11] F. Kuntz, "Congestion management in germany the impact of renewable generation on congestion management costs," 2011. [Online]. Available: http://idei.fr/doc/conf/eem/papers_2011/kunz.pdf

[12] T. Potluri and K. W. Hedman, "Network topology optimization with acopf," *IEEE PES General Meeting*, pp. 1–7, July 22-26 2012.

[13] K. W. Hedman, M. C. Ferris, R. P. O'Neill, E. B. Fisher, and S. S. Oren, "Co-optimization of generation unit commitment and transmission switching with n-1 reliability," *IEEE Trans. Power Syst.*, vol. 25, pp. 1052 – 1063, May 2010.

[14] H. Glavitsch, "State of the art review: switching as means of control in the power system," *INTL. JNL. Elect. Power Energy Syst.*, vol. 7, no. 2, pp. 92–100, Apr. 1985.

[15] B. G. Gorenstin, L. A. Terry, M. F. Pereira, and L. M. V. G. Pinto, "Integrated network topology optimization and generation rescheduling for power system security applications," *in IASTED International Symposium: High Tech. in the Power Industry, Bozeman, MT*, pp. 110–114, Aug. 1986.

[16] J. G. Rolim and L. J. B. Machado, "A study of the use of corrective switching in transmission systems," *IEEE Trans. Power Syst.*, vol. 14, pp. 336–341, 1999.

[17] K. W. Hedman, R. P. O'Neill, E. B. Fisher, and S. S. Oren, "Optimal transmission switching with contingency analysis," *IEEE Trans. Power Syst.*, vol. 24, no. 3, pp. 1577–1586, Aug. 2009.

[18] P. Balasubramanian and K. Hedman, "Real-time corrective switching in response to simul-

taneous contingencies," *JNL of Energy Engineering*, accepted for publication.
[19] R. P. O'Neill, R. Baldick, U. Helman, M. H. Rothkopf, and W. S. Jr., "Dispatchable transmission in RTO markets," *IEEE Trans. Power Syst.*, vol. 20, no. 1, pp. 171 – 179, Feb. 2005.
[20] K. W. Hedman, R. P. O'Neill, E. B. Fisher, and S. S. Oren, "Optimal transmission switching - sensitivity analysis and extensions," *IEEE Trans. Power Syst.*, vol. 23, pp. 1469–1479, Aug. 2008.
[21] R. P. O'Neill, K. W. Hedman, E. A. Krall, A. Papavasiliou, and S. S. Oren, "Economic analysis of the isos multi-period n-1 reliable unit commitment and transmission switching problem using duality concepts," *Energy Systems Journal*, vol. 1, no. 2, pp. 165–195, 2010.
[22] K. W. Hedman, R. P. O'Neill, E. B. Fisher, and S. S. Oren, "Smart flexible just-in-time transmission and flowgate bidding," *IEEE Trans. Power Syst.*, vol. 26, no. 1, pp. 93–102, Feb. 2011.
[23] K. W. Hedman, S. S. Oren, and R. P. ONeill, "A review of transmission switching and network topology optimization," in *IEEE Power and Energy Society General Meeting*, July 2011.
[24] ISO-NE, *ISO New England Outlook:Smart Grid is About Consumers*, Apr. 2010. [Online]. Available: http://www.isone.com/nwsiss/nwltrs/outlook/2009/outlook_may_2009_final.pdf
[25] J.C.Villumsen, G. Bronmo, and A. B. Philpott, "Line capacity expansion and transmission switching in power systems with large-scale wind power," *IEEE Trans. Power Syst.*, vol. 28, no. 2, pp. 731–739, May 2013.
[26] A. Khodaei, M. Shahidehpour, and S. Kamalinia, "Transmission switching in expansion planning," *IEEE Trans. Power Syst.*, vol. 25, no. 3, pp. 1722–1733, Aug. 2010.
[27] PJM, *Manual 3: Transmission Operations, Revision: 40*, 2012. [Online]. Available: http://www.pjm.com/~/media/documents/manuals/m03.ashx
[28] ——, *Manual 3: Transmission Operations, Revision: 44*, Nov. 2013. [Online]. Available: http://www.pjm.com/markets-andoperations/compliance/nercstandards/~/media/documents/manuals/m03.ashx
[29] A. Ott, VP, *Private communication*. PJM, Norristown, PA, Nov. 2012.
[30] J. Birge and F. Louveaux, *Introduction to Stochastic Programming*. Springer Verlag, 1997.
[31] A. Préopa, *Stochastic Programming*. Kluwer Academic Publishers, 1995.
[32] A. J. Kleywegt, A. Shapiro, and T. Homem-de Mello, "The sample average approximation method for stochastic discrete optimization," *SIAM Journal on Optimization*, vol. 12, no. 2, pp. 479–502, 2002.
[33] S. Ahmed and A. Shapiro, "The sample average approximation method for stochastic programs with integer recourse," ISyE, Georgia Institute of Technology, GA, Tech. Rep., 2002.
[34] P. Artzner, F. Delbaen, J. M. Eber, and D. Heath, "Coherent measures of risk," *Mathematical Finance*, vol. 9, no. 3, p. 203, 1999.
[35] B. K. Pagnoncelli, S. Ahmed, and A. Shapiro, "Sample average approximation method for chance constrained programming: theory and applications," *Journal of Optimization Theory and Applications*, vol. 142, no. 2, pp. 399–416, 2009.
[36] J. Luedtke, S. Ahmed, and G. Nemhauser, "An integer programming approach for linear programs with probabilistic constraints," *Math. Program.*, vol. 122, no. 2, pp. 247–272, 2010.
[37] J. Luedtke, "A branch-and-cut decomposition algorithm for solving general chance-

constrained mathematical programs," *Preprint available at: www.optimization-online.org*, 2011.
[38] A. L. Soyster, "Convex programming with set-inclusive constraints and applications to inexact linear programming," *Oper. Res.*, vol. 21, no. 5, pp. 1154–1157, Sep.-Oct. 1973.
[39] P. Kouvelis and G. Yu, *Robust Discrete Optimization and Its Applications*. Kluwer Academic Pub, 1997.
[40] A. Ben-Tal and A. Nemirovski, "Robust convex optimization," *Mathematics of Oper. Res.*, vol. 23, pp. 769–805, 1998.
[41] ——, "Robust solutions of linear programming problems contaminated with uncertain data," *Math. Program.*, vol. 88, no. 3, pp. 411–424, Sep. 2000.
[42] ——, "Robust optimization - methodology and applications," *Math. Program.*, vol. 92, pp. 453–480, 2002.
[43] D. Bertsimas and M. Sim, "Robust discrete optimization and network flows," *Math. Program.*, vol. 98, no. 1–3, pp. 49–71, Sep. 2003.
[44] ——, "The price of robustness," *Oper. Res.*, vol. 52, pp. 35–53, 2004.
[45] A. Ben-Tal, A. Goryashko, E. Guslitzer, and A. Nemirovski, "Adjustable robust solutions of uncertain linear programs." *Math. Program.*, vol. 99, pp. 351–376, 2004.
[46] D. Bertsimas and A. Thiele, "A robust optimization approach to supply chain management," *Oper. Res.*, vol. 54, no. 1, pp. 150–168, 2006.
[47] S. Takriti, J. R. Birge, and E. Long, "A stochastic model for the unit commitment problem," *IEEE Trans. Power Syst.*, vol. 11, no. 3, pp. 1497–1508, Aug. 1996.
[48] P. Carpentier, G. Gohen, J.-C. Culioli, and A. Renaud, "Stochastic optimization of unit commitment: a new decomposition framework," *IEEE Trans. Power Syst.*, vol. 11, no. 2, pp. 1067–1073, May 1996.
[49] D. Dentcheva and W. Römisch, "Optimal power generation under uncertainty via stochastic programming," in *Stochastic Programming Methods and Technical Applications*, ser. Lecture Notes in Economics and Mathematical Systems, K. Marti and P. Kall, Eds. Springer-Verlag, 1997, pp. 22–56.
[50] R. Gollmer, M. P. Nowak, W. Römisch, and R. Schultz, "Unit commitment in power generation–a basic model and some extensions," *Ann. Oper. Res.*, vol. 96, no. 1–4, pp. 167–189, Nov. 2000.
[51] S. W. Wallace and S.-E. Fleten, "Stochastic programming models in energy," *Handbooks in Oper. Res. and Management Science*, vol. 10, pp. 637–677, 2003.
[52] A. Tuohy, P. Meibom, E. Denny, and M. O'Malley, "Unit commitment for systems with significant wind penetration," *IEEE Trans. Power Syst.*, vol. 24, no. 2, pp. 592–601, May 2009.
[53] P. A. Ruiz, C. R. Philbrick, E. Zak, K. W. Cheung, and P. W. Sauer, "Uncertainty management in the unit commitment problem," *IEEE Trans. Power Syst.*, vol. 24, no. 2, pp. 642–651, May 2009.
[54] A. Papavasiliou, S. S. Oren, and R. P. O'Neill, "Reserve requirements for wind power integration: a scenario-based stochastic programming framework," *IEEE Trans. Power Syst.*, vol. 26, no. 4, pp. 2197–2206, Nov. 2011.
[55] A. Papavasiliou, "Coupling renewable energy supply with deferrable demand," Ph.D. dissertation, University of California, Berkeley, 2012.
[56] M. Shahidehpour, H. Yamin, and Z. Li, *Market Operations in Electric Power Systems*. Wi-

ley, 2002.
[57] L. Wu, M. Shahidehpour, and T. Li, "Stochastic security-constrained unit commitment," *IEEE Trans. Power Syst.*, vol. 22, no. 2, pp. 800–811, May 2007.
[58] F. Bouffard, F. D. Galiana, and A. J. Conejo, "Market-clearing with stochastic security-Part I: Formulation," *IEEE Trans. Power Syst.*, vol. 20, no. 4, pp. 1818–1826, Nov. 2005.
[59] ——, "Market-clearing with stochastic security-Part II: Case studies," *IEEE Trans. Power Syst.*, vol. 20, no. 4, pp. 1827–1835, Nov. 2005.
[60] Q. Wang, Y. Guan, and J. Wang, "A chance-constrained two-stage stochastic program for unit commitment with uncertain wind power output," *IEEE Trans. Power Syst.*, vol. 27, no. 1, pp. 206–215, Feb. 2012.
[61] D. M. Falcão, "High performance computing in power system applications," in *Vector and Parallel Processing–VECPAR'96*, ser. Lecture Notes in Computer Science, J. Palma and J. Dongarra, Eds. Springer, 1997, vol. 1215, pp. 1–23.
[62] D. Bertsimas, E. Litvinov, X. Sun, J. Zhao, and T. Zheng, "Adaptive robust optimization for the security constrained unit commitment problem," *IEEE Trans. Power Syst.*, vol. 28, no. 1, pp. 52 – 63, Feb. 2013.
[63] R. Jiang, M. Zhang, G. Li, and Y. Guan, "Two-stage robust power grid optimization problem," *JNL Operations Research*, submitted, 2010. [Online]. Available: http://www.optimization-online.org/DB_FILE/2010/10/2769.pdf
[64] P. Kouvelis and G. Yu, *Robust Discrete Optimization and Its Applications*. Kluwer Academic Pub, 1997.
[65] B. G. Gorenstin, N. M. Campodonico, J. P. Costa, and M. V. F. Pereira, "Power system expansion planning under uncertainty," *IEEE Trans. Power Syst.*, vol. 8, no. 1, pp. 129–136, Feb. 1993.
[66] E. O. Crousillat, P. Dörfner, P. Alvarado, and H. M. Merrill, "Conflicting objectives and risk in power system planning," *IEEE Trans. Power Syst.*, vol. 8, no. 3, pp. 887–893, Aug. 1993.
[67] P. Linares, "Multiple criteria decision making and risk analysis as risk management tools for power systems planning," *IEEE Trans. Power Syst.*, vol. 17, no. 3, pp. 895–900, Aug. 2002.
[68] T. De la Torre, J. W. Feltes, T. Gómez San Román, and H. M. Merrill, "Deregulation, privatization, and competition: Transmission planning under uncertainty," *IEEE Trans. Power Syst.*, vol. 14, no. 2, pp. 460–465, May 1999.
[69] V. Miranda and L. M. Proença, "Why risk analysis outperforms probabilistic choice as the effective decision support paradigm for power system planning," *IEEE Trans. Power Syst.*, vol. 13, no. 2, pp. 643–648, May 1998.
[70] J. M. Arroyo, N. Alguacil, and M. Carrión, "A risk-based approach for transmission network expansion planning under deliberate outages," *IEEE Trans. Power Syst.*, vol. 25, no. 3, pp. 1759–1766, Aug. 2010.
[71] A. Wald, *Statistical decision functions*. John Wiley, 1950.
[72] D. Bertsimas and S. Melvyn, "The price of robustness," *Oper. Res.*, vol. 52, no. 1, pp. 35–53, Jan.-Feb. 2004.
[73] P. Khargonekar, I. R. Petersen, and K. Zhou, "Robust stabilization of uncertain linear systems: quadratic stabilizability and H^∞ control theory," *IEEE Tras. Auto. Ctrl.*, vol. 35, no. 3, pp. 356–361, Mar. 1990.
[74] C. S. Yu and H. L. Li, "A robust optimization model for stochastic logistic problems," *Inter.*

JNL Prod. Eco., vol. 64, no. 1-3, pp. 385 – 397, Mar. 2000. [Online]. Available: http://www.sciencedirect.com/science/article/pii/S0925527399000742

[75] F. J. Fabozzi, P. N. Kolm, D. Pachamanova, and S. M. Focardi, *Robust Portfolio Optimization and Management*. Wiley, 2007.

[76] M. Chu, Y. Zinchenko, S. G. Henderson, and M. B. Sharpe, "Robust optimization for intensity modulated radiation therapy treatment planning under uncertainty," *Phys. Med. Biol.*, vol. 50, no. 23, pp. 54–63, 2005.

[77] F. P. Bernardo and P. M. Saraiva, "A robust optimization framework for process parameter and tolerance design," *AIChE JNL*, vol. 44, no. 9, pp. 2007–2017, 1998.

[78] L. El Ghaoui, F. Oustry, and H. Lebret, "Robust solutions to uncertain semidefinite programs," *SIAM JNL Optimization*, vol. 9, no. 1, pp. 33–52, 1998.

[79] A. Ben-tal and A. Nemirovski, "Robust solutions of linear programming problems contaminated with uncertain data," *Mathematical Programming*, vol. 88, pp. 411–424, 2000.

[80] A. Ben-Tal, L. E. Ghaoui, and A. Nemirovski, *Robust Optimization*. Princeton Univ. Press, 2009.

[81] P. C. Gupta, "A stochastic approach to peak power-demand forecasting in electric utility systems," *IEEE Trans. Power Apparatus Syst.*, vol. PAS-90, no. 2, pp. 824–832, Mar. 1971.

[82] A. Ben-Tal and A. Nemirovski, "Robust convex optimization," *Math. Oper. Res.*, vol. 23, no. 4, pp. 769–805, Nov. 1998.

[83] D. Bertsimas and M. Sim, "Robust discrete optimization and network flows," *Math. Prog.*, vol. 98, no. 1-3, pp. 49–71, Sep. 2003.

[84] D. Mejia-Giraldo and J. McCalley, "Adjustable decisions for reducing the price of robustness of capacity expansion planning," *IEEE Trans. Power Syst.*, 2014.

[85] E. B. Fisher, R. P. O'Neill, and M. C. Ferris, "Optimal transmission switching," *IEEE Trans. Power Syst.*, vol. 23, no. 3, pp. 1346–1355, Aug. 2008.

[86] P. A. Ruiz, A. Rudkevich, M. C. Caramanis, E. Goldis, E. Ntakou, and C. R. Philbrick, "Reduced mip formulation for transmission topology control," in *50th Annual Allerton Conference on Communication, Control, and Computing*, 2012.

[87] T. Guler, G. Gross, and M. Liu, "Generalized line outage distribution factors," *IEEE Trans. Power Syst.*, vol. 22, no. 2, pp. 879–881, May 2007.

[88] ISO-NE, *ISO New England Operating Procedure no. 19: Transmission Operations, Revision 5*, June 1, 2010. [Online]. Available: http://www.iso-ne.com/rules_proceds/operating/isone/op19/op19_rto_final.pdf

[89] California ISO, *Minimum Effective Threshold Report*, March 1, 2010. [Online]. Available: http://www.caiso.com/274c/274ce77df630.pdf

[90] J. D. Fuller, R. Ramasra, and A. Cha, "Fast heuristics for transmission-line switching," *IEEE Trans. Power Syst.*, vol. 27, no. 3, pp. 1377–1386, Aug. 2012.

[91] P. A. Ruiz, J. M. Foster, A. Rudkevich, and M. C. Caramanis, "On fast transmission topology control heuristics," *IEEE PES General Meeting*, July 2011.

[92] J. M. Foster, P. A. Ruiz, A. Rudkevich, and M. C. Caramanis, "Economic and corrective applications of tractable transmission topology control," *in Proc. 49th Allerton Conference on Communications, Control and Computing, Monticello, IL,*, Sep. 2011.

[93] M. Li, P. Luh, L. Michel, Q. Zhao, and X. Luo, "Corrective line switching with security constraints for the base and contingency cases," *IEEE Trans. Power Syst.*, vol. 27, no. 1, pp. 125–133, Feb. 2012.

[94] PJM, Switching Solutions. [Online]. Available: http://www.pjm.com/markets-and-operations/etools/oasis/system-information/switching-solutions.aspx
[95] Power System Test Case Archive, Univ. of Washington, Dept. of Elect. Eng., 2007. [Online]. Available: http://www.ee.washington.edu/research/pstca/
[96] California ISO, *Spinning Reserve and Non-Spinning Reserve*, 2006. [Online]. Available: http://www.caiso.com/docs/2003/09/08/2003090815135425649.pdf
[97] Reuters, "Loss of wind causes texas power grid emergency," Feb. 2008. [Online]. Available: http://www.reuters.com/article/2008/02/28/us-utilities-ercot-wind-idUSN2749522920080228
[98] K. Galbraith, "The rolling chain of events behind texas blackouts," The Texas Tribune, Feb. 2008. [Online]. Available: http://www.texastribune.org/2011/02/03/the-rolling-chain-of-events-behind-texas-blackouts/
[99] A. Korad and K.W, "Robust corrective topology control for system reliability," *IEEE Trans. Power Syst.*, vol. 28, no. 4, pp. 4042 – 4051, Nov. 2013.
[100] L. Chen, O. Sangyo, Y. Tada, H. Okamoto, R. Tanabe, and H. Mitsuma, "Optimal reconfiguration of transmission systems with transient stability constraints," *International Conference on Power System Technology*, p. 1346 1350, Aug. 1998.
[101] B. Perunicic, M. Ilic, and A. Stankovic, "Short time stabilization of power systems via line switching," *IEEE International Symposium on Circuits and Systems*, pp. 917 – 921, June 1988.
[102] P. Kundur, J. Paserba, V. Ajjarapu, G. Andersson, A. Bose, C. Canizares, N. Hatziargyriou, D. Hill, A. Stankovic, C. Taylor, T. V. Cutsem, and V. Vittal, "Definition and classification of power system stability IEEE/CIGRE joint task force on stability terms and definitions," *IEEE Trans. Power Syst.*, vol. 19, no. 2, pp. 1387 – 1401, May 2004.
[103] J. Zhao, T. Zheng, and E. Litvinov, "Variable resource dispatch through do-not-exceed limit," *IEEE Trans. Power Syst.*, vol. pp, no. 99, pp. 1–10, 2014.
[104] NREL Western Wind Resources Dataset. [Online]. Available: http://wind.nrel.gov/Web_nrel/
[105] California ISO, Flexible Resource Adequacy Criteria and Must Offer Obligation, Dec. 20 2012.
[106] R. H. Byrd, J. Nocedal, and R. A. Waltz, "KNITRO: An integrated package for nonlinear optimization," *Nonconvex Optimization and Its Applications*, vol. 83, pp. 35–59, 2006.
[107] K. Clark, N. W. Miller, and J. J. Sanchez-Gasca, "Modeling of GE wind turbine-generators for grid studies," *GE Energy, Ver. 4.5*, 16 Apr. 2010.
[108] L. Bu, W. Xu, L. Wang, F. Howell, and P. Kundur, "A PSS tuning toolbox and its applications," *IEEE PES General Meeting*, pp. 2090–2095, 13-17 July 2003.
[109] N. W. Miller, M. Shao, and S. Venkataraman, "Report California ISO (CAISO) frequency response study," *GE Energy*, 9 Nov. 2011. [Online]. Available: http://www.caiso.com/Documents/Report-FrequencyResponseStudy.pdf
[110] PJM, *PJM Statistics*, 26 Mar. 2014. [Online]. Available: http://www.pjm.com/~/media/about-pjm/newsroom/fact-sheets/pjm-statistics.ashx
[111] P. A. Ruiz, J. M. Foster, A. Rudkevich, and M. C. Caramanis, "Tractable transmission topology control using sensitivity analysis," *IEEE Trans. Power Syst.*, vol. 27, no. 3, pp. 1550–1559, Aug. 2012.
[112] R. Baldick, "Border flow rights and contracts for differences of differences: models for

electric transmission property rights," *IEEE Trans. Power Syst.*, vol. 22, no. 4, pp. 1495–1506, Nov. 2007.

[113] M. Soroush and J. D. Fuller, "Accuracies of optimal transmission switching heuristics based on dcopf and acopf," *IEEE Trans. Power Syst.*, vol. 29, no. 2, pp. 924–932, Mar. 2014.

[114] R. D. Zimmerman, C. E. Murillo-Sanchez, and R. J. Thomas, "MATPOWER's extensible optimal power flow architecture," *IEEE PES General Meeting*, pp. 1–7, July 26-30 2009.

[115] ——, "MATPOWER: steady-state operations, planning, and analysis tools for power systems research and education," *IEEE Trans. Power Syst.*, vol. 26, no. 1, pp. 12–19, Feb. 2011.

[116] Y. Al-Abdullah, M. A. Khorsand, and K. W. Hedman, "Analyzing the impacts of out-of-market corrections," *2013 IREP Symposium IX -Bulk Power System Dynamics and Control, Rethymnon, Greece*, pp. 1–10, 2013.

[117] B. Whittle, J. Yu, S. Teng, and J. Mickey, "Reliability unit commitment in ERCOT," in *Proceedings of the IEEE Power Engineering Society General Meeting*, Montreal, Qubec, 2006.

[118] P. Meibom, R. Barth, B. Hasche, H. Brand, C. Weber, and M. O'Malley, "Stochastic optimization model to study the operational impacts of high wind penetrations in Ireland," *IEEE Trans. Power Syst.*, vol. 26, no. 3, pp. 1367–1379, Aug. 2011.

[119] J. F. Restrepo and F. D. Galiana, "Assessing the yearly impact of wind power through a new hybrid deterministic/stochastic unit commitment," *IEEE Trans. Power Syst.*, vol. 26, no. 1, pp. 401–410, Feb. 2011.

[120] R. Jiang, J. Wang, and Y. Guan, "Robust unit commitment with wind power and pumped storage hydro," *IEEE Trans. Power Syst.*, vol. 27, no. 2, pp. 800–810, May 2012.

[121] A. Philpott and R. Schultz, "Unit commitment in electricity pool markets," *Math. Program.*, vol. 108, no. 2–3, pp. 313–337, Sep. 2006.

[122] S. Sen, L. Yu, and T. Genc, "A stochastic programming approach to power portfolio optimization," *Oper. Res.*, vol. 54, no. 1, pp. 55–72, Jan. 2006.

[123] N. Gröwe-Kuska, K. C. Kiwiel, M. P. Nowak, W. Römisch, and I. Wegner, "Power management in a hydro-thermal system under uncertainty by Lagrangian relaxation," in *IMA Volumes in Mathematics and Its Applications*, vol. 128. Springer, 2002, pp. 39–70.

[124] L. El Ghaoui and H. Lebret, "Robust solutions to least-squares problems with uncertain data," *SIAM J. Matrix Anal. Appl.*, vol. 18, no. 4, pp. 1035–1064, Oct. 1997.

[125] L. Baringo and A. J. Conejo, "Offering strategy via robust optimization," *IEEE Trans. Power Syst.*, vol. 26, no. 3, pp. 1418–1425, Aug. 2011.

[126] A. Street, F. Oliveira, and J. M. Arroyo, "Contingency-constrained unit commitment with n-K security criterion: a robust optimization approach," *IEEE Trans. Power Syst.*, vol. 26, no. 3, pp. 1581–1590, Aug. 2011.

[127] A. H. Hajimiragha, C. A. Cañizares, M. W. Fowler, S. Moazeni, and A. Elkamel, "A robust optimization approach for planning the transition to plug-in hybrid electric vehicles," *IEEE Trans. Power Syst.*, vol. 26, no. 4, pp. 2264–2274, Nov. 2011.

[128] D. Bertsimas, E. Litvinov, X. A. Sun, J. Zhao, and T. Zheng, "Adaptive robust optimization for the security constrained unit commitment problem," *IEEE Trans. Power Syst.*, vol. 28, no. 1, pp. 52–63, 2013.

[129] A. T. Al-Awami and M. A. El-Sharkawi, "Coordinated trading of wind and thermal energy," *IEEE Trans. on Sustainable Energy*, vol. 2, no. 3, pp. 277–287, Jul. 2011.

[130] A. Botterud, Z. Zhou, J. Wang, R. J. Bessa, H. Keko, J. Sumaili, and V. Miranda, "Wind

power trading under uncertainty in LMP markets," *IEEE Trans. Power Syst.*, vol. 27, no. 2, pp. 894–903, May 2012.

[131] H. Aissi, C. Bazgan, and D. Vanderpooten, "Min-max and min-max regret versions of combinatorial optimization problems: a survey," *Eur. J. Oper. Res.*, vol. 197, no. 2, pp. 427–438, Sep. 2009.

[132] A. O. Kazakçi, S. Rozakis, and D. Vanderpooten, "Energy crop supply in France: a min-max regret approach," *J. Oper. Res. Soc.*, vol. 58, no. 11, pp. 1470–1479, Nov. 2007.

[133] X. Guan, P. B. Luh, H. Yan, and J. A. Amalfi, "An optimization-based method for unit commitment," *Int. J. Electr. Power Energy Syst.*, vol. 14, no. 1, pp. 9–17, Feb. 1992.

[134] S. J. Wang, S. M. Shahidehpour, D. S. Kirschen, S. Mokhtari, and G. D. Irisarri, "Short-term generation scheduling with transmission and environmental constraints using an augmented Lagrangian relaxation," *IEEE Trans. Power Syst.*, vol. 10, no. 3, pp. 1294–1301, 1995.

[135] C. Tseng, S. Oren, C. Cheng, C. Li, A. Svoboda, and R. Johnson, "A transmission-constrained unit commitment method in power system scheduling," *Decision Support Systems*, vol. 24, no. 3, pp. 297–310, 1999.

[136] R. Jiang, M. Zhang, G. Li, and Y. Guan, "Benders decomposition for the two-stage security constrained robust unit commitment problem," *Preprint available at: www.optimization-online.org*, 2011.

[137] G. Nemhauser and L. Wolsey, *Integer and Combinatorial Optimization*. Wiley, 1988.

[138] H. Konno, "A cutting plane algorithm for solving bilinear programs," *Math. Program.*, vol. 11, no. 1, pp. 14–27, Dec. 1976.

[139] F. Bouffard and F. D. Galiana, "Stochastic security for operations planning with significant wind power generation," in *Power and Energy Society General Meeting - Conversion and Delivery of Electrical Energy in the 21st Century*, Pittsburgh, PA, 2008.

[140] A. Kleywegt, A. Shapiro, and T. Homem-de Mello, "The sample average approximation method for stochastic discrete optimization," *SIAM J. Optim.*, vol. 12, no. 2, pp. 479–502, Jan. 2002.

[141] H. Zareipour, "Wind power ramp events classification and forecasting: A data mining approach," in *Proceedings of the IEEE Power Engineering Society General Meeting*, Detroit, MI, 2011.

[142] R. Billinton and R. Karki, "Capacity reserve assessment using system well-being analysis," *IEEE Trans. Power Syst.*, vol. 14, p. 433438, 1999.

[143] H. Gooi, D. Mendes, K. Bell, and D. Kirschen, "Optimum scheduling of spinning reserve," *IEEE Trans. Power Syst.*, vol. 14, p. 14851490, 1999.

[144] R. Billinton and M. Fotuhi-Firuzabad, "A reliability framework for generating unit commitment," *Elect. Power Syst. Res.*, vol. 56, no. 1, pp. 81–88, 2000.

[145] F. Aminifar, M. Fotuhi-Firuzabad, and M. Shahidehpour, "Unit commitment with probabilistic spinning reserve and interruptible load considerations," *IEEE Trans. Power Syst.*, vol. 24, no. 1, p. 388397, 2009.

[146] M. A. Ortega-Vazquez and D. S. Kirschen, "Estimating the spinning reserve requirements in systems with significant wind power generation penetration," *IEEE Trans. Power Syst.*, vol. 24, no. 1, p. 114124, 2009.

[147] Y. Guan and J. Wang, "Uncertainty sets for robust unit commitment," *IEEE Trans. Power Syst.*, vol. 29, no. 3, pp. 1439–1440, 2014.

[148] J. Lyon, K. W. Hedman, and M. Zhang, "Reserve requirements to efficiently manage intra-

zonal congestion," *IEEE Trans. Power Syst.*, vol. 29, no. 1, pp. 251–258, Jan. 2014.

Intentionally Blank Page

Part II

A Zonotope-Based Method for Capturing the Effect of Variable Generation on the Power Flow

Alejandro Domínguez-García
Xichen Jiang
University of Illinois at Urbana-Champaign

For information about this part of the project report, contact:

Alejandro Domínguez-García
Department of Electrical and Computer Engineering
306 N. Wright Street,
Urbana, IL 61801
Phone: 217 333-0394
Email: aledan@illinois.edu

Power Systems Engineering Research Center

The Power Systems Engineering Research Center (PSERC) is a multi-university Center conducting research on challenges facing the electric power industry and educating the next generation of power engineers. More information about PSERC can be found at the Center's website: http://www.pserc.org.

For additional information, contact:

Power Systems Engineering Research Center
Arizona State University
527 Engineering Research Center
Tempe, Arizona 85287-5706
Phone: 480-965-1643
Fax: 480-965-0745

Contents

List of Tables

List of Figures

Chapter 1

Introduction

The integration of renewable resources such as wind and solar introduces additional uncertainty on the generation side of a power system since these power sources are intermittent and difficult to forecast. Such uncertainty invariably affects the system operation across all time scales, from day-ahead scheduling to automatic generation control, and across all subsystems, including transmission and generation. Our work focuses on capturing the effect of this uncertainty in electricity generation using a set-theoretic approach. Given the uncertainty in renewable-based electricity generation, it is possible to determine whether the system static state variables, i.e., bus voltage magnitudes and angles, are within their acceptable ranges using the proposed method.

Deterministic power flow analysis does not capture the uncertainty associated with renewable-based electricity generation as it only provides a snapshot of the system states at a particular time for a specific generation and load profile. In order to assess the effects of uncertain generation on the power flow solution, two main approaches have been developed; they include probabilistic and set-theoretic methods. In probabilistic power flow analysis (see, e.g., [1]), uncertainty in load and generation is modeled as a random vector, which results in the power flow solution also being described by a random vector. Both numerical and analytical methods have been proposed to address the probabilistic power flow problem [2]–[5]. Other researchers have addressed the issues of efficiency and accuracy in calculating the probability density functions of the bus voltages and line flows [6]–[10]. In set-theoretic methods, some of the system parameters and variables are assumed to be unknown, but constrained to lie within a bounded set [11]. For example, in interval analysis [12]–[15], it is assumed that some line parameters and loads take values within a symmetric polytope. This uncertainty is propagated through the power system model, resulting in a solution that is also constrained within some symmetric polytope. A disadvantage of this method is that the polytope, which contains the set of all possible solutions, may be overly conservative and contains non-solutions as well. In our previous work, we used ellipsoids to capture the uncertainty in renewable-based electricity generation [16]; however, that method becomes progressively less efficient when applied to larger systems.

In the analysis method proposed in this report, we capture the uncertain variations in renewable-based generation with a zonotope where its center is the nominal forecast value. As an example, the power produced by a rooftop solar installation can be assumed to lie within some interval around a nominal power output value, which may be based on the

forecasted solar insolation level. Using set operations, we propogate this zonotope through a linearized model of the power system. The result is a zonotope which bounds the bus voltage magnitudes and angles. To determine whether renewable-based power generation variability has a significant impact on power system static performance, we verify that this zonotope is contained within the region of the static state space defined by system operational requirements, such as minimum and maximum bus voltage values. Zonotopes are ideal candidates for uncertainty analysis because they can be efficiently encoded, are computationally tractable, and are closed under linear transformations [17]. Additionally, our method is equally applicable to both distribution and transmission systems and scales with the size of the system.

Zonotopes have been used in several power and energy system applications to capture the impact of uncertainty on dynamic performance [18, 19, 20, 21]. Specifically, in [18], [19], zonotopes are used to address the general problem of quantifying the impact of uncertainty in initial states and inputs on power system dynamics. Similarly, [20] proposes the use of zonotopes to study the impact of high-capacity transmission on power system frequency dynamics. In the context of wind-energy conversion systems, zonotopes have also been used in design verification problems pertaining to voltage ride-through capabilities of the system's power electronics converter [21].

It is important to note that in relation to the works in [18, 19, 20], while we also use zonotopes for uncertainty modeling, our setting is very different in the sense that we are interested in capturing the impact of uncertainty in variable generation on the power flow. In other words, instead of dealing with a dynamic problem as in [18, 19, 20], we solve a static problem similar to the one we worked on in our earlier papers [22], [16], where we used ellipsoids instead of zonotopes; however, ellipsoids bounding the system uncertainty become more difficult to compute as its size increases. In this report, we show that the use of zonotopes complements the ellipsoidal methods we proposed in [22], [16], as they fill in many of the shortcomings associated with ellipsoids.

The remainder of this report is organized as follows. In Chapter 2, we introduce the fundamental ideas behind uncertainty modeling using zonotopes and apply them to study the impact of uncertain renewable-based electricity generation in power systems. We illustrate these ideas through a simple 4-bus example. Chapter 3 presents the results of the proposed methodology applied to the IEEE 34-bus and 123-bus distribution systems, and the IEEE 145-bus transmission system. We compare the performance of our method against the linearized and the nonlinear power flow computations and present the results in Chapter 4. Concluding remarks are made in Chapter 5.

Chapter 2

Uncertainty in Power Systems

In this chapter, we introduce a set-theoretic method for capturing the effect of uncertainty in renewable-based electricity generation on the power system state variables, i.e., voltage magnitudes and angles. The unknown-but-bounded uncertainty in the renewable-based generation is upper-bounded with a zonotope. We linearize the power flow equations around a nominal operating point (based on the nominal forecast of renewable-based power generation profile), and propagate the zonotope through the linearized system to obtain another zonotope that bounds the power system static states.

2.1 Power System Model Fundamentals

In order to capture the impact of uncertainty in renewable-based electricity generation connected to the power system network, we first present the conventional power flow equations. Let V_i and θ_i denote the voltage magnitude and angle of bus i and P_i^g (P_i^d) and Q_i^g (Q_i^d) denote the generation (demand) of real and reactive power at bus i. Then, the power balance equations for real and reactive power at bus i can be written as,

$$\begin{aligned} P &= V_i \sum_{k=1}^{n} V_k \left[G_{ik} \cos(\theta_i - \theta_k) + B_{ik} \sin(\theta_i - \theta_k) \right], \\ Q &= V_i \sum_{k=1}^{n} V_k \left[G_{ik} \sin(\theta_i - \theta_k) - B_{ik} \cos(\theta_i - \theta_k) \right], \end{aligned} \tag{2.1}$$

where $P = P_i^g - P_i^d$, $Q = Q_i^g - Q_i^d$; G_{ik} and B_{ik} are the real and imaginary parts of the (i,k) entry in the network admittance matrix, respectively. For an n bus system, let m denote the number of PQ buses. Then, after removing the slack bus active and reactive power balance equations (assumed to be bus 1), and the reactive power balance equations for the PV buses, we can write the remaining equations of (2.1) as

$$u + w = f(x), \tag{2.2}$$

where the nonlinear vector function $f : \mathbb{R}^{n+m-1} \mapsto \mathbb{R}^{n+m-1}$ denotes the mapping between the system states and the power injections; $x \in \mathbb{R}^{n+m-1}$ represents unknown quantities to be

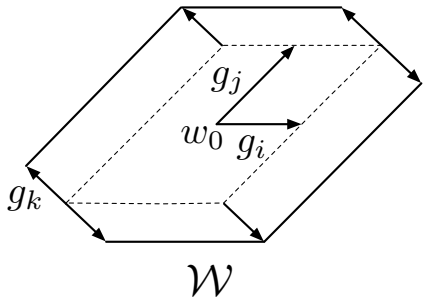

Figure 2.1: Construction of a zonotope.

solved for, which includes V_i and θ_i for PQ buses and θ_i for PV buses; $u \in \mathbb{R}^{n+m-1}$ contains active power injections in PV buses arising from conventional sources and the demands of active power in PV buses and the demand of both active and reactive power in PQ buses; $w \in \mathbb{R}^{n+m-1}$ contains renewable-based active power generation in the PV and PQ buses, and the reactive power injections in PQ buses. Note that in (2.2), the entries of u corresponding to reactive power balance equations in PQ buses and the entries of w corresponding to buses without renewable-based generation and load are all zero.

2.2 Zonotopes

Zonotopes are a special instance of polytopes which can be defined as the Minkowski sum of a finite number of line segments. Formally, a zonotope is defined as

$$\mathcal{W} = \{w : w = w_0 + \sum_{j=1}^{s} \alpha_j g_j,\ -1 \leq \alpha_j \leq 1\}. \tag{2.3}$$

where $w_0 \in \mathbb{R}^{n+m-1}$ is the center of the zonotope and $g_1, g_2, \ldots, g_s \in \mathbb{R}^{n+m-1}$ form the set of linearly independent generators [17]. Figure 2.1 illustrates how a zonotope is constructed from the Minkowski sum of its generators.

Zonotopes also have the useful property of being closed under linear transformations. Thus, given a zonotope $\mathcal{W}$ and a linear transformation matrix $H \in \mathbb{R}^{(n+m-1)\times(n+m-1)}$, we can obtain another zonotope $\mathcal{X}$ after applying the linear transformation as follows:

$$\begin{aligned} \mathcal{X} &= H\mathcal{W} \\ &= \{x : x = Hw_0 + H\sum_{j=1}^{s} \alpha_j g_j,\ -1 \leq \alpha_j \leq 1\}. \end{aligned} \tag{2.4}$$

2.3 Problem Statement: Unknown-but-bounded Model

In general, load forecasts are more accurate than renewable-generation forecast [23]. Therefore, we assume that uncertainty in the power injections only appear in w (although we can easily extend our formulation to include uncertainty in the load). The vector w can be

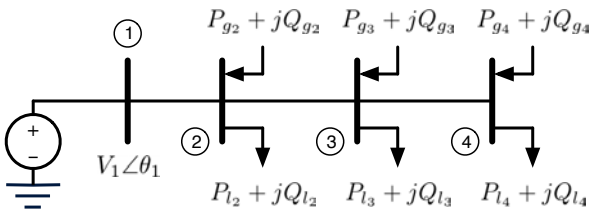

Figure 2.2: Four-bus system with renewable power injection.

expressed as $w = w_0 + \Delta w$ where w_0 denotes the vector of nominal values that w takes from the generation forecast. Assuming the values that w can take are unknown-but-bounded, we can capture the uncertainty in w with a zonotope $\mathcal{W}$ according to (2.3). The magnitudes of the generators correspond to the amount of uncertainty in the values of w. In addition, the angles between each pair of generator vectors provide a measure of correlation between the variables of w.

Example 1 (Four-bus system) *Consider the four-bus system shown in Fig. 2.2 with renewable-based resources connected to buses 2, 3, and 4. Suppose the nominal forecast for renewable generation is* $w_0 = [P^0_{g2}\ P^0_{g3}\ P^0_{g4}]^T = [0.4\ 0.3\ 0.5]^T$ *p.u. with an uncertainty of* $\pm 50\%$ *of the nominal forecast. Then, following the notation of* (2.3)*, the generator vectors are* $g_1 = [0.2\ 0\ 0]^T$*,* $g_2 = [0\ 0.15\ 0]^T$*, and* $g_3 = [0\ 0\ 0.25]^T$*. For this particular example, the zonotope* $\mathcal{W}$ *capturing the uncertainty in* w *is a rectangular prism with sides having lengths of* 0.4*,* 0.3*, and* 0.5*, centered at* $[0.4\ 0.3\ 0.5]^T$*.* ■

We are interested in propagating this uncertainty set $\mathcal{W}$ through the power system model of (2.1) to obtain a set $\mathcal{X}$ that bounds all possible values that the system state x can take. To do this, we first linearize the nonlinear mapping $f(\cdot)$ about its nominal solution x_0 corresponding to $w = w_0$ and $u = u_0$. Let $\Delta w := w - w_0$ where $w \in \mathcal{W}$. Then for sufficiently small w,

$$\Delta w \approx J \Delta x, \tag{2.5}$$

where $J = \frac{\partial f}{\partial x}\Big|_{x_0}$ is the power flow Jacobian evaluated at x_0. Thus, inverting the Jacobian, we can express the sensitivity of the state variable x to w as

$$\Delta x \approx M \Delta w, \tag{2.6}$$

where $M = J^{-1}$.

Zonotopes have the useful property of being closed under linear transformations. Thus, given the input uncertainty set $\mathcal{W}$ defined in (2.3), we can propagate the zonotope through (2.6) to obtain a set $\mathcal{X}$ that contains all possible values that x can attain as follows:

$$\begin{aligned} \mathcal{X} &= H\mathcal{W} \\ &= \{x : x = Hw_0 + H\sum_{j=1}^{s} \alpha_j g_j,\ -1 \le \alpha_j \le 1\}. \end{aligned} \tag{2.7}$$

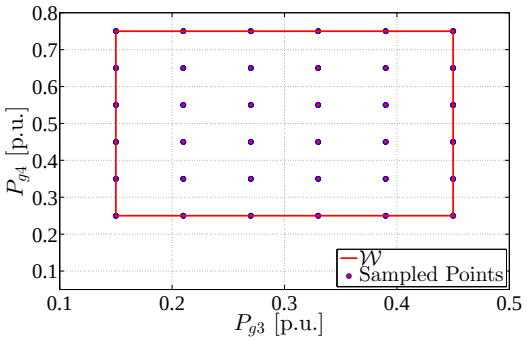

(a) Input uncertainty set and bounding zonotope $\mathcal{W}$

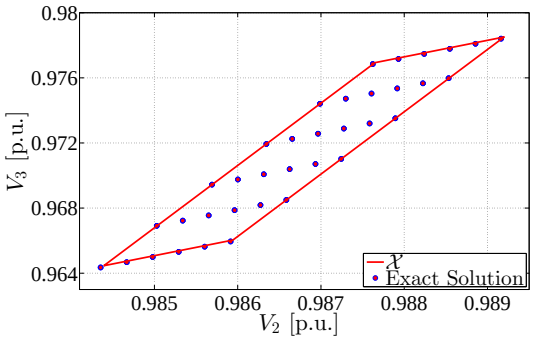

(b) State-bounding zonotope $\mathcal{X}$ and exact solution points.

Figure 2.3: Four-bus test system's input and state bounding zonotopes.

Example 2 (Four-bus system) *Continuing with the four-bus system of Example 1, we compute the zonotope $\mathcal{X}$ that bounds the possible values of the state vector x resulting from uncertainty in the active power injections in w using* (2.7)*. The center of zonotope $\mathcal{X}$, x_0, is computed from w_0 using the nonlinear power flow equations of* (2.1)*. Table 2.1 shows the nominal power flow solutions of this system. The zonotope $\mathcal{W}$ capturing the uncertainty in w is projected onto the $P_{g3} - P_{g4}$ axis and shown in Fig. 2.3(a) and the resulting zonotope $\mathcal{X}$ bounding the system states V_2 and V_3 is shown in Fig. 2.3(b). In addition, we sampled the input space $\mathcal{W}$ and calculated the corresponding exact solutions to the power flow equations of* (2.1)*. In Fig. 2.3(b), we see that one of the solutions points lie on the outside of the zonotope $\mathcal{X}$, which can be attributed to error from linearization.* ■

2.3.1 Performance Requirements Verification

In a power system, static performance requirements include constraints in the form of interval ranges on i) the values that system states can take, and/or ii) the values that functions of these states can take. For example, bus voltage magnitudes are generally required to remain within ±5% of its nominal value. Also, transmission line flows, which can be obtained as a function of the states, are constrained by maximum capacity limits. Thus, once $\mathcal{X} \approx \{x_0\} \oplus \Delta\mathcal{X}$ is obtained, we can verify whether a system meets all its performance criteria for the renewable-based generation scenario described by $\mathcal{W}$.

Table 2.1: Four-bus system nominal power flow solution.

w_0	$P^0_{g_2}$	$Q^0_{g_2}$	$P^0_{g_3}$	$Q^0_{g_3}$	$P^0_{g_4}$	$Q^0_{g_4}$
	0.4	0	0.3	0	0.5	0
u_0	$P^0_{l_2}$	$Q^0_{l_2}$	$P^0_{l_3}$	$Q^0_{l_3}$	$P^0_{l_4}$	$Q^0_{l_4}$
	0.8	0.25	0.5	0.1	0.9	0.5
x_0	V^0_2	θ^0_2	V^0_3	θ^0_3	V^0_4	θ^0_4
	0.987	$-0.124°$	0.972	$-0.273°$	0.965	$-0.302°$

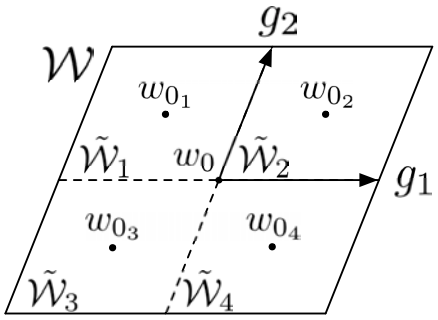

Figure 2.4: Input uncertainty set partition.

Let $z = h(x)$ define some performance metric of interest, where $h : \mathbb{R}^{n+m-1} \mapsto \mathbb{R}^p$, and let Φ denote a set in $\mathbb{R}^p$ defined by performance requirements. Then, for the system to meet all its performance criteria, the set $\mathcal{Z}$ that results from $\mathcal{X}$ and the mapping $h(\cdot)$, i.e., $\mathcal{Z} = \{z : z = h(x),\ x \in \mathcal{X}\}$, must be contained in Φ. As already mentioned, unless $h(\cdot)$ is linear, mapping a set through a nonlinear function is not an easy task. Therefore, as before, we resort to linearization to obtain $\mathcal{Z} \approx \{z_0\} \oplus \Delta\mathcal{Z}$, where $z_0 = h(x_0)$, and then check whether or not $\{z_0\} \oplus \Delta\mathcal{Z} \subseteq \Phi$.

Requirements on the values that system states can take

In this case $z = x$, thus performance requirements constrain the values that the state x can take to some region of the state space Φ defined by the symmetric polytope

$$\Phi = \{x : |\pi_i^T(x - x_0)| \leq 1 \quad \forall i = 1, \ldots, n + m - 1\}. \tag{2.8}$$

where $\pi_i \in \mathbb{R}^n$ is a unitary vector parallel to the i^{th} axis. Since $z = x$, then $\mathcal{Z} = \mathcal{X}$; thus in order to verify that the system meets performance requirements for any $w \in \mathcal{W}$, we need to verify whether or not $\{x_0\} + \Delta\mathcal{X} \subseteq \Phi$.

2.3.2 Very Large Variations in Renewable-Based Power

The linearization in (2.5) is justified for a small change in w around w_0. If the uncertainty in w is large, then the accuracy of the linearization degrades and the exact solutions may lie outside of the zonotope bound $\mathcal{X}$, which was exemplified in Example 2. However, for large variability, we can improve the accuracy of $\mathcal{X}$ by subdividing $\mathcal{W}$ into a partition of l disjoint subsets $\{\tilde{\mathcal{W}}_1, \tilde{\mathcal{W}}_2, \ldots, \tilde{\mathcal{W}}_l\}$, i.e., $\mathcal{W} = \bigcup_{i=1}^{l} \tilde{\mathcal{W}}_i$, where $\tilde{\mathcal{W}}_i \bigcap \tilde{\mathcal{W}}_j = \emptyset$, $\forall i \neq j$. While the shape of the $\tilde{\mathcal{W}}_i$'s could be arbitrary as long as they form a partition of $\mathcal{W}$, we choose them to also be zonotopes with the same shape and orientation as $\mathcal{W}$ and all of equal size; the idea is graphically depicted in Fig. 2.4 for a two-dimensional set. The centers of all the $\tilde{\mathcal{W}}_i$'s can be obtained from (2.3) and are given by

$$\begin{aligned} \mathcal{C} = \{w : w =& w_0 + \sum_{j=1}^{s} \alpha_j g_j,\ \alpha_j = \pm(1 + 2k)/(2n_j), \\ & k = 0, 1, ..., n_j - 1\}, \end{aligned} \tag{2.9}$$

where $2n_j$ is the number of segments into which the segment that spans the set $\mathcal{W}$ in the direction of the j^{th} axis is divided. Then, $\tilde{\mathcal{W}}_i$, which corresponds to $w_{0_i} \in \mathcal{C}$, is described by

$$\tilde{\mathcal{W}}_i = \{w : w = w_{0_i} + \sum_{j=1}^{s} \alpha_j g_j,\ -1/(2n_j) \leq \alpha_j \leq 1/(2n_j)\}$$

Each $\tilde{\mathcal{W}}_i$ is constructed, via appropriate choice of n_j, so that the variations in w around w_{0_i} are sufficiently small such that $\Delta w \approx J_i \Delta x$, where J_i is the power flow Jacobian evaluated at $x = x_{0_i}$, i.e., the power flow solution that corresponds to w_{0_i}. In this way, the problem is divided into several subproblems. By applying the same ideas as previously mentioned to each zonotope $\tilde{\mathcal{W}}_i$, we obtain $\tilde{\mathcal{X}}_i$, the set that bounds all bus voltage magnitudes and angles corresponding to variations in $\tilde{\mathcal{W}}_i$. Finally, the set $\mathcal{X}$ that bounds all possible values that bus voltage magnitudes and angles can take as a result of $\mathcal{W}$ is given by

$$\mathcal{X} = \bigcup_{i=1}^{l} \tilde{\mathcal{X}}_i. \tag{2.10}$$

Chapter 3

Case Studies

In this chapter, we validate the framework developed in Chapter 2 by comparing the results obtained using the proposed analysis method against the exact solutions computed from the power flow equations (2.1). The case studies are performed on the IEEE 34-bus and 123-bus test systems taken from the IEEE PES Distribution System Analysis Subcommittee and have a power base of 100 kVA and a voltage base of 4.16 kV [24]. To show the applicability of this method to large transmission systems, we apply the method to the IEEE 145-bus, 50-machine transmission system [25, 26]. These systems are modified to include power injection resulting from renewable resources at a subset of buses. For each case study we linearize the system before propagating the uncertainty in renewable-based generation through the model. Then we examine the impact of uncertainty on bus voltage magnitudes. The MatLab code for simulating the case studies are provided in Appendix B.

3.1 34-bus System

The one-line diagram and complete description for this system can be found in [24]. Suppose that for this system, renewable-based electricity resources are installed at buses 3, 7, 10, 15, 18, 23, 27, 29, 30, and 34, with nominal real power injection of 1 p.u. and an uncertainty of ±50% (±0.5 p.u.) around the nominal value. In order to determine whether the system states will remain within bounds dictated by performance requirements, we first we bound

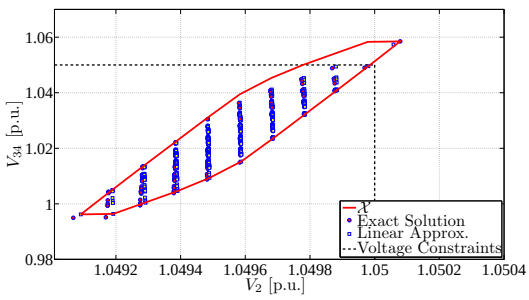

(a) Renewable-based power injections with variability of ±50% around each nominal value of 1 p.u.

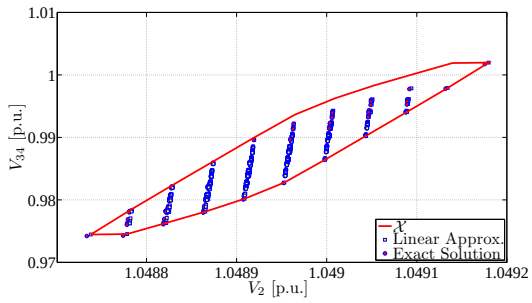

(b) Renewable-based power injections with variability around each nominal value of 0.4 p.u.

Figure 3.1: 34-bus system: power flow solutions and state-bounding zonotope projections.

the power injection space with zonotope $\mathcal{W}$. Then we compute the corresponding state-bounding zonotope $\mathcal{X}$ using (2.7). The resulting zonotope is projected onto the subspace defined by the V_2-V_{34} axis and shown in Fig. 3.1(a). Additionally, we also sampled the input power injection space and obtained the corresponding solutions of the linearized power flow as well as the exact solutions of the nonlinear power flow and depicted them with squares and circles, respectively. The resulting projection of the zonotope $\mathcal{X}$ contained all the linearized power flow solutions and all but the extrema of the nonlinear power flow solution. Thus, we can conclude that the linearization is fairly accurante. In fact, for this case study, we computed the percent error between the voltage magnitudes obtained through linearized power flow and nonlinear power flow for each sample point and found the maximum to be only 3.14%. From the figure, we can also conclude that for the uncertainty levels selected, a portion of the input space maps to a region in the solution state space that violates the voltage constraints of 1.05 p.u., which are depicted with dashed lines. This conclusion is also verified by the linearized and exact nonlinear power flow solutions. Therefore, we cannot conclude that the system states will remain within the performance requirements if this system is subjected to this level of uncertainty in power injection arising from renewable resources.

Now suppose the nominal real power injection is 0.4 p.u. (instead of 1 p.u.) at the same buses and that the uncertainty of the power injections at the affected buses remains at $\pm 50\%$ (± 0.5 p.u.) around the nominal value. The result is shown in Fig. 3.1(b) along with the linearized and exact nonlinear power flow solutions. We conclude that for the the power injection and uncertainty levels chosen, no voltage magnitude violations for buses 2 and 34 are detected.

The one-line diagram and complete description for this system can be found in [24]. Suppose that for this system, renewable-based electricity generation resources are installed at buses 80, 95, 96, 103, 108, 110, 115, 121, 122, and 123, with nominal real power injection of 1 p.u. and an uncertainty of $\pm 50\%$ (± 0.5 p.u.) around the nominal value. In order to determine whether the system states will remain within bounds dictated by performance requirements, we first bound the power injection space with zonotope $\mathcal{W}$. Then we compute the corresponding state-bounding zonotope $\mathcal{X}$ using (2.7). The resulting zonotope is projected onto the subspace defined by the V_{110}-V_{123} axis and shown in Fig. 4.1(a). Additionally, we sampled the input power injection space and obtained the corresponding solutions of the linearized power flow as well as the exact solutions of the nonlinear power flow and depicted them with squares and circles, respectively. The resulting projection of the zonotope $\mathcal{X}$ contained all the linearized power flow solutions and all but the extrema of the nonlinear power flow solution. Thus, we can conclude that the linearization is fairly accurate. In fact, for this case study, we computed the percent error between the voltage magnitudes obtained through the linearized power flow and the nonlinear power flow for each sample point and found the maximum to be only 2.5%.

3.2 123-bus Distribution System

From Fig. 4.1(a), we can also conclude that for the uncertainty levels selected, a portion of the input space maps to a region in the solution state space that violates the voltage constraints of 1.05 p.u., which are depicted with dashed lines. This conclusion is also verified by the linearized and exact nonlinear power flow solutions. Therefore, we cannot conclude that the system states will remain within the performance requirements if this system were subjected to this level of uncertainty in power injection arising from renewable resources.

Now suppose the nominal real power injection is 0.8 p.u. (instead of 1 p.u.) at the same buses and that the uncertainty of the power injections at the affected buses remains at ±50% (±0.4 p.u.) around the nominal value. The result is shown in Fig. 4.1(b) along with the linearized and exact nonlinear power flow solutions. We conclude that for the the power injection and uncertainty levels chosen, no voltage magnitude violations for buses 110 and 123 are detected.

Next, we show how the proposed method can be used to assess whether or not the active power flow through Lines 2 and 100 violate corresponding requirements. In Fig. 3.3, we plot the line flow bounding zonotope $\mathcal{Z}$ computed from a corresponding $\mathcal{X}$ bounding the state variable uncertainty. We also plot several exact line flow solution points obtained from the nonlinear power flow equations by sampling the input space; note that all these points are contained in $\mathcal{Z}$.

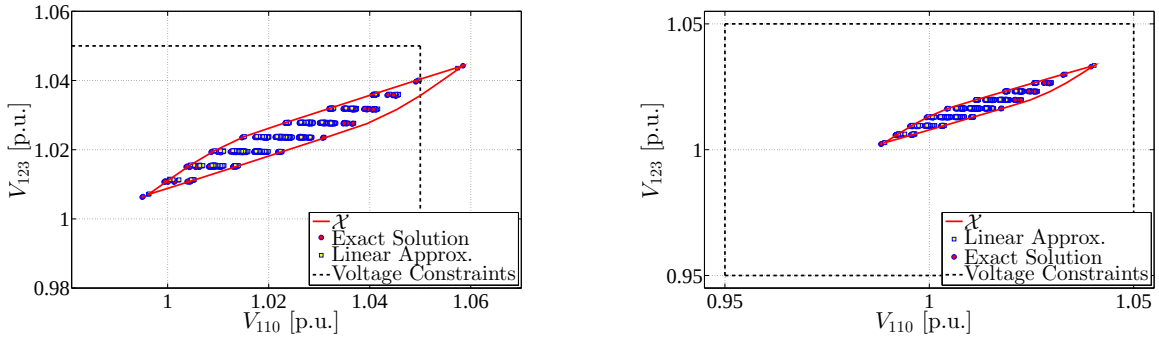

(a) Renewable-based power injections with variability of ±50% around each nominal value of 1 p.u.

(b) Renewable-based power injections with variability of ±50% around each nominal value of 0.8 p.u.

Figure 3.2: 123-bus system: nonlinear and linearized power flow solutions, and state-bounding zonotope projections.

3.3 145-bus Transmission System

A full description of the IEEE 145-bus transmission system can be found in [25]. Suppose renewable-based electricity resources are installed at the buses listed in Table 3.1, which also specifies their respective nominal power outputs and uncertainty in power injection. We capture this uncertainty with a zonotope $\mathcal{W}$, and use it to compute the state-bounding zonotope $\mathcal{X}$ that contains all possible values of x. The projection of $\mathcal{X}$ onto the V_{100}-V_{133} axes is shown in Fig. 3.4 along with the exact power flow solutions. As in the 123-bus case,

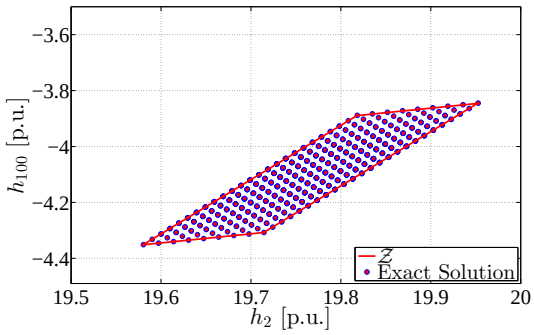

Figure 3.3: 123-bus power system.

all of the solution points lie within $\mathcal{X}$ except for one lower extreme point, which can be attributed to the error resulting from linearization. Again, we computed the maximum error of the voltage magnitudes between the linearized power flow and nonlinear power flow to be only 1.13%. Therefore, with this particular level of uncertainty in the power injection, the linearization provides an accurate estimate for the nonlinear power flow solutions.

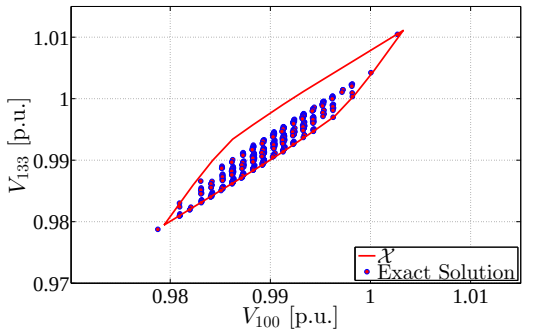

Figure 3.4: 145-bus power system.

Table 3.1: 145-bus system: data for renewable-based power injection variations.

Bus	70	85	96	110	112	120	125	128	130	133
Nominal Value [p.u.]	1	1.5	1	1	1	1.5	1	1.5	1	1
Variation [p.u.]	0.3	0.4	0.2	0.3	0.6	0.7	0.4	0.4	0.5	0.4

Chapter 4

Performance Evaluation

In this chapter, the computation time of our method is evaluated against those of solving the linearized and nonlinear power flows in MATLAB. We also compare the computation time of zonotopes against those of using ellipsoids (see Appendix A for a review of elliposoids). Our code is run on a computer equipped with Intel Core 2 Quad 8400 processor running at 2.66 GHz. For our method, we provide the time required to compute $\mathcal{X}$ from the input uncertainty space $\mathcal{W}$ along with the time required to compute the linearized and nonlinear power flow solutions by sampling the extremas of $\mathcal{W}$. For the ellipsoidal method, we provide the overall amount of time required to obtain the minimum-volume ellipsoid enclosing the system state variables. For the ellipsoidal method, the majority of the time is spent on computing the ellipsoid bounding the input uncertainty.

The computation times required for each of the test cases in Chapter 3 and the 4-bus example are shown in Table 4.1. As the number of buses with renewable-based generation increase, the time required to compute the nonlinear power flow solutions corresponding to the extremas of $\mathcal{W}$ grows much more quickly than that required for the linearized power flow, zonotope, and ellipsoidal methods. In fact, obtaining the exact power flow solutions required more than 12 hours to solve when there are more than 12 buses with renewable-based generation, while the computation time for the zonotope and ellispoidal method remained nearly constant. Lastly, if interior points of the input space were also sampled in addition to the extremas of $\mathcal{W}$, then significantly longer times are required for obtaining the corresponding nonlinear and linearized power flow solution points, rendering the computations intractable. On the other hand, our proposed method does not exhibit any significant increase in computation time when used on a larger system. Although the computational times for both ellipsoids and zonotopes seem low, zonotopes do have the extra flexibility of being able to

Table 4.1: Comparison of overall computation times [s] for for 4-,34-, 123-, and 145-bus systems.

	4-bus	34-bus	123-bus	145-bus
Ellipsoid	1.29	2.96	2.62	2.55
Zonotope	0.00037	0.012	0.038	0.15
Linear Approx.	0.00002	0.007	0.046	0.057
Nonlinear PF	0.011	13.45	173.55	219.15

handle asymmetrical power injections. If ellipsoids were used to capture asymmetrical power injections, then the optimization used to compute the minimum-volume input ellipsoids does not scale well to the size of the system.

For comparison, we computed the state bounding ellipsoid, $\mathcal{E}$, for the same 123-bus example shown in Fig. 3.2 and show the results in Fig. 4.1. For this example, we conclude that the ellipsoids captured additional points that are extraneous to the zonotopes; that is, the zonotopes provide a better bound to the uncertainty in power system state variables than ellipsoids.

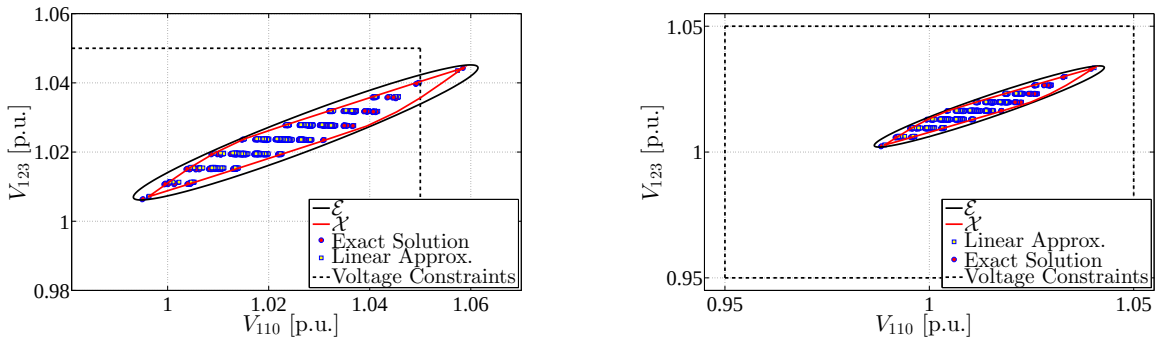

(a) Renewable-based power injections with variability of ±50% around each nominal value of 1 p.u.

(b) Renewable-based power injections with variability of ±50% around each nominal value of 0.8 p.u.

Figure 4.1: 123-bus system: zonotopes and ellipsoids.

Chapter 5

Conclusion

This report proposes a set-theoretic method to assess the impact of unknown-but-bounded power injections resulting from renewable resources. The unknown-but-bounded uncertainty in the power injections are captured using a zonotope which is subsequently propagated through the linearized power-flow model of the system to obtain another zonotope that bounds the worst-case deviation of the system state variables. From this method, we can determine whether the system state variables will remain within the ranges specified by operational requirements when subjected to the uncertainty in renewable generation. This proposed method can be combined with other set-theoretic methods such as using ellipsoids to provide a more comprehensive tool set for uncertainty analysis.

The validity of this method is verified on three test systems. From the test cases, we have shown that the results using our method matches closely to those obtained from repeatedly solving the nonlinear power flow for different power injections associated with various levels of uncertainty. We have also shown that our method is highly scalable with the dimensionality and the size of the system. The performance of the method is compared against those of ellipsoids and power flow equations.

Future work may include an analysis of the limits of the small-signal approximation to the power flow model. In this regard, we may wish to bound the higher-order Taylor series terms to obtain more accurate bounds for the variations in systems states caused by even deeper penetration levels than those considered in the case studies of this report. An error analysis on the linear approximation can be conducted by bounding the higher-order terms of a Taylor series expansion with the Lagrange remainder. By including the higher-order terms, we might be able to capture solution points that may lie outside of the set obtained from the linearized model.

Appendix A

Ellipsoids

In this appendix, we review a method to obtain a family of ellipsoids whose intersection provides a tight over-approximation of the input uncertainty set. Consider a static linear system described by

$$x = Hw, \tag{A.1}$$

where $x \in \mathbb{R}^r$ are the system states, $w \in \mathbb{R}^s$ are the system inputs, and $H \in \mathbb{R}^{r \times s}$. Assume that the values w can take are unknown but bounded, i.e., the possible values of w are contained in some closed and bounded zonotope set $\mathcal{W} \subseteq \mathbb{R}^s$. The objective is to obtain a set $\mathcal{X} \subseteq \mathbb{R}^r$ that contains all possible values that x can attain. In order to achieve this, we first approximate the zonotope $\mathcal{W}$ by the intersection of a family of ellipsoids $\mathcal{E} = \{\mathcal{E}_1, \mathcal{E}_2, \dots, \mathcal{E}_j, \dots\}$, each of which upper bounds $\mathcal{W}$, i.e.,

$$w \in \mathcal{W} \subseteq \bigcap_i \mathcal{E}_i, \tag{A.2}$$

with

$$\mathcal{E}_i = \{w : (w - w_0)^T \Psi_i^{-1} (w - w_0) \leq 1\}, \tag{A.3}$$

where Ψ_i is a positive definite matrix known as the *shape matrix* and w_0 is the center of the ellipsoid $\mathcal{E}_i$. Now, we propagate each ellipsoid $\mathcal{E}_i$ through (A.1) with the objective of obtaining a set $\mathcal{F}_i$ that contains all possible values of x that results from all possible values that $w \in \mathcal{E}_i$ can take. Since $w \in \mathcal{W} \subseteq \mathcal{E}_i,\ \forall i$, it immediately follows that $x \in \mathcal{X} \subseteq \mathcal{F}_i,\ \forall i$, and hence,

$$x \in \mathcal{X} \subseteq \bigcap_i \mathcal{F}_i. \tag{A.4}$$

Furthermore, it turns out that ellipsoids are closed under linear transformations; therefore the set $\mathcal{F}_i$ is also an ellipsoid and thus can be defined as

$$\mathcal{F}_i = \{x : (x - x_0)^T \Gamma_i^{-1} (x - x_0) \leq 1\}, \tag{A.5}$$

where $x_0 = Hw_0$ and $\Gamma_i = H \Psi_i H^T$ (see, e.g., [27]). The ideas introduced above are graphically depicted by Fig. A.1 for a two-dimensional system with an input set $\mathcal{W}$ upper bounded by the intersection of two ellipsoids, $\mathcal{E}_1$ and $\mathcal{E}_2$, which map to $\mathcal{F}_1$ and $\mathcal{F}_2$ respectively. As

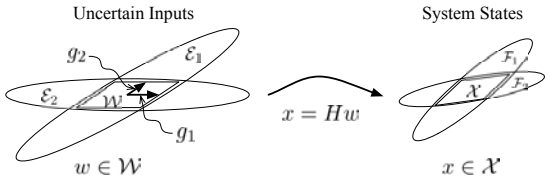

Figure A.1: Ellipsoids $\mathcal{E}_1$ and $\mathcal{E}_2$ bounding $\mathcal{W}$ (the set of all possible values that w can take), and corresponding ellipsoids $\mathcal{F}_1$ and $\mathcal{F}_2$ bounding $\mathcal{X}$.

shown in the figure, the intersection of $\mathcal{F}_1$ and $\mathcal{F}_2$ contains the set $\mathcal{X}$. The accuracy of the upper-bounding approximation of $\mathcal{X}$ provided by (A.4) depends on the choice of the ellipsoids in the family $\mathcal{E} = \{\mathcal{E}_1, \mathcal{E}_2, \ldots, \mathcal{E}_j, \ldots\}$ upper bounding the set $\mathcal{W}$.

The approach to obtaining a family of ellipsoids $\mathcal{E} = \{\mathcal{E}_1, \mathcal{E}_2, \ldots, \mathcal{E}_j, \ldots\}$ whose intersection tightly upper bounds $\mathcal{W}$ is to choose each $\mathcal{E}_i$ to contain $\mathcal{W}$ while minimizing its projection onto some direction defined by a unitary vector η_i normal to the hyperplanes of $\mathcal{W}$, $\mathcal{H}_i^+$ and $\mathcal{H}_i^-$. Thus, by minimizing the projection of the ellipsoid onto the direction defined by η_i we obtain an ellipsoid that is tight to the hyper-faces $\mathcal{H}_i^+$ and $\mathcal{H}_i^-$ of $\mathcal{W}$. This is graphically represented in Fig. A.2.

The hyperplanes $\mathcal{H}_i^+$ and $\mathcal{H}_i^-$ are defined by

$$\begin{aligned} \mathcal{H}_i^+ &= \{w : \eta_i^T[w - (w_0 + g_i)] = 0\}, \\ \mathcal{H}_i^- &= \{w : \eta_i^T[w - (w_0 - g_i)] = 0\}, \end{aligned} \tag{A.6}$$

and η_i is the unitary vector defining the hyperplane $\mathcal{H}_i^+$, such that $\eta_i^T(w + g_i) > 0,\ \forall w \notin \mathcal{W}$. Then, η_i is the vector normal to the hyperplane $\mathcal{H}_i^+$ that contains the corresponding hyperface of the zonotope $\mathcal{W}$. The projection of the ellipsoid $\mathcal{E}_i = \{w : (w - w_0)^T \Psi_i^{-1} (w - w_0) \leq 1\}$ onto the direction defined by η_i is given by $\pi_{\mathcal{E}_i}(\eta_i) = 2\sqrt{\eta_i^T \Psi_i \eta_i}$ [28]. Thus, the problem of obtaining $\mathcal{E}_i$ can be cast into an optimization program as follows:

$$\begin{aligned} \text{minimize} \quad & \sqrt{\eta_i^T \Psi_i \eta_i} \\ \text{subject to} \quad & v^T \Psi_i^{-1} v \leq 1; \qquad \forall v \in \mathcal{V}, \\ & \sqrt{\eta_j^T \Psi_i \eta_j} \leq k_j; \quad \forall j \neq i, \end{aligned} \tag{A.7}$$

where $\mathcal{V}$ is the set of vertices of $\mathcal{W}$, and k_j is the maximum length of the semi-major axis in the η_j direction. The first inequality enforces that the resulting $\mathcal{E}_i$ contains $\mathcal{W}$. The second

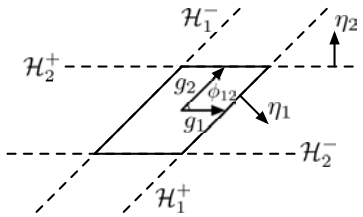

Figure A.2: Hyperplanes ($\mathcal{H}_i^+,\ \mathcal{H}_i^-$) and directions of minimum span (η_i),

set of inequalities constrains the projection of $\mathcal{E}_i$ onto the directions defined by the vectors normal to all other hyperplanes $\mathcal{H}_j^+,\ j \neq i$ and are included for solvability.

While the method described in (A.7) provides in general an accurate approximation of the input set $\mathcal{W}$ by obtaining a family of ellipsoids $\mathcal{E} = \{\mathcal{E}_i,\ i = 1, \ldots, s\}$, it requires solving the optimization program in (A.7) for each of input-bounding ellipsoids, up to the dimension of the input set, s; this computation can be parallelized using, e.g., the MATLAB parallel toolbox. In this regard, tightly upper bounding $\mathcal{W}$ results in a very accurate upper-bound on the set $\mathcal{X}$.

In certain cases, it may be convenient to obtain a single bounding ellipsoid for $\mathcal{W}$ and conduct the analysis for just this ellipsoid. While any of the ellipsoids in the family $\mathcal{E} = \{\mathcal{E}_i,\ i = 1, \ldots, s\}$ would serve this purpose, recall that each $\mathcal{E}_i \in \mathcal{E}$ is tight to $\mathcal{W}$ in a particular direction defined by η_l in the sense that projection of of the ellipsoid onto the direction defined by η_l is minimal, but its projection onto other directions $\eta_i,\ i \neq l$ might be much larger than the actual projection of $\mathcal{W}$ onto that direction. Thus, an alternative to this problem is to obtain an ellipsoid $\mathcal{E}_0 = \{w : (w - w_0)^T \Psi_0^{-1} (w - w_0) \leq 1\}$ that minimizes the sum of the projections onto all directions defining the semi-axes of $\mathcal{E}_0$, which is equivalent to minimizing the sum of the squared semi-axes of $\mathcal{E}_0$ [28]. The sum of the squared semi-axis of $\mathcal{E}_0$ is given by the $\tau_{\mathcal{E}_0} = \text{trace}(\Psi_0)$. Thus, the problem of obtaining $\mathcal{E}_0$ can be casted into an optimization program:

$$\begin{array}{ll} \text{minimize} & \text{trace}(\Psi_0) \\ \text{subject to} & v^T \Psi_0^{-1} v \leq 1, \quad \forall v \in \mathcal{V}. \end{array} \tag{A.8}$$

Appendix B

MATLAB Simulation Code

B.1 Four-Bus System

```
clear all;
close all;
clc;

load Node4.mat;
bus(2,4) = 0.4;
bus(3,4) = 0.3;
bus(4,4) = 0.5;

[soln ybus L J] = get_pf(bus,line);

H = inv(J);
S=get_pf_v3(soln,line);
P=real(S);
Q=imag(S);

[row col] = size(H);

Psi_g1 = 1e-9 * eye(size(H));
Psi_output = Psi_g1;
Psi_output_circum = Psi_g1;
Psi_g2 = Psi_g1;
Psi_g3 = Psi_g1;
Psi_g4 = Psi_g1;

%Circumscribed Ellipsoid, 0.4 0.3 0.5
Psi_g1(1,1)=0.019200359813707;
Psi_g1(2,2)=0.010800200973839;
Psi_g1(3,3)=0.029998879653079;
```

```
30
31 %Rectangular Bounds, Tight, 0.4 0.3, 0.5
32 Psi_g2(1,1)=1.166400001020240;
33 Psi_g2(2,2)=0.007239848297445;
34 Psi_g2(3,3)=0.020109999995486;
35
36 Psi_g3(1,1)=0.012841364416638;
37 Psi_g3(2,2)=1.123600000627010;
38 Psi_g3(3,3)=0.020063939576689;
39
40
41 %Generate Max inscribed ellip at output bounds
42 n=3;
43
44 V_max=zeros(n ,2^n);
45 d_V=0.05*ones(1,n);
46
47 m = 2*n;
48
49 A = zeros(m,n); b = zeros(m,1);
50
51 for i=1:m
52   A(i,ceil(i/2)) = (-1)^(i-1);
53   b(i) = d_V(ceil(i/2));
54
55 end
56
57 cvx_begin
58     variable B(n,n) symmetric
59     variable d(n)
60     maximize( det_rootn( B ) )
61     subject to
62         for i = 1:m
63             norm( B*A(i,:)', 2 ) + A(i,:)*d <= b(i);
64         end
65 cvx_end
66 Psi_out = B'*B;
67 Psi_output(4:6,4:6)=Psi_out;
68 d=ones(1,n);
69
70 R_squared=3*0.05^2
71 Psi_out_circum=diag(ones(3,1)*R_squared)
72 Psi_output_circum(4:6,4:6)=Psi_out_circum;
73
74 %generate zonotope
```

```
g=[0 0 0 0.05 0 0; 0 0 0 0 0.05 0; 0 0 0 0 0 0.05]';
c=[0; 0; 0; 0; 0; 0]; %center of zonotope
Z_out=[];
for i=1:2
    for j=1:2
        for k=1:2

            Z_out=[Z_out c+(-1)^i*g(:,1)+(-1)^j*g(:,2)+(-1)^k*g
                (:,3)]; %Vertices of zonotope
        end
    end
end
[a,b]=size(Z_out)


numout=zeros(a, b);
for numin=0:b-1
    numout(:,numin+1)=de2bi(bitxor(numin,bitshift(numin,-1)),a)';
end

for i=1:b
    Z_out(:,i)=c+(-1)^numout(1,i)*g(:,1)+(-1)^numout(2,i)*g(:,2)
        +(-1)^numout(3,i)*g(:,3);
end


 %Maximum Output Ellipsoid Bound
  figure
  hold on
    proj = zeros(2, row);
    x = 2;  % voltage at bus x
    y = 3;  % voltage at bus y
    volt_x = 1;
    volt_y = 1;
    proj(1,x-1+row/2) = 1;
    proj(2,y-1+row/2) = 1;
    Psi_proj1 = proj * Psi_output * proj';
    Psi_proj1_circum = proj * Psi_output_circum * proj';


    angles = 200;
    theta   = linspace( 0, 2 * pi, angles );
    ellipsoid1= sqrtm(Psi_proj1) * [ cos(theta) ; sin(theta) ] ;
    ellipsoid1_circum= sqrtm(Psi_proj1_circum) * [ cos(theta) ;
        sin(theta) ] ;
```

```
117
118
119       p1=plot(ellipsoid1(1,:), ellipsoid1(2,:), ...
120               '-k','LineWidth',3);
121       p2=plot(ellipsoid1_circum(1,:), ellipsoid1_circum(2,:), ...
122               '-r','LineWidth',3);
123
124        axis([-0.09 0.09 -0.09 0.09])
125       grid on;
126
127  proj_zonotope=zeros(a/2,2);
128  proj_zonotope(x-1,1)=1; proj_zonotope(y-1,2)=1;
129  g_in=g*proj_zonotope;
130  Z_in=[];
131  for i=1:2
132       for j=1:2
133
134               Z_in=[Z_in c+(-1)^i*g_in(:,1)+(-1)^j*g_in(:,2)]; %
                     Vertices of zonotope
135       end
136  end
137  [a,b]=size(Z_in)
138
139  numout=zeros(a, b);
140  for numin=0:b-1
141       numout(:,numin+1)=de2bi(bitxor(numin,bitshift(numin,-1)),a)';
142  end
143
144  for i=1:b
145       Z_in(:,i)=c+(-1)^numout(1,i)*g_in(:,1)+(-1)^numout(2,i)*g_in
             (:,2);
146  end
147
148  k=convhull(Z_out(x-1+row/2,:),Z_out(y-1+row/2,:)) %project the
     zonotope and get convex hull
149  p2=plot(Z_out(x-1+row/2,k), Z_out(y-1+row/2,k), 'b', 'LineWidth',
     4); %plot the zonotope
150  set(gca,'fontsize',36,'fontname','times new roman'); ...
151     xl=xlabel('$ V_2 $ [p.u.] ','fontsize',38,'fontname','times new
           roman');
152     set(xl,'Interpreter','latex');
153     yl=ylabel('$ V_3 $ [p.u.]','fontsize',38,'fontname','times new
          roman');
154     set(yl,'Interpreter','latex');
155     l1=legend([p1], '$\Delta\mathcal{E}_0$', 'location', 'SouthEast
```

```
        ');
156     set(l1,'FontSize',37, 'Interpreter','latex')
157
158
159 x = 2;  % voltage at bus x
160 y = 3;  % voltage at bus y
161 volt_x = soln(x,2);
162 volt_y = soln(y,2);
163
164
165 %Monte Carlo for Finding exact Reach set
166 Percent1=0.2;
167 Percent2=0.2;
168 Percent3=0.2;
169 Rating1=0.4; %rated output
170 Rating2=0.3;
171 Rating3=0.5;
172 i=-Percent1*Rating1:0.04:Percent1*Rating1;
173 j=-Percent2*Rating2:0.04:Percent2*Rating2;
174 k=-Percent3*Rating3:0.04:Percent3*Rating3;
175 figure
176 hold on
177 Out=[];
178 Out_nonlinear = [];
179 draw = 1;
180 for counti=1:length(i)
181     for countj=1:length(j)
182         for countk=1:length(k)
183             bus_loop = bus;
184             bus_loop(2,4) = bus(2,4) + i(counti);
185             bus_loop(3,4) = bus(3,4) + j(countj);
186             bus_loop(4,4) = bus(4,4) + k(countk);
187             [soln ybus L J] = get_pf(bus_loop,line);
188             Out_nonlinear = [soln(2:4,3); soln(2:4,2)];
189
190             if draw == 1
191     p3=plot(Out_nonlinear(x-1+row/2), Out_nonlinear(y-1+row/2), 'o'
        , 'MarkerSize',8, 'MarkerFaceColor', 'r');
192                 draw = 1;
193             else
194                 draw = 1;
195             end
196         end
197     end
198 end
```

```
199
200 x_p = 3;  % power at bus x_p
201 y_p = 4;  % power at bus y_p
202
203
204 Gamma1 = H * Psi_g1 * H';
205 Gamma2 = H * Psi_g2 * H';
206 Gamma3 = H * Psi_g3 * H';
207 Gamma_input=J*Psi_output*J';
208 Gamma_input_circum=J*Psi_output_circum*J';
209     proj_input=zeros(2,row);
210
211     proj_input(1,x_p-1) = 1;
212     proj_input(2,y_p-1) = 1;
213     proj = zeros(2, row);
214     proj(1,x-1+row/2) = 1;
215     proj(2,y-1+row/2) = 1;
216
217     Gamma_proj_input = proj_input * Gamma_input * proj_input';
218     Gamma_proj_input_circum = proj_input * Gamma_input_circum *
        proj_input';
219     Gamma_proj1 = proj * Gamma1 * proj';
220     Gamma_proj2 = proj * Gamma2 * proj';
221     Gamma_proj3 = proj * Gamma3 * proj';
222
223     angles = 200;
224     theta   = linspace( 0, 2 * pi, angles );
225     ellipsoid_input=sqrtm(Gamma_proj_input) * [ cos(theta) ; sin(
        theta) ] ;
226     ellipsoid_input_circum=sqrtm(Gamma_proj_input_circum) * [ cos(
        theta) ; sin(theta) ] ;
227     ellipsoid1= sqrtm(Gamma_proj1) * [ cos(theta) ; sin(theta) ] ;
228     ellipsoid2= sqrtm(Gamma_proj2) * [ cos(theta) ; sin(theta) ] ;
229     ellipsoid3= sqrtm(Gamma_proj3) * [ cos(theta) ; sin(theta) ] ;
230     p1=plot(ellipsoid1(1,:)+volt_x, ellipsoid1(2,:)+volt_y, ...
231             '-k','LineWidth',3);
232     p2=plot(ellipsoid2(1,:)+volt_x, ellipsoid2(2,:)+volt_y, ...
233             '--k','LineWidth',2);
234     plot(ellipsoid3(1,:)+volt_x, ellipsoid3(2,:)+volt_y, ...
235             '--k','LineWidth',2);
236
237 %plot the zonotope bounding power injectinos
238 g_in=J*g;
239 Z_in=[];
240 for i=1:2
```

```
241         for j=1:2
242             for k=1:2
243 
244             Z_in=[Z_in  c+(-1)^i*g_in(:,1)+(-1)^j*g_in(:,2)+(-1)^k*g_in
                    (:,3)]; %Vertices of zonotope
245             end
246         end
247 end
248 k=convhull(Z_in(x_p-1,:),Z_in(y_p-1,:)); %project the zonotope and
        get convex hull
249 
250 
251     figure();
252     hold on;
253     grid on;
```

B.2 34-Bus System

```
clear all;
close all;
clc;
load Node34.mat;

%Power Injections, All symmetric
Rating=0.8;
Percentage=0.5;
num_gen=10;

changed_bus = [3 7 10 15 18 23 27 29 30 34];

for i = 1:numel(changed_bus)
    bus(changed_bus(i),4) = Rating;
end

[soln ybus L J] = get_pf(bus,line);
H = inv(J);
[row col] = size(H);

% Zonotopes
g_in=zeros(row/2,numel(changed_bus));
for i=1:numel(changed_bus)
    g_in(changed_bus(i)-1, i)=Rating*Percentage;
end
Psi_g1 = 1e-7 * eye(size(H));

%Circumscribed Ellipsoid
R_squared=num_gen*(Rating*Percentage)^2;
for i = 1:numel(changed_bus)
    Psi_g1(changed_bus(i)-1,changed_bus(i)-1) = R_squared;
end

%voltage
x=28;
y=11;
volt_x = soln(x,2);
volt_y = soln(y,2);

c=soln(:,2); %center of zonotope

%Monte Carlo for Finding exact Reach set
```

```
43
44 num_step = 2;
45 i1 = linspace(-Percentage*Rating, Percentage*Rating, num_step);
46 i2 = linspace(-Percentage*Rating, Percentage*Rating, num_step);
47 i3 = linspace(-Percentage*Rating, Percentage*Rating, num_step);
48 i4 = linspace(-Percentage*Rating, Percentage*Rating, num_step);
49 i5 = linspace(-Percentage*Rating, Percentage*Rating, num_step);
50 i6 = linspace(-Percentage*Rating, Percentage*Rating, num_step);
51 i7 = linspace(-Percentage*Rating, Percentage*Rating, num_step);
52 i8 = linspace(-Percentage*Rating, Percentage*Rating, num_step);
53 i9 = linspace(-Percentage*Rating, Percentage*Rating, num_step);
54 i10 = linspace(-Percentage*Rating, Percentage*Rating, num_step);
55
56 figure('position', [20 80 1300 800]);
57 axes('position', [0.14 0.14 0.8 0.8]);
58 hold on; box on; grid on;
59
60 Out=zeros(1,66)';
61 draw = 1;
62 toggle=1;
63 for counti1=1:length(i1)
64     for counti2=1:length(i2)
65         for counti3=1:length(i3)
66             for counti4=1:length(i4)
67                 for counti5=1:length(i5)
68                     for counti6=1:length(i6)
69                         for counti7=1:length(i7)
70                             for counti8=1:length(i8)
71                                 for counti9=1:length(i9)
72                                     for counti10=1:length(i10)
73
74  Out(changed_bus-1)=[i1(counti1) i2(counti2) i3(counti3) i4(
       counti4) i5(counti5) i6(counti6) i7(counti7) i8(counti8) i9(
       counti9) i10(counti10)];
75  Out_linear=H*Out;
76
77              bus_loop = bus;
78              bus_loop(3,4) = bus(3,4) + i1(counti1);
79              bus_loop(7,4) = bus(7,4) + i2(counti2);
80              bus_loop(10,4) = bus(10,4) + i3(counti3);
81              bus_loop(15,4) = bus(15,4) + i4(counti4);
82              bus_loop(18,4) = bus(18,4) + i5(counti5);
83              bus_loop(23,4) = bus(23,4) + i6(counti6);
84              bus_loop(27,4) = bus(27,4) + i7(counti7);
85              bus_loop(29,4) = bus(29,4) + i8(counti8);
```

```
86                bus_loop(30,4) = bus(30,4) + i9(counti9);
87                bus_loop(34,4) = bus(34,4) + i10(counti10);
88                [soln ybus L J] = get_pf(bus_loop,line);
89                Out_nonlinear = [soln(2:34,3); soln(2:34,2)];
90
91                if draw == 1
92                    if toggle==1
93                        p3=plot(Out_nonlinear(x-1+row/2),
                              Out_nonlinear(y-1+row/2), 'o', 'MarkerSize
                              ',8, 'MarkerFaceColor', 'r');
94                        p2=plot(Out_linear(x-1+row/2)+volt_x,
                              Out_linear(y-1+row/2)+volt_y, 's', '
                              MarkerSize',8, 'MarkerFaceColor', 'y');
95                        toggle=0;
96                    else
97                        p2=plot(Out_linear(x-1+row/2)+volt_x,
                              Out_linear(y-1+row/2)+volt_y, 's', '
                              MarkerSize',8, 'MarkerFaceColor', 'y');
98                        p3=plot(Out_nonlinear(x-1+row/2),
                              Out_nonlinear(y-1+row/2), 'o', 'MarkerSize
                              ',8, 'MarkerFaceColor', 'r');
99                        toggle=1;
100                   end
101                   draw = 0;
102               else
103                   draw = draw + 1;
104               end
105                                       end
106                                   end
107                               end
108                           end
109                       end
110                   end
111               end
112           end
113       end
114   end
115
116   plot(Out_nonlinear(x-1+row/2), Out_nonlinear(y-1+row/2), 'o', '
          MarkerSize',8, 'MarkerFaceColor', 'r');
117   plot(Out_linear(x-1+row/2)+volt_x, Out_linear(y-1+row/2)+volt_y, '
          s', 'MarkerSize',8, 'MarkerFaceColor', 'y');
118
119
120   Gamma1 = H * Psi_g1 * H';
```

```
proj = zeros(2, row);
proj(1,x-1+row/2) = 1;
proj(2,y-1+row/2) = 1;
Gamma_proj1 = proj * Gamma1 * proj';

angles = 200;
theta  = linspace( 0, 2 * pi, angles );
ellipsoid1= sqrtm(Gamma_proj1) * [ cos(theta) ; sin(theta) ] ;

g_out=H*[g_in; zeros(row/2,numel(changed_bus))];
Z_out=[];
for k1=1:2
    for k2=1:2
        for k3=1:2
            for k4=1:2
                for k5=1:2
                    for k6=1:2
                        for k7=1:2
                            for k8=1:2
                                for k9=1:2
                                    for k10=1:2

Z_out=[Z_out c(2:34,:)+(-1)^k1*g_out(34:66,1)+(-1)^k2*g_out
    (34:66,2)+(-1)^k3*g_out(34:66,3)+(-1)^k4*g_out(34:66,4)+(-1)^k5
    *g_out(34:66,5)+...
 +(-1)^k6*g_out(34:66,6)+(-1)^k7*g_out(34:66,7)+(-1)^k8*g_out
    (34:66,8)+(-1)^k9*g_out(34:66,9)+(-1)^k10*g_out(34:66,10)]; %
    Vertices of zonotope
                                    end
                                end
                            end
                        end
                    end
                end
            end
        end
    end
end

k=convhull(Z_out(x-1,:),Z_out(y-1,:)); %project the zonotope and
    get convex hull
p5=plot(Z_out(x-1,k), Z_out(y-1,k), 'r', 'LineWidth', 3);
%%%
line1x = [1.05  1.05];
line1y = [1.05  0.95];
```

```
line2x = [0.95 0.95];
line2y = [0.95 1.05];
line3x = [0.95 1.05];
line3y = [0.95 0.95];
line4x = [0.95 1.05];
line4y = [1.05 1.05];
p4=plot(line1x, line1y, 'Color', 'black', 'LineWidth', 3, '
    LineStyle', '--');
plot(line2x, line2y, 'Color', 'black', 'LineWidth', 3, 'LineStyle'
    , '--');
plot(line3x, line3y, 'Color', 'black', 'LineWidth', 3, 'LineStyle'
    , '--');
plot(line4x, line4y, 'Color', 'black', 'LineWidth', 3, 'LineStyle'
    , '--');

axis([0.945 1.055 0.945 1.055]);

for i = 1:numel(gamma)

    Gamma = H* ((1-gamma(i))^(-1)*Psi_g + 1/gamma(i)*Psi_l) *H';

    proj = zeros(2, row);
    proj(1,x-1+row/2) = 1;
    proj(2,y-1+row/2) = 1;
    Gamma_proj = proj * Gamma * proj';

    angles = 200;
    theta  = linspace( 0, 2 * pi, angles );
    ellipsoid= sqrtm(Gamma_proj) * [ cos(theta) ; sin(theta) ] ;
    plot(ellipsoid(1,:)+volt_x, ellipsoid(2,:)+volt_y, ...
            'c','LineWidth',1);
    grid on; hold on;

end

set(gca,'fontsize',36,'fontname','times new roman'); ...
   xl=xlabel('$ V_{110} $ [p.u.] ','fontsize',40,'fontname','times
       new roman');
   set(xl,'Interpreter','latex');
   yl=ylabel('$ V_{123} $ [p.u.]','fontsize',40,'fontname','times
      new roman');
   set(yl,'Interpreter','latex');
   l1=legend([p5, p2, p3, p4], '$\mathcal{X}$', 'Linear Approx.',
      'Exact Solution', 'Voltage Constraints', 'location', '
      SouthEast');
```

```
198     set(l1,'FontSize',37, 'Interpreter','latex')
```

B.3 123-Bus System

```
clear all;
close all;
clc;
load Node123.mat;
%Power Injections, Asymmetric
Rating=[1.5 1 1.5 1 1 1.5 1 1 1 1.5]; %Per unit ratings 100kVA base?
Percentage=[0.4 0.4 0.4 0.4 0.4 0.4 0.4 0.4 0.4 0.4]; %percentage of variation
num_gen=10;

changed_bus = [80 95 96 103 108 110 115 121 122 123]; %123 bus system

for i = 1:numel(changed_bus)
    bus(changed_bus(i),4) = Rating(i); %Asymmetrical Power Injection
end
[soln ybus L J] = get_pf(bus,line);
H = inv(J);

[row col] = size(H);
num_bus=row/2+1;
Psi_g = 1e-7 * eye(size(H));

% Zonotopes
g_in=zeros(row/2,numel(changed_bus));
for i=1:numel(changed_bus)
    g_in(changed_bus(i)-1, i)=Rating(i)*Percentage(i);
end

%tight bounding in three directions
Psi_g1 = Psi_g;
Psi_g2 = Psi_g;
Psi_g3 = Psi_g;

%Compute shape matrix, Asymmetrical Injections
gen=Rating.*Percentage;
V=[];
for i1=1:2
for i2=1:2
for i3=1:2
```

```
for i4=1:2
for i5=1:2
for i6=1:2
for i7=1:2
for i8=1:2
for i9=1:2
for i10=1:2
    V=[V; gen(1)*(-1)^i1 gen(2)*(-1)^i2 gen(3)*(-1)^i3 gen(4)*(-1)
        ^i4 gen(5)*(-1)^i5 gen(6)*(-1)^i6 gen(7)*(-1)^i7 gen(8)
        *(-1)^i8 gen(9)*(-1)^i9 gen(10)*(-1)^i10];

end
end
end
end
end
end
end
end
end
end
V=V';

%%
e = ell_enclose(V)
x = V;
[n,m] = size(x);
% Find the shape matrix of input bound, minimum volume
cvx_begin
    variable A(n,n) symmetric
    variable b(n)
    maximize( det_rootn( A ) )
    subject to
        norms( A * x + b * ones( 1, m ), 2 ) <= 1;
cvx_end
P=inv(A'*A)


%Elongated/tight in other directions
elongate=3;
dir1=3;
dir2=6;
dir3=10;
changed_bus([dir1, dir2, dir3])
additional_points_1=zeros(1,numel(changed_bus));
```

```
82 additional_points_2=zeros(1,numel(changed_bus));
83 additional_points_3=zeros(1,numel(changed_bus));
84 additional_points_1(dir1)=gen(dir1)+elongate;
85 additional_points_2(dir2)=gen(dir2)+elongate;
86 additional_points_3(dir3)=gen(dir3)+elongate;
87
88 V_1=[V additional_points_1' -additional_points_1'];
89 V_2=[V additional_points_2' -additional_points_2'];
90 V_3=[V additional_points_3' -additional_points_3'];
91
92 e1 = ell_enclose(V_1)
93 x=V_1;
94 [n,m] = size(x);
95 % Find the shape matrix of input bound, minimum volume
96 cvx_begin
97     variable A(n,n) symmetric
98     variable b(n)
99     maximize( det_rootn( A ) )
100    subject to
101        norms( A * x + b * ones( 1, m ), 2 ) <= 1;
102 cvx_end
103 P1=inv(A'*A)
104
105 e2 = ell_enclose(V_2)
106 x=V_2;
107 [n,m] = size(x);
108 % Find the shape matrix of input bound, minimum volume
109 cvx_begin
110     variable A(n,n) symmetric
111     variable b(n)
112     maximize( det_rootn( A ) )
113     subject to
114         norms( A * x + b * ones( 1, m ), 2 ) <= 1;
115 cvx_end
116 P2=inv(A'*A)
117
118 e3 = ell_enclose(V_3)
119 x=V_3;
120 [n,m] = size(x);
121 % Find the shape matrix of input bound, minimum volume
122 cvx_begin
123     variable A(n,n) symmetric
124     variable b(n)
125     maximize( det_rootn( A ) )
126     subject to
```

```
127         norms( A * x + b * ones( 1, m ), 2 ) <= 1;
128 cvx_end
129 P3=inv(A'*A)
130
131
132
133
134 for i = 1:numel(changed_bus)
135     %minimum volume
136     Psi_g(changed_bus(i)-1,changed_bus(i)-1) = P(i, i);
137
138     %tight in directions
139     Psi_g1(changed_bus(i)-1,changed_bus(i)-1) = P1(i, i);
140     Psi_g2(changed_bus(i)-1,changed_bus(i)-1) = P2(i, i);
141     Psi_g3(changed_bus(i)-1,changed_bus(i)-1) = P3(i, i);
142 end
143
144 %bus voltage of interest
145 x=103;
146 y=123;
147 volt_x = soln(x,2);
148 volt_y = soln(y,2);
149
150 c=soln(:,2); %center of zonotope
151 num_step = 2;
152
153 %Aymmetrical Power Injection
154 i1 = linspace(-Percentage(1)*Rating(1), Percentage(1)*Rating(1),
    num_step);
155 i2 = linspace(-Percentage(2)*Rating(2), Percentage(2)*Rating(2),
    num_step);
156 i3 = linspace(-Percentage(3)*Rating(3), Percentage(3)*Rating(3),
    num_step);
157 i4 = linspace(-Percentage(4)*Rating(4), Percentage(4)*Rating(4),
    num_step);
158 i5 = linspace(-Percentage(5)*Rating(5), Percentage(5)*Rating(5),
    num_step);
159 i6 = linspace(-Percentage(6)*Rating(6), Percentage(6)*Rating(6),
    num_step);
160 i7 = linspace(-Percentage(7)*Rating(7), Percentage(7)*Rating(7),
    num_step);
161 i8 = linspace(-Percentage(8)*Rating(8), Percentage(8)*Rating(8),
    num_step);
162 i9 = linspace(-Percentage(9)*Rating(9), Percentage(9)*Rating(9),
    num_step);
```

```
163 i10 = linspace(-Percentage(10)*Rating(10), Percentage(10)*Rating
    (10), num_step);
164
165 figure
166 axes('position', [0.14 0.14 0.8 0.8]);
167 hold on; grid on; box on;
168 Out=zeros(1,2*(num_bus-1))';
169 draw = 1;
170 for counti1=1:length(i1)
171     for counti2=1:length(i2)
172         for counti3=1:length(i3)
173             for counti4=1:length(i4)
174                 for counti5=1:length(i5)
175                     for counti6=1:length(i6)
176                         for counti7=1:length(i7)
177                             for counti8=1:length(i8)
178                                 for counti9=1:length(i9)
179                                     for counti10=1:length(i10)
180                                         linear
181                                         Out(changed_bus-1)=[i1(
                                            counti1) i2(counti2) i3
                                            (counti3) i4(counti4)
                                            i5(counti5) i6(counti6)
                                             i7(counti7) i8(counti8
                                            ) i9(counti9) i10(
                                            counti10)];
182                                         Out_linear=H*Out;
183
184                                         %nonlinear
185                                         bus_loop = bus;
186                                         bus_loop(changed_bus(1),4)
                                                = bus(changed_bus(1)
                                            ,4) + i1(counti1);
187                                         bus_loop(changed_bus(2),4)
                                                = bus(changed_bus(2)
                                            ,4) + i2(counti2);
188                                         bus_loop(changed_bus(3),4)
                                                = bus(changed_bus(3)
                                            ,4) + i3(counti3);
189                                         bus_loop(changed_bus(4),4)
                                                = bus(changed_bus(4)
                                            ,4) + i4(counti4);
190                                         bus_loop(changed_bus(5),4)
                                                = bus(changed_bus(5)
                                            ,4) + i5(counti5);
```

```
191                                     bus_loop(changed_bus(6),4)
                                            = bus(changed_bus(6)
                                        ,4) + i6(counti6);
192                                     bus_loop(changed_bus(7),4)
                                            = bus(changed_bus(7)
                                        ,4) + i7(counti7);
193                                     bus_loop(changed_bus(8),4)
                                            = bus(changed_bus(8)
                                        ,4) + i8(counti8);
194                                     bus_loop(changed_bus(9),4)
                                            = bus(changed_bus(9)
                                        ,4) + i9(counti9);
195                                     bus_loop(changed_bus(10)
                                        ,4) = bus(changed_bus
                                        (10),4) + i10(counti10)
                                        ;
196                                     [soln ybus L J] = get_pf(
                                        bus_loop,line);
197                                     Out_nonlinear = [soln(2:
                                        num_bus,3); soln(2:
                                        num_bus,2)];
198
199                                     if draw == 1
200                                         p2=plot(Out_linear(x
                                            -1+row/2)+volt_x,
                                            Out_linear(y-1+row
                                            /2)+volt_y, 's', '
                                            MarkerFaceColor', '
                                            y'); %voltage
201                                         p3=plot(Out_nonlinear(
                                            x-1+row/2),
                                            Out_nonlinear(y-1+
                                            row/2), 'o', '
                                            MarkerSize',8, '
                                            MarkerFaceColor', '
                                            r'); %voltage
202                                         draw = 0;
203                                     else
204                                         draw = draw + 1;
205                                     end
206                                 end
207                             end
208                         end
209                     end
210                 end
```

```
211                     end
212                 end
213             end
214         end
215 end
216
217 plot(Out_nonlinear(x-1+row/2), Out_nonlinear(y-1+row/2), 'o', '
    MarkerSize',8, 'MarkerFaceColor', 'r'); %voltage
218 %minimum volume
219 Gamma = H * Psi_g * H';
220 %Tight in specific directions
221 Gamma1 = H * Psi_g1 * H';
222 Gamma2 = H * Psi_g2 * H';
223 Gamma3 = H * Psi_g3 * H';
224
225 proj = zeros(2, row);
226 proj_angles = proj;
227 proj(1,x-1+row/2) = 1;
228 proj(2,y-1+row/2) = 1;
229
230 %minimum volumne
231 Gamma_proj = proj * Gamma * proj'; %voltage
232
233 %Tight in specific directions
234 Gamma_proj1 = proj * Gamma1 * proj';
235 Gamma_proj2 = proj * Gamma2 * proj';
236 Gamma_proj3 = proj * Gamma3 * proj';
237
238 angles = 200;
239 theta  = linspace( 0, 2 * pi, angles );
240 %minimum volumne
241 ellipsoid= sqrtm(Gamma_proj) * [ cos(theta) ; sin(theta) ];
242 ellipsoid1= sqrtm(Gamma_proj1) * [ cos(theta) ; sin(theta) ] ;
243 ellipsoid2= sqrtm(Gamma_proj2) * [ cos(theta) ; sin(theta) ] ;
244 ellipsoid3= sqrtm(Gamma_proj3) * [ cos(theta) ; sin(theta) ] ;
245
246 %%% zonotopes
247 g_out=H*[g_in; zeros(row/2,numel(changed_bus))];
248 Z_out=[];
249 for k1=1:2
250     for k2=1:2
251         for k3=1:2
252             for k4=1:2
253                 for k5=1:2
254                     for k6=1:2
```

```
                                for k7=1:2
                                    for k8=1:2
                                        for k9=1:2
                                            for k10=1:2
Z_out=[Z_out c(2:123,:)+(-1)^k1*g_out(123:244,1)+(-1)^k2*g_out
    (123:244,2)+(-1)^k3*g_out(123:244,3)+(-1)^k4*g_out(123:244,4)
    +(-1)^k5*g_out(123:244,5)+...
+(-1)^k6*g_out(123:244,6)+(-1)^k7*g_out(123:244,7)+(-1)^k8*g_out
    (123:244,8)+(-1)^k9*g_out(123:244,9)+(-1)^k10*g_out(123:244,10)
    ]; %Vertices of zonotope
                                            end
                                        end
                                    end
                                end
                            end
                        end
                    end
                end
            end
        end
    end
k=convhull(Z_out(x-1,:),Z_out(y-1,:)); %project the zonotope and
    get convex hull
p5=plot(Z_out(x-1,k), Z_out(y-1,k), 'r', 'LineWidth', 3); %plot
    the zonotope, which should be inside circumscribed ellipsoid

%%
line1x = [1.05 1.05];
line1y = [1.05 0.95];
line2x = [0.95 0.95];
line2y = [0.95 1.05];
line3x = [0.95 1.05];
line3y = [0.95 0.95];
line4x = [0.95 1.05];
line4y = [1.05 1.05];
p4=plot(line1x, line1y, 'Color', 'black', 'LineWidth', 3, '
    LineStyle', '--');
plot(line2x, line2y, 'Color', 'black', 'LineWidth', 3, 'LineStyle'
    , '--');
plot(line3x, line3y, 'Color', 'black', 'LineWidth', 3, 'LineStyle'
    , '--');
plot(line4x, line4y, 'Color', 'black', 'LineWidth', 3, 'LineStyle'
    , '--');
axis([0.974 1.02 0.945 1.045]);

set(gca,'fontsize',36,'fontname','times new roman'); ...
```

```
290     xl=xlabel('$ V_{103} $ [p.u.] ','fontsize',38,'fontname','times
            new roman');
291     set(xl,'Interpreter','latex');
292     yl=ylabel('$ V_{123} $ [p.u.]','fontsize',38,'fontname','times
            new roman');
293     set(yl,'Interpreter','latex');
294     l1=legend([p5, p3, p4], '$\mathcal{X}$', 'Exact Solution', '
            Voltage Constraints', 'location', 'SouthEast');
295     set(l1,'FontSize',37, 'Interpreter','latex')
```

B.4 145-Bus System

```
clear all;
close all;
clc;
load data50m.mat;

x=6;
y=34;
x_PQ=length(find(bus(1:x-1,10)==3));
y_PQ=length(find(bus(1:y-1,10)==3));
x_PV=length(find(bus(1:x-1,10)==2));
y_PV=length(find(bus(1:y-1,10)==2));
slack=find(bus(:,10)==1); %the slack bus

%inject power 10 buses
Rating=1; %nominal P injection
Percentage=0.50;
num_gen=10;
num_bus=length(bus(:,1)); %number of buses in this system
PQ=find(bus(1:end,10)==3);
num_PQ=length(PQ); %number of PQ buses in this system

changed_bus = [3 7 10 15 18 23 27 29 30 34];
num_changed_bus=numel(changed_bus);

if any(bus(changed_bus,10)==2)
    disp('injection at PV bus')
end
if any(bus(changed_bus,10)==1)
    error('slack bus cannot have uncertain power injection')
end

for i = 1:num_changed_bus
    bus(changed_bus(i),4) = Rating;
end

[soln ybus dVdQ H K N L] = get_pf_v4(bus,line);
soln(:,[1 2 10]);
J = [H N; K L];

M = inv(J);

[row col] = size(M);
```

```
43
44 % Zonotopes
45 g_in=zeros(row,num_changed_bus);
46 shift_logic=lt(slack, changed_bus);
47 for i=1:num_changed_bus
48     if (shift_logic(i)==1)
49         g_in(changed_bus(i)-1, i)=Rating*Percentage;
50     else
51         g_in(changed_bus(i), i)=Rating*Percentage;
52     end
53 end
54 Psi_g1 = 1e-7 * eye(size(M));
55
56 %Circumscribed Ellipsoid
57 R_squared=num_gen*(Rating*Percentage)^2;
58 for i = 1:num_changed_bus
59     if (shift_logic(i)==1)
60         Psi_g1(changed_bus(i)-1, changed_bus(i)-1)=R_squared;
61     else
62         Psi_g1(changed_bus(i), changed_bus(i))=R_squared;
63     end
64 end
65
66 %voltage
67 volt_x = soln(x,2);
68 volt_y = soln(y,2);
69 if (bus(x,10)==2 || bus (y,10)==2)
70     error('voltage uncertainty at incorrect bus')
71 end
72 c=soln(:,2); %center of zonotope
73
74 %Monte Carlo for Finding exact Reach set
75 num_step = 2;
76
77 i1 = linspace(-Percentage*Rating, Percentage*Rating, num_step);
78 i2 = linspace(-Percentage*Rating, Percentage*Rating, num_step);
79 i3 = linspace(-Percentage*Rating, Percentage*Rating, num_step);
80 i4 = linspace(-Percentage*Rating, Percentage*Rating, num_step);
81 i5 = linspace(-Percentage*Rating, Percentage*Rating, num_step);
82 i6 = linspace(-Percentage*Rating, Percentage*Rating, num_step);
83 i7 = linspace(-Percentage*Rating, Percentage*Rating, num_step);
84 i8 = linspace(-Percentage*Rating, Percentage*Rating, num_step);
85 i9 = linspace(-Percentage*Rating, Percentage*Rating, num_step);
86 i10 = linspace(-Percentage*Rating, Percentage*Rating, num_step);
87
```

```
figure
axes('position', [0.14 0.14 0.8 0.8]);
hold on; grid on; box on;
Out=zeros(1,col)'; %[P, Q]'

draw = 0;
for counti1=1:length(i1)
    for counti2=1:length(i2)
        for counti3=1:length(i3)
            for counti4=1:length(i4)
                for counti5=1:length(i5)
                    for counti6=1:length(i6)
                        for counti7=1:length(i7)
                            for counti8=1:length(i8)
                                for counti9=1:length(i9)
                                    for counti10=1:length(i10)

                                        Out(changed_bus-shift_logic)
                                            =[i1(counti1) i2(counti2)
                                             i3(counti3) i4(counti4)
                                            i5(counti5) i6(counti6)
                                            i7(counti7) i8(counti8)
                                            i9(counti9) i10(counti10)
                                            ];
                                        Out_linear=J\Out; %[theta, V
                                            ]'

            bus_loop = bus;
            bus_loop(changed_bus,4) = bus(changed_bus,4)+ [i1(
                counti1) i2(counti2) i3(counti3) i4(counti4) i5(
                counti5) i6(counti6) i7(counti7) i8(counti8) i9(
                counti9) i10(counti10)]';
            bus_loop(3,4) = bus(3,4) + i1(counti1);
            bus_loop(7,4) = bus(7,4) + i2(counti2);
            bus_loop(10,4) = bus(10,4) + i3(counti3);
            bus_loop(15,4) = bus(15,4) + i4(counti4);
            bus_loop(18,4) = bus(18,4) + i5(counti5);
            bus_loop(23,4) = bus(23,4) + i6(counti6);
            bus_loop(27,4) = bus(27,4) + i7(counti7);
            bus_loop(29,4) = bus(29,4) + i8(counti8);
            bus_loop(30,4) = bus(30,4) + i9(counti9);
            bus_loop(34,4) = bus(34,4) + i10(counti10);
            [soln ybus dVdQ H K N L] = get_pf_v4(bus_loop,line);

            Out_nonlinear = [soln(:,3); soln(:,2)]; %[theta, V]'
```

```
123
124                 if ~mod(draw,1)
125                         p2=plot(Out_nonlinear(x+num_bus),
                                Out_nonlinear(y+num_bus), 'o', 'MarkerSize
                                ',8, 'MarkerFaceColor', 'r');
126                         p3=plot(Out_linear(x_PQ+num_bus)+volt_x,
                                Out_linear(y_PQ+num_bus)+volt_y, 's', '
                                MarkerSize',8, 'MarkerFaceColor', 'y');
127                 end
128                 draw=draw+1;
129                                             end
130                                         end
131                                     end
132                                 end
133                             end
134                         end
135                 end
136             end
137         end
138 end
139 plot(Out_nonlinear(x+num_bus), Out_nonlinear(y+num_bus), 'o', '
        MarkerSize',8, 'MarkerFaceColor', 'r');
140 plot(Out_linear(x_PQ+num_bus)+volt_x, Out_linear(y_PQ+num_bus)+
        volt_y, 's', 'MarkerSize',8, 'MarkerFaceColor', 'y');
141
142 Gamma1 = M * Psi_g1 * M';
143 proj = zeros(2, row);
144
145
146 proj(1,x_PQ+num_bus) = 1; %%% make sure indices are correct
147 proj(2,y_PQ+num_bus) = 1;
148
149 Gamma_proj1 = proj * Gamma1 * proj';
150
151 angles = 200;
152 theta  = linspace( 0, 2 * pi, angles );
153 ellipsoid1= sqrtm(Gamma_proj1) * [ cos(theta) ; sin(theta) ] ;
154 p1=plot(ellipsoid1(1,:)+volt_x, ellipsoid1(2,:)+volt_y, ...
155         'k','LineWidth',3);
156
157 line1x = [1.05 1.05];
158 line1y = [1.05 0.95];
159 line2x = [0.95 0.95];
160 line2y = [0.95 1.05];
161 line3x = [0.95 1.05];
```

```
line3y = [0.95 0.95];
line4x = [0.95 1.05];
line4y = [1.05 1.05];
p4=plot(line1x, line1y, 'Color', 'black', 'LineWidth', 3, '
    LineStyle', '--');
plot(line2x, line2y, 'Color', 'black', 'LineWidth', 3, 'LineStyle'
    , '--');
plot(line3x, line3y, 'Color', 'black', 'LineWidth', 3, 'LineStyle'
    , '--');
plot(line4x, line4y, 'Color', 'black', 'LineWidth', 3, 'LineStyle'
    , '--');

%%% zonotopes
disp('zonotope timing')
tic
g_out=M*g_in;
[row col]=size(g_in);
Z_out=zeros(num_PQ,2^col);
count=0;
for k1=1:2
    for k2=1:2
        for k3=1:2
            for k4=1:2
                for k5=1:2
                    for k6=1:2
                        for k7=1:2
                            for k8=1:2
                                for k9=1:2
                                    for k10=1:2
                                    count=count+1;
                                        Z_out(:,count)=c(PQ)+(-1)^
                                            k1*g_out(num_bus:end,1)
                                            +(-1)^k2*g_out(num_bus:
                                            end,2)+(-1)^k3*g_out(
                                            num_bus:end,3)+(-1)^k4*
                                            g_out(num_bus:end,4)
                                            +(-1)^k5*g_out(num_bus:
                                            end,5)+...

                                            +(-1)^k6*g_out(num_bus:
                                            end,6)+(-1)^k7*g_out(
                                            num_bus:end,7)+(-1)^k8*
                                            g_out(num_bus:end,8)
                                            +(-1)^k9*g_out(num_bus:
                                            end,9)+(-1)^k10*g_out(
```

```
                                                    num_bus:end,10); %
                                                    Vertices of zonotope
189                                                 end
190                                             end
191                                         end
192                                     end
193                                 end
194                             end
195                         end
196                     end
197                 end
198 end
199 k=convhull(Z_out(x_PQ+1,:),Z_out(y_PQ+1,:)); %project the zonotope
        and get convex hull
200 toc
201 p5=plot(Z_out(x_PQ+1,k), Z_out(y_PQ+1,k), 'r', 'LineWidth', 4);
202
203 set(gca,'fontsize',36,'fontname','times new roman'); ...
204     xl=xlabel('$ V_{2} $ [p.u.] ','fontsize',38,'fontname','times
        new roman');
205     set(xl,'Interpreter','latex');
206     yl=ylabel('$ V_{34} $ [p.u.]','fontsize',38,'fontname','times
        new roman');
207     set(yl,'Interpreter','latex');
208     l1=legend([p5, p2, p3, p4], '$\mathcal{X}$', 'Exact Solution',
        'Linear Approx.', 'Voltage Constraints', 'location', '
        SouthEast');
209     set(l1,'FontSize',37, 'Interpreter','latex')
```

References

[1] B. Borkowska, "Probabilistic load flow," *IEEE Transactions on Power Apparatus and Systems*, vol. 93, no. 3, pp. 752–759, Aug. 1974.

[2] P. Jorgensen, J. Christensen, and J. Tande, "Probabilistic load flow calculation using monte carlo techniques for distribution network with wind turbines," in *Proc. of the 8th International Conference on Harmonics And Quality of Power*, vol. 2, oct 1998, pp. 1146 – 1151.

[3] C.-L. Su, "Probabilistic load-flow computation using point estimate method," *IEEE Transactions on Power Systems*, vol. 20, no. 4, pp. 1843 – 1851, Nov. 2005.

[4] A. Leite da Silva and V. Arienti, "Impact of power generation uncertainty on power system static performance," in *IEE Proc. of Generation, Transmission and Distribution C*, vol. 137, no. 4, Jul. 1990, pp. 276–282.

[5] A. Meliopoulos, G. Cokkinides, and X. Chao, "A new probabilistic power flow analysis method," *IEEE Transactions on Power Systems*, vol. 5, no. 1, pp. 182 – 190, Feb. 1990.

[6] P. Sauer, "A generalized stochastic power flow algorithm," in *Proc. of IEEE Power Engineering Society Summer Meeting*, 1978, pp. 544–549.

[7] R. Allan and A. Leite da Silva, "Evaluation methods and accuracy in probabilistic load flow solutions," *IEEE Transactions on Power Systems*, vol. PAS-100, no. 5, pp. 2539 – 2546, May 1981.

[8] P. Sauer and B. Hoveida, "Constrained stochastic power flow analysis," *Electric Power Systems Research*, vol. 5, no. 2, pp. 87 – 95, 1982.

[9] G. Anders, "Modelling operator action to balance system in probabilistic load-flow computations," *International Journal of Electric Power and Energy Systems*, vol. 4, no. 3, pp. 162 – 168, 1982.

[10] M. Brucoli, F. Torelli, and R. Napoli, "Quadratic probabilistic load flow with linearly modelled dispatch," *International Journal of Electric Power and Energy Systems*, vol. 7, pp. 138 – 146, 1985.

[11] A. Sarić and A. Stanković, "Model uncertainty in security assessment of power systems," *IEEE Transactions on Power Systems*, vol. 20, no. 3, pp. 1398–1407, 2005.

[12] L. Jaulin, M. Kieffer, O. Didrit, and E. Walter, *Applied Interval Analysis*. Springer, 2001.

[13] Z. Wang and F. Alvarado, "Interval arithmetic in power flow analysis," *IEEE Transactions on Power Systems*, vol. 7, no. 3, pp. 1341–1349, 1992.

[14] H. Mori and A. Yuihara, "Contingency screening using interval analysis in power systems," in *Proc. of the IEEE International Symposium on Circuits and Systems*, vol. 3, May 1998, pp. 444 – 447.

[15] A. Sarić and A. Stanković, "An application of interval analysis and optimization to electric energy markets," *IEEE Transactions on Power Systems*, vol. 21, no. 2, pp. 515 – 523, May 2006.

[16] X. Jiang, Y. Chen, and A. Dominguez-Garcia, "A set-theoretic framework to assess the impact of variable generation on the power flow," *IEEE Transactions on Power Systems*, vol. 28, no. 2, pp. 855–867, May 2013.

[17] A. Girard, "Reachability of uncertain linear systems using zonotopes," *Hybrid Systems: Computation and Control*, pp. 291–305, 2005.

[18] M. Althoff, O. Stursberg, and M. Buss, "Reachability analysis of linear systems with uncertain parameters and inputs," in *2007 46th IEEE Conference on Decision and Control*, Dec 2007, pp. 726–732.

[19] M. Althoff, "Formal and compositional analysis of power systems using reachable sets," *IEEE Transactions on Power Systems*, vol. PP, no. 99, pp. 1–11, 2014.

[20] H. Pico, D. Aliprantis, and E. Hoff, "Reachability analysis of power system frequency dynamics with new high-capacity hvac and hvdc transmission lines," in *Bulk Power System Dynamics and Control - IX Optimization, Security and Control of the Emerging Power Grid (IREP), 2013 IREP Symposium*, Aug 2013, pp. 1–9.

[21] H. Villegas Pico and D. Aliprantis, "Voltage ride-through capability verification of wind turbines with fully-rated converters using reachability analysis," *IEEE Transactions on Energy Conversion*, vol. 29, no. 2, pp. 392–405, June 2014.

[22] Y. Chen, X. Jiang, and A. Domínguez-García, "Impact of power generation uncertainty on power system static performance," in *Proc. of the North American Power Symposium*, 2011.

[23] Y. Makarov, P. Etingov, J. Ma, Z. Huang, and K. Subbarao, "Incorporating uncertainty of wind power generation forecast into power system operation, dispatch, and unit commitment procedures," *IEEE Transactions on Sustainable Energy*, vol. 2, no. 4, pp. 433–442, Oct. 2011.

[24] W. Kersting, "Radial distribution test feeders," *IEEE Transactions on Power Systems*, vol. 6, no. 3, pp. 975 –985, Aug. 1991.

[25] "Transient stability test systems for direct stability methods," *IEEE Transactions on Power Systems*, vol. 7, no. 1, pp. 37–43, Feb. 1992.

[26] Power System Toolbox ver. 2.0: Dynamic Tutorial and Functions, Cherry Tree Scientific Software. Colborne, ON, Canada, 1999.

[27] F. Schweppe, *Uncertain Dynamic Systems*. Englewood Cliffs, NJ: Prentice-Hall Inc., 1973.

[28] F. Chernousko and A. Ovseevich, "Properties of the optimal ellipsoids approximating the reachable sets of uncertain systems," *Optimization Theory and Applications*, vol. 120, no. 2, pp. 223–246, February 2004.